GABRIEL PEREIRA DAS NEVES

Contributions to LPV modeling and gain-scheduled control applied to mechatronic systems

São Paulo
2022

GABRIEL PEREIRA DAS NEVES

Contributions to LPV modeling and gain-scheduled control applied to mechatronic systems

Corrected Version

Thesis presented to the Escola Politécnica da Universidade de São Paulo to obtain the degree of Doctor of Science.

São Paulo
2022

GABRIEL PEREIRA DAS NEVES

Contributions to LPV modeling and gain-scheduled control applied to mechatronic systems

Corrected Version

Thesis presented to the Escola Politécnica da Universidade de São Paulo to obtain the degree of Doctor of Science.

Concentration area:

3139 - System Engineering

Advisor:

Prof. Dr. Bruno Augusto Angélico

São Paulo
2022

Este exemplar foi revisado e corrigido em relação à versão original, sob responsabilidade única do autor e com a anuência de seu orientador.

São Paulo, _____ de _____ de _____

Assinatura do autor: _____

Assinatura do orientador: _____

Catalogação-na-publicação

Neves, Gabriel
Contributions to LPV modeling and gain-scheduled control applied to mechatronic systems / G. Neves -- versão corr. -- São Paulo, 2022.
125 p.

Tese (Doutorado) - Escola Politécnica da Universidade de São Paulo. Departamento de Engenharia de Telecomunicações e Controle.

1.CONTROLE (TEORIA DE SISTEMAS E CONTROLE) 2.SISTEMAS DINÂMICOS 3.MODELOS NÃO LINEARES I.Universidade de São Paulo. Escola Politécnica. Departamento de Engenharia de Telecomunicações e Controle II.t.

ACKNOWLEDGMENTS

To Prof. Dr. Bruno Augusto Angélico, for his guidance, friendship, trust and all the help during the whole work.

To my unofficial co-advisor Prof. Dr. Ricardo C.L.F Oliveira, that without his help we would not have made it halfway through this job. Thank you for your help, for your teachings and for your friendship.

To my girfriend Rayra Destro for all her help and understanding throughout this time. In addition to all this for the constant encouragement to walk this path.

To my mother, Cassia and my sisters Fernanda, Marina and Bianca, who always encouraged me to continue studying and were always available to help.

To Fábio Yukio Toriume, Mateus Mussi Brugnolli, Rafael Pereira Bachega, Arthur Castelo Branco de Oliveira, Leonardo de Paula Carvalho, Caio Igor Gonçalves Chinelato and Jorge Augusto Vasconcelos Alves for the support and fellowship during the doctorate period.

To Prof. Dr. Edvaldo Assunção, Prof. Dr. Grace Silva Deaecto, Prof. Dr. Guilherme Vianna Raffo and Prof. Dr. André Marcorin de Oliveira for participating on the defense, and to Prof. Dr. José Jaime da Cruz, for participating on the qualification. Thank you for all the comments and suggestions about the thesis.

To the Laboratório de Automação e Controle (LAC) of the Escola Politécnica of USP for the availability of physical resources.

To all who helped, directly or indirectly, throughout the project.

To CAPES for the grant number 88882.333359/2019-01 and Finance Code 001.

"Those who dream by day are cognizant of many things which escape those who dream only by night."

-Edgar Allan Poe

RESUMO

Esta tese propõe contribuições para modelagem e controle de uma classe de sistemas não lineares utilizando modelos lineares a parâmetros variantes (do inglês, *Linear Parameter-Varying — LPV*). Como primeira contribuição, são propostas duas técnicas de modelagem especializadas na geração de modelos LPV com dependência polinomial nos parâmetros (denominados parâmetros LPV). Caso os parâmetros estejam relacionados com os estados ou entradas, o modelo é chamado de quasi-LPV. A primeira técnica, baseada na expansão em série de Taylor, produz um modelo mais acurado em torno de um ponto de operação quando comparada com as técnicas clássicas de linearização. A segunda abordagem é baseada em um algoritmo de interpolação polinomial e produz uma família de modelos lineares dentro de uma faixa de operação pré-estabelecida, sendo especialmente adequada para lidar com problemas de seguimento de trajetória. A segunda contribuição da tese é um conjunto de condições para controle escalonado de sistemas LPV ou quasi-LPV. São propostas condições de estabilização, controle $\mathcal{H}_2$ e $\mathcal{H}_\infty$ por realimentação de estados e de saída (estática e dinâmica de ordem completa), que são resolvidas por meio de desigualdade matriciais lineares e busca em um parâmetro escalar confinado no intervalo $(-1, 1)$. Todas as classes de controladores podem ter ganhos com dependência polinomial de grau arbitrário nos parâmetros LPV, em geral fornecendo resultados menos conservadores à medida que os graus aumentam. Com vistas a validar as contribuições desta tese, as técnicas de modelagem e controle propostas são aplicadas em alguns sistemas mecatrônicos, considerando simulações e experimentos físicos.

Palavras-Chave – Modelo LPV, Modelo quasi-LPV, Desigualdade matricial linear, Ganho escalonado, Realimentação de estado, Realimentação estática de saída, Realimentação dinâmica de saída, Norma $\mathcal{H}_2$, Norma $\mathcal{H}_\infty$.

ABSTRACT

This thesis proposes contributions for modeling and control of a class of nonlinear systems using linear parameter-varying (LPV) models. As a first contribution, two modeling techniques specialized in the generation of LPV models with polynomial dependence on the parameters (called LPV parameters) are proposed. If the parameters are related to states or inputs, the model is called quasi-LPV. The first technique, based on Taylor series expansion, produces a more accurate model around an operating point when compared to classical linearization techniques. The second approach is based on a polynomial interpolation algorithm and yields a family of linear models within a pre-established operating range, being especially suitable for dealing with reference tracking problems. The second contribution of the thesis is a set of conditions for gain-scheduled control of LPV or quasi-LPV systems. Stabilization, $\mathcal{H}_2$ and $\mathcal{H}_\infty$ control design conditions by state and output feedback static and full-order dynamic are proposed, being solved in terms of linear matrix inequalities and search on a scalar parameter confined in the range $(-1, 1)$. All classes of controllers can present gains with arbitrary degree polynomial dependence on the LPV parameters, in general providing less conservative results as the degrees increase. In order to validate the contributions of this thesis, the proposed modeling and control techniques are applied in some mechatronic systems, considering simulations and practical experiments.

Keywords – Quasi-LPV model, LPV model, Linear matrix inequality, Gain-scheduled, State-feedback, Static output-feedback, Dynamic output-feedback, $\mathcal{H}_2$ norm, $\mathcal{H}_\infty$ norm.

LIST OF FIGURES

LIST OF TABLES

CONTENTS

1 INTRODUCTION

In the absence of a general theory to cope with stability analysis and control design of nonlinear dynamical systems, the *linear parameter-varying* (LPV) modeling arises as an appealing framework to address such systems in a practical manner (RUGH; SHAMMA, 2000; HOFFMANN; WERNER, 2015; BIANCHI et al., 2014). Moreover, the attractiveness of LPV models has become more prominent in the last decades due to the growing maturity of the numerical methods available for analysis and control synthesis of linear models subject to uncertain and time-varying parameters (MOHAMMADPOUR; SCHERER, 2012; BRIAT, 2015). As a matter of fact, the Lyapunov stability theory, supported by semidefinite programming based methods (BOYD et al., 1994), has been extensively extended and improved along the years. In this context one can mention the use of parameter-dependent Lyapunov functions (DE OLIVEIRA; BERNUSSOU; GEROMEL, 1999; WU, 2001; DAAFOUZ; BERNUSSOU, 2001; WANG; BALAKRISHNAN, 2002; DE SOUZA; TROFINO, 2006), the possibility of designing gain-scheduled controllers (APKARIAN; GAHINET, 1995; APKARIAN; GAHINET; BECKER, 1995), the consideration of bounded rates of variation for the time-varying parameters (WU et al., 1996; APKARIAN; ADAMS, 1998; DE SOUZA; BARBOSA; TROFINO, 2006), extensions to deal with time-varying parameters with polynomial dependence of arbitrary degree (MONTAGNER; OLIVEIRA; PERES, 2006; MONTAGNER et al., 2009; SATO, 2005; CHESI et al., 2007), switching control laws (GEROMEL; COLANERI, 2006b; DEAECTO et al., 2010; HANIFZADEGAN; NAGAMUNE, 2014), to mention a few.

Nonlinear dynamics can present a wide range of particular features and behaviors and, as a consequence, it is difficult to claim that there exist one best strategy to derive a linear model affected by time-varying parameters from a set of nonlinear differential equations (TANAKA; WANG, 2001). Among the possibilities, two main modeling techniques can be considered the main streams explored in the literature. The first one is known as *Takagi-Sugeno fuzzy modeling*, where a linear model affected by time-varying parameters is constructed (through the sector nonlinearity approach) to represent a non-

linear dynamics in a closed region of the state space in terms of fuzzy rules. As a result, one has a model where the state-space matrices are represented in terms of a convex combination of time-varying parameters (also known as membership functions). The second approach, broadly known as *LPV modeling*, is generally based on standard linearization techniques but presenting the state-space matrices depending linearly on bounded time-varying parameters (possibly with bounded rates of variation). In the case where some time-varying parameters are related to the states or inputs of the system, then the resulting model is particularly named as a *quasi-LPV* system (HUANG; JADBABAIE, 1999; TAN; PACKARD; BALAS, 2000; BIANCHI; MANTZ; CHRISTIANSEN, 2005; ROTONDO; NEJJARI; PUIG, 2013; TÓTH, 2010; ABBAS et al., 2014). The modeling of quasi-LPV systems is usually based on techniques that maintain the nonlinear features of the dynamics (SHU-QING; SHENG-XIU, 2010), in general expressing the model in terms of the state vector multiplied by a matrix with nonlinear terms (RUGH; SHAMMA, 2000). In this context it is important to mention that LPV models do not arise necessarily from nonlinear dynamics. As a matter of fact, some systems may present a linear dynamics with parameters that may vary over time, as for instance, switched systems, which comprises a relevant class of dynamical systems with important practical applications (LIBERZON, 2003; GEROMEL; COLANERI, 2006a; DEAECTO et al., 2010; HANIFZADEGAN; NAGAMUNE, 2014). Moreover, some time-varying parameters may not be physical quantities but artificially created to represent some phenomenon. For instance, some properties or issues as packet dropout, time-varying sampling rates (or bandwidth) and time-delays in the context of Networked Control Systems (HESPANHA; NAGHSHTABRIZI; XU, 2007) may be modeled as bounded time-varying parameters. Finally, LPV models can also be obtained considering identification techniques where a precise model for the dynamics is not known (DE CAIGNY; CAMINO; SWEVERS, 2011).

In the context of synthesis of gain-scheduled controllers for LPV systems, the most prominent approach is certainly the Lyapunov stability theory, where design conditions can be formulated in terms of semidefinite programming, which is a class of optimization procedures where efficient (polynomial time) algorithms are available (APKARIAN; GAHINET, 1995; TOH; TODD; TÜTÜNCÜ, 1999; STURM, 1999; ANDERSEN; ANDERSEN, 2000). Stabilizing controllers with performance criteria based on the $\mathcal{H}_2$ and $\mathcal{H}_\infty$ norms are the most considered approaches, with synthesis conditions in general given in terms of linear matrix inequalities (LMIs) (BOYD et al., 1994; DE SOUZA; TROFINO, 2006; GEROMEL; KOROGUI; BERNUSSOU, 2007; DE CAIGNY et al., 2010; APKAR-

IAN; ADAMS, 1998; SATO; PEAUCELLE, 2013). Certainly, this field of research was highly benefited by the arising of techniques based on Lyapunov functions depending on the time-varying parameters (GAHINET; APKARIAN; CHILALI, 1996; GEROMEL; DE OLIVEIRA; HSU, 1998; TROFINO; DE SOUZA, 2001), providing a new class of methods after the *quadratic stability* paradigm, where controllers and filters were designed using a fixed (parameter-independent) Lyapunov function. Besides less conservative in general, analysis and synthesis conditions based on parameter-dependent Lyapunov functions allow the consideration, whenever available, of bounded rates of variation for the time-varying parameters, which is a realistic assumption in most physical systems. Moreover, the development of the so called *LMI relaxations* to check parameter-dependent LMIs with polynomial dependence on the time-varying parameters (BLIMAN, 2004, 2005; OLIVEIRA; PERES, 2007) gave rise to design methods capable to provide gain-scheduled controllers with arbitrary polynomial dependence, providing in general less conservative results than controllers with affine dependence on the parameters. To reduce the conservativeness of the results, some approaches combine LMI conditions with the search of scalar variables or perform the synthesis in two steps, generally improving the performance indices at the price of a higher computational effort (EBIHARA; HAGIWARA, 2004; XIE, 2005; Oliveira; de Oliveira; Peres, 2011; AGULHARI; OLIVEIRA; PERES, 2012).

This thesis presents contributions regarding modeling, synthesis of controllers and experimental validations in physical plants, as detailed in what follows.

1. The first contribution addresses the problem of designing LPV or quasi-LPV models for a class of nonlinear systems. The first proposed technique consists of generating a linear model affected by time-varying parameters around an operating point, with the purpose of increasing the representability of the system. For this task, high-order Taylor series expansion is used. Next, it is proposed a generic polynomial regression algorithm to obtain polynomial quasi-LPV models from a set of nonlinear ordinary differential equations. The procedure has as inputs the number of time-varying parameters (an arbitrary choice of the designer), a generic degree associated to each parameter, and an arbitrary number of local operating points. As a result, one has a polynomial quasi-LPV model, which presents as main appealing feature the ability to address tracking problems without demanding the insertion of integrators or pre-filter design. This approach is somewhat similar to the LPV identification techniques, as the one presented in (DE CAIGNY; CAMINO; SWEVERS, 2011; DE CAIGNY et al., 2010), where the main strategy is the interpolation of linear models.

2. Motivated by the first contribution, that is, by the capability of producing polynomial LPV or quasi-LPV models, the second contribution are synthesis conditions for the design of gain-scheduled controllers for continuous-time polynomial LPV or quasi-LPV models. The conditions are formulated in terms of LMIs combined with a search in a scalar parameter. Differently from previous state-feedback approaches for LPV systems from the literature, a theoretical bound for the scalar parameter is provided, being an advantage when implementing a search procedure (RODRIGUES; OLIVEIRA; CAMINO, 2015, 2018). Three control techniques are considered in this line of investigation: State-feedback, static output-feedback and full-order dynamic output-feedback control. Furthermore, design conditions that minimize an upper bound for the $\mathcal{H}_2$ and $\mathcal{H}_\infty$ norms are also proposed.

3. Finally, the modeling and control design techniques are experimentally validated in four mechatronic systems: Inverted pendulum with reaction wheel, rotational pendulum, unicycle and a control moment gyroscope (CMG). Details of each one of these systems, including the mechanical model, are presented in Appendix.

The text is organized as follows: Chapter 2 presents modeling techniques for LPV and quasi-LPV systems for a class of nonlinear systems; Then, in Chapter 3, synthesis conditions for stabilizing, $\mathcal{H}_2$ and $\mathcal{H}_\infty$ gain-scheduled controllers are proposed; In Chapter 4, simulation and practical results are presented; Finally, in Chapter 5, conclusions and perspectives of future works are presented.

2 MODELING

This chapter presents modeling techniques to obtain a linear model depending polynomially on time-varying parameters from a class of nonlinear systems. If the time-varying parameters are not related to the states or inputs, the resulting model is called LPV model. Otherwise, it is called quasi-LPV model. As terminology, we may call the time-varying parameters as *LPV variables*. Rigorously, an LPV model has an affine dependency with respect to the LPV variables. However, we choose to keep the nomenclature "LPV model" (or quasi-LPV) even in the situation where the dependency is polynomial of arbitrary degree.

Two modeling techniques are proposed. The first one employs a Taylor series expansion of arbitrary order, producing an LPV (or quasi-LPV) model capable to represent the dynamics of the plant around the operating point with more precision, at least with more accuracy than the linear models obtained with standard linearization techniques. The resulting model is particularly suitable to treat the problem of regulation.

In the second approach, a polynomial interpolation algorithm is proposed to generate an LPV (or quasi-LPV) model composed by a family of linear models defined inside a pre-specified region. This approach is specially appropriate to cope with problems involving the tracking of trajectories. Through this method, it is possible to solve the tracking problem without the need for pre-filtering techniques or insertion of integrators.

2.1 Problem definition

A nonlinear model of a dynamic system, in general, can be represented by the state-space differential equation

$$\dot{x}(t) = f(x(t), k(t)) + b(x(t), k(t))u(t), \tag{2.1}$$

where $x(t)$ and $u(t)$ are the vectors of states and inputs, respectively. The vector k contains time-varying parameters not related to $x(t)$ and $u(t)$, and $f(x, k)$ and $b(x, k)$ are

nonlinear functions depending on $x(t)$ and $k(t)$. A simplifying hypothesis well established in mechanical systems, and adopted in this work, is that the model depends linearly on the inputs.

Typically, in the design of linear controllers, it is calculated a linear approximation for the model (2.1) considering an operation point (x_0, u_0), yielding the following linear model

$$\dot{x}(t) = A(x(t) - x_0) + B(u(t) - u_0), \tag{2.2}$$

where A and B are the states and inputs matrices, respectively. In general the accuracy of this model can only be guaranteed for small variations around the operation point, thus causing a limitation of performance.

We consider the problem of finding a time-varying model for a plant modeled as in (2.2) but with matrices $A(\cdot)$ and $B(\cdot)$ represented with more precision than the conventional linear approximation. To accomplish this task, two modeling techniques are considered. The first one is focused on systems that actually operate around an operation point, and the motivation is to increase the performance of the closed-loop system considering a larger region in which the model represents accurately the system. The second is focused on systems that must follow a trajectory. All approaches can address LPV and quasi-LPV models.

For ease of representation, some definitions and hypotheses are defined in the next section.

2.2 Definitions and hypotheses

Some definitions that are used throughout the text are presented in the sequence.

- $x(t)$ is the state vector;
- $u(t)$ is the input vector;
- x_0 is the operation point;

- $J(v,u)$ is the Jacobian matrix of v for a given u, that is

$$J(v,u) = \begin{bmatrix} \frac{\partial v_1}{\partial u_1} & \cdots & \frac{\partial v_1}{\partial u_n} \\ \vdots & \ddots & \vdots \\ \frac{\partial v_n}{\partial u_1} & \cdots & \frac{\partial v_n}{\partial u_n} \end{bmatrix};$$

- ρ is the vector of time-varying parameters (or LPV variables);
- D^γ is the mixed derivatives at γ. In other words

$$D^\gamma f = \frac{\partial^{|\gamma| f}}{\partial x_1^{\gamma_1} \dots \partial x_n^{\gamma_n}};$$

- γ is a multi-index notation;

Two hypotheses regarding the vector field are assumed:

- $f(x)$ is of class C^g, and g is the maximum degree of the polynomial form considered for the LPV or quasi-LPV models to be designed;
- $\dot{x}_0$ is negligible in relation to the rest of the system, that is, it is a smooth variable of the operation point.

2.3 Modeling based on Taylor expansion

The main motivation for this approach is the problem of stabilization of plants that operate around an operation point in closed-loop. The aim is to increase the region around the operating point where the proposed LPV or quasi-LPV models can represent the dynamics of the plant with accuracy.

2.3.1 LPV model

Although this work does not focus primarily on simple LPV models (where LPV variables are not state variables), this section shows one way to obtain a model with polynomial dependency on the time-varying parameters. Considering the nonlinear model (2.1), a linear approximation can be obtained by

$$A = J(\dot{x}, x)|_{x_0,u_0}, \tag{2.3}$$

$$B = J(\dot{x}, u)|_{x_0,u_0}, \tag{2.4}$$

where matrices A and B depend on the vector of time-varying parameters ρ that does not present components related with x neither with u. Thus, one has the following LPV system

$$\dot{x}(t) = A(\rho)x(t) + B(\rho)u(t).$$

However, in most cases, the dependency on ρ is non-polynomial. As a matter of fact, in most mechatronic cases this dependence is through trigonometric functions, for example. As the interest is to produce models with polynomial dependency on ρ, a Taylor series expansion of a given order is performed, such that $A(\rho)$ and $B(\rho)$ are expressed in terms of polynomial matrices.

To exemplify this approach, consider the Control Moment Gyroscope (CMG) given in Appendix D with the following choices of state variables

$$x = \begin{bmatrix} \theta_A & \theta_B & \dot{\theta}_A & \dot{\theta}_B & \dot{\theta}_C \end{bmatrix}^\top.$$

Note that θ_C and $\dot{\theta}_D$ are not state variables and, in this example, they are considered LPV variables, resulting in a pure LPV model.

The first step to obtain the dynamic matrices of the LPV model is to compute the Jacobian of the nonlinear equation (D.2), that is

$$A = J(\dot{x}, x)|_{x_{op}, u_{op}}, \quad B = J(\dot{x}, u)|_{x_{op}, u_{op}},$$

where

$$\dot{x} = \begin{bmatrix} \dot{\theta}_A & \dot{\theta}_B & \ddot{\theta}_A & \ddot{\theta}_B & \ddot{\theta}_C \end{bmatrix}^\top, \quad u = \begin{bmatrix} T_3 & T_4 \end{bmatrix}^\top,$$

and (x_{op}, u_{op}) are the values of the states and inputs at the operation point, in this example chosen as

$$x_{op} = \begin{bmatrix} 0 & 20^\circ & 0 & 0 & 0 \end{bmatrix}^\top, \quad u_{op} = \begin{bmatrix} 0 & 0 \end{bmatrix}^\top,$$

for arbitrary θ_C and $\dot{\theta}_D$. Defining $\rho = \{\theta_C, \dot{\theta}_D\}$ one has the following matrices

$$A(\theta_C, \dot{\theta}_D) = \begin{bmatrix} 0 & 0 & 1 & 0 & 0 \\ 0 & 0 & 0 & 1 & 0 \\ 0 & 0 & a_1 & a_2 & a_3 \\ 0 & 0 & a_2 & a_4 & a_5 \\ 0 & a_6 & a_7 & a_8 & -0.43 \end{bmatrix}, \quad B(\theta_C) = \begin{bmatrix} 0 & 0 \\ 0 & 0 \\ 0 & \frac{-1.4\times10^5 \sin(\theta_C)}{1.2\times10^3 \sin(\theta_C)^2 + 1.6\times10^4} \\ 0 & \frac{6.7\times10^6 \cos(\theta_C)}{2.4\times10^4 \cos(\theta_C)^2 - 3.3\times10^5} \end{bmatrix},$$

where

$$
\begin{aligned}
a_1 &= \frac{-1.4(29\cos(\theta_C)^2 - 266)}{1.2\times 10^3\cos(\theta_C)^2 - 1.7\times 10^4},\\
a_2 &= \frac{788\sin(2\theta_C)}{2.4\times 10^4\cos(2\theta_C) - 6.3\times 10^5},\\
a_3 &= \frac{3.3\times 10^3\dot{\theta}_D\cos(\theta_C)}{1.2\times 10^3\cos(\theta_C)^2 - 1.7\times 10^4},\\
a_4 &= \frac{0.71(58\cos(\theta_C)^2 + 1.3\times 10^3)}{1.2\times 10^3\cos(\theta_C)^2 - 1.7\times 10^4},\\
a_5 &= \frac{9.1\times 10^3\dot{\theta}_D\sin(\theta_C)}{1.2\times 10^3\sin(\theta_C)^2 + 1.6\times 10^4},\\
a_6 &= \frac{25\dot{\theta}_D\sin(\theta_C)}{1.2\times 10^3\sin(\theta_C)^2 + 1.6\times 10^4},\\
a_7 &= \dot{\theta}_D\cos(\theta_C),\\
a_8 &= -\dot{\theta}_D\sin(\theta_C).
\end{aligned}
$$

As can be seen, matrices $A(\theta_C, \dot{\theta}_D)$ and $B(\theta_C)$ present trigonometric terms and also rational functions involving θ_C and $\dot{\theta}_D$. To produce an LPV representation with polynomial dependence on θ_C and $\dot{\theta}_D$, a second order Taylor series expansion is applied to all nonlinear terms, providing the following LPV polynomial matrices

$$
A(\theta_C, \dot{\theta}_D) = A_0 + \dot{\theta}_D A_1 + \theta_C A_2 + \dot{\theta}_D\theta_C A_3 + \theta_C^2 A_4 + \dot{\theta}_D\theta_C^2 A_5, \tag{2.5}
$$

$$
B(\theta_C) = B_0 + \theta_C B_1 + \theta_C^2 B_2, \tag{2.6}
$$

where A_i and B_j are known matrices. As can be noted, the proposed representation is a polynomial LPV model since none of the state variables has been transformed into a time-varying parameter. Higher-order expansions can be considered to improve the model, but this also increases the numerical complexity of the simulations and to perform the synthesis of controllers.

2.3.2 Quasi-LPV model based on high order Taylor expansion

This section deals with a more generic case where the LPV variables can be state variables of the model. Unlike the previous case, it is not possible to apply the Jacobian matrix directly, because this action would result in a first-order model around the operation point of the state variable. Thus, the strategy is to consider a high order Taylor expansion, from which it is possible to represent a larger region around the operation point where the model is still accurate.

For this, it is considered the nonlinear model (2.1) such that the vector $f(x)$ can be decomposed as

$$f(x) = \begin{bmatrix} f_1(x) \\ f_2(x) \\ \vdots \\ f_n(x) \end{bmatrix}.$$

The multivariables Taylor's series is defined as

$$f_i(x) = \sum_{|\gamma| \leq p} \frac{D^\gamma f(x_0)}{\gamma!}(x - x_0)^\gamma + R_{x_0,p}(x - x_0),$$

where p is the desired degree of the polynomial and $R_{x_0,p}(x - x_0)$ are the terms with degree greater than p. Therefore, a polynomial approximation of degree p is given by

$$f_i(x) \approx \hat{f}_i(x) = \sum_{|\gamma| \leq p} \frac{D^\gamma f(x_0)}{\gamma!}(x - x_0)^\gamma.$$

Applying this procedure for each f_i, one has

$$\hat{f}(x) = \begin{bmatrix} \hat{f}_1(x) \\ \hat{f}_2(x) \\ \vdots \\ \hat{f}_n(x) \end{bmatrix}.$$

The same is done for $b(x)$ to obtain $\hat{b}(x)$, such that (2.1) can be represented as

$$\dot{x}(t) \approx \hat{f}(x) + \hat{b}(x)u(t). \tag{2.7}$$

Equation (2.7) represents a polynomial model to all variables in x. When dealing with models where some states are not available for measurement, it is also possible to work with only a subset of state variables, approximating the non measured ones in their respective linearization points (a practical example is presented later to clarify this point). Therefore, the LPV variables (defined by the vector of time-varying parameters ρ) are organized in a matrix form to get the quasi-LPV model

$$\dot{x}(t) = A(\rho)(x(t) - x_0) + B(\rho)(u(t) - u_0). \tag{2.8}$$

This methodology is simple and increases the region around the operation point where

the model can represent the dynamics with accuracy. Regarding the closed-loop operation, this strategy can be used to increase the robustness against plant variations and disturbances, since the model can represent the dynamics with more accuracy than the standard linear model.

To exemplify this approach, consider a rotational inverted pendulum (Furuta pendulum) (MORI; NISHIHARA; FURUTA, 1976), with nonlinear model presented in Appendix B, where θ_0 and θ_1 are the arm and pendulum angle, respectively, and V_p is the PWM duty-cycle input. For more details see the Appendix B.

Applying the Taylor expansion of fourth-order, yields

$$\begin{aligned}
\ddot{\theta}_0 &\approx -68.923\theta_1^3 + 1.5577\theta_1^2\dot{\theta}_0 + 0.06746\theta_1^2\dot{\theta}_1 - 125.867V_p\theta_1^2 + 0.4623\theta_1\dot{\theta}_0^2 \ldots \\
&-0.6164\theta_1\dot{\theta}_0\dot{\theta}_1 - 0.6164\theta_1\dot{\theta}_1^2 + 36.2838\theta_1 - 1.263\dot{\theta}_0 - 0.03893\dot{\theta}_1 + 102.092V_p, \qquad (2.9) \\
\ddot{\theta}_1 &\approx -140.407\theta_1^3 + 3.28414\theta_1^2\dot{\theta}_0 + 0.1304\theta_1^2\dot{\theta}_1 - 265.37V_p\theta_1^2 + 1.4435\theta_1\dot{\theta}_0^2 \ldots \\
&-0.9246\theta_1\dot{\theta}_0\dot{\theta}_1 - 0.9246\theta_1\dot{\theta}_1^2 + 113.286\theta_1 - 1.8952\dot{\theta}_0 - 0.1215\dot{\theta}_1 + 153.137V_p. \qquad (2.10)
\end{aligned}$$

As quasi-LPV variables, only the pendulum angle θ_1 is selected because the arm angle θ_0 does not influence the dynamics (see Appendix B), only its derivative (arm velocity) s present in the model. Finally, it is defined $\rho = \{\theta_1\}$.

As can be seen, the Taylor expansion considers all variables of the model, but the only LPV variable in this example is θ_1. Thus, a simplifying hypothesis is adopted. It is considered that the other parameters, namely $\dot{\theta}_0$ and $\dot{\theta}_1$, are linear around the operation point, such that

$$\begin{aligned}
\ddot{\theta}_0 &\approx -68.923\theta_1^3 + 1.5577\theta_1^2\dot{\theta}_0 + 0.06746\theta_1^2\dot{\theta}_1 - 125.867V_p\theta_1^2 \ldots \\
&\quad +36.2838\theta_1 - 1.263\dot{\theta}_0 - 0.03893\dot{\theta}_1 + 102.092V_p, \\
\ddot{\theta}_1 &\approx -140.407\theta_1^3 + 3.28414\theta_1^2\dot{\theta}_0 + 0.1304\theta_1^2\dot{\theta}_1 - 265.37V_p\theta_1^2 \ldots \\
&\quad +113.286\theta_1 - 1.8952\dot{\theta}_0 - 0.1215\dot{\theta}_1 + 153.137V_p.
\end{aligned}$$

In a matrix notation form (numbers truncated with two decimal digits), one has

$$\begin{bmatrix} \dot{\theta}_0 \\ \dot{\theta}_1 \\ \ddot{\theta}_0 \\ \ddot{\theta}_1 \end{bmatrix} \approx \begin{bmatrix} 0 & 0 & 1 & 0 \\ 0 & 0 & 0 & 1 \\ 0 & 36.28 - 68.92\theta_1^2 & -1.26 + 1.56\theta_1^2 & -0.04 + 0.07\theta_1^2 \\ 0 & 113.29 - 140.41\theta_1^2 & -1.9 + 3.28\theta_1^2 & -0.12 + 0.13\theta_1^2 \end{bmatrix} \begin{bmatrix} \theta_0 \\ \theta_1 \\ \dot{\theta}_0 \\ \dot{\theta}_1 \end{bmatrix} + \begin{bmatrix} 0 \\ 0 \\ 102.09 - 125.87\theta_1^2 \\ 153.14 - 265.37\theta_1^2 \end{bmatrix} V_p. \qquad (2.11)$$

Eq. (2.11) can be written in a quasi-LPV form

$$\dot{x}(t) = A(\theta_1)x(t) + B(\theta_1)u(t) \tag{2.12}$$

where,

$$\begin{aligned}
u &= V_p, \\
x &= \begin{bmatrix}\theta_0 & \theta_1 & \dot{\theta}_0 & \dot{\theta}_1\end{bmatrix}^\top, \\
A(\theta_1) &= \underbrace{\begin{bmatrix} 0 & 0 & 1 & 0 \\ 0 & 0 & 0 & 1 \\ 0 & 36.28 & -1.26 & -0.04 \\ 0 & 113.29 & -1.9 & -0.12 \end{bmatrix}}_{A_0} + \theta_1^2 \underbrace{\begin{bmatrix} 0 & 0 & 1 & 0 \\ 0 & 0 & 0 & 1 \\ 0 & -68.92 & 1.56 & 0.07 \\ 0 & -140.41 & 3.28 & 0.13 \end{bmatrix}}_{A_1}, \\
B(\theta_1) &= \underbrace{\begin{bmatrix} 0 \\ 0 \\ 102.09 \\ 153.14 \end{bmatrix}}_{B_0} + \theta_1^2 \underbrace{\begin{bmatrix} 0 \\ 0 \\ -125.87 \\ -265.37 \end{bmatrix}}_{B_1}.
\end{aligned}$$

To evaluate the quality (accuracy) of this quasi-LPV model, a simulation was performed considering Taylor expansions of third, fourth and fifth orders, besides the nonlinear and linear models. This experiment considers the original polynomial models (as the one in (2.9) and (2.10) for degree four) and the associated quasi-LPV models (as the one in (2.12)). In the first simulation the input is zero ($V_p = 0$) and the initial condition is $x(0) = \begin{bmatrix}0 & 0.1\frac{\pi}{180} & 0 & 0\end{bmatrix}^\top$. The results are shown in Figures 1-2, where the curves indicated by Taylor$_i$ are the models obtained by the Taylor expansion, and qLPV$_i$ are the associated quasi-LPV models. As can be seen, curves qLPV$_4$ and qLPV$_5$ are superimposed, and the LPV models represent the system quite well, even for large angles.

As a new investigation, the pendulum is considered at the equilibrium point and a step in the input is applied ($V_p = 0.05$ in $t = 0.3s$). The results are shown in Figures 3-4. In this simulation, it is possible to see that the quasi-LPV models represented θ_0 significantly better than the linear model, but only when θ_1 presents high values. In this case it is possible to see the difference between qLPV$_4$ and qLPV$_5$, because their input matrices B are different.

Although the quasi-LPV models showed significantly better results than the linear

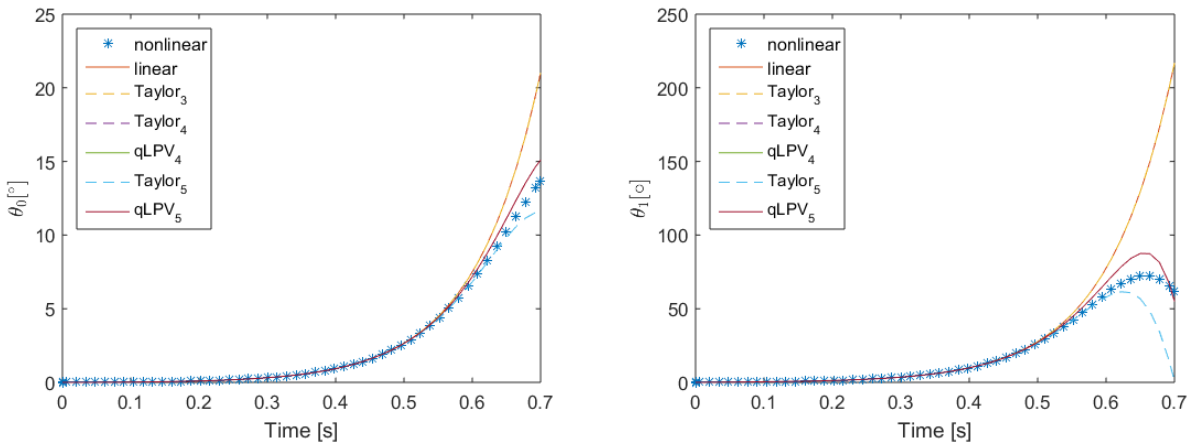

(a) θ_0 (b) θ_1

Figure 1: Angular positions of the Furuta pendulum simulation considering the initial condition $\theta_1 = 0.1°$ and without input ($V_p = 0$).

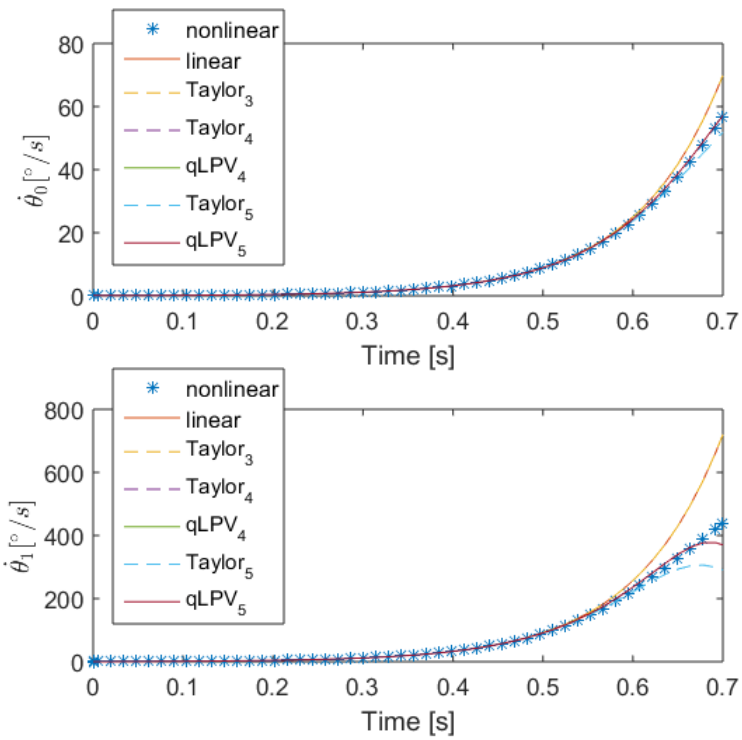

Figure 2: Velocities of the Furuta pendulum simulation considering the initial condition $\theta_1 = 0.1°$ and without input ($V_p = 0$).

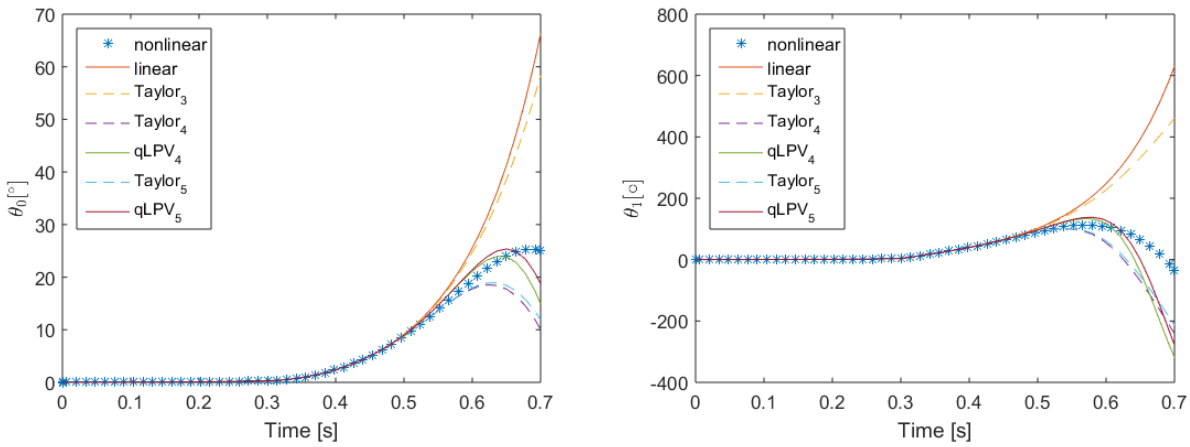

(a) θ_0 (b) θ_1

Figure 3: Angular positions of the Furuta pendulum simulation considering the input $V_p = 0.05$ applied at $0.3s$.

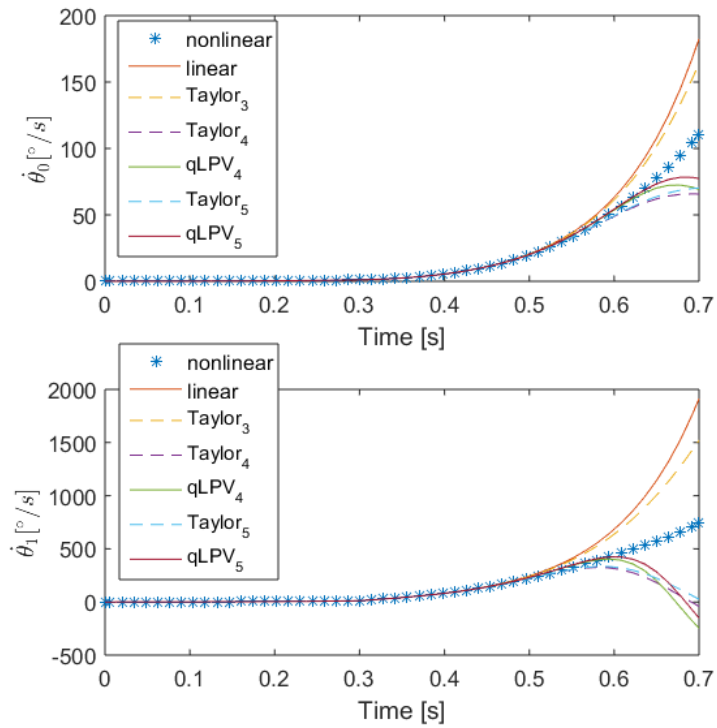

Figure 4: Velocities of the Furuta pendulum simulation considering the input $V_p = 0.05$ applied at $0.3s$.

model for relatively high angles, at small angles the quasi-LPV models are still very close to linear. However, the quasi-LPV models can be used to design controllers that may improve the system performance in the presence of input disturbances.

Besides that, the Furuta pendulum is a very simple system and the quasi-LPV model has only one LPV variable.

As a more complex example, consider a reaction wheel unicycle, where the nonlinear model can be seen in the Appendix C, and the θ_r, θ_w, φ and ψ are the reaction wheel, travel wheel, roll and pitch angles, respectively, and V_r and V_w are the voltage motor of each wheel. For more details see the Appendix C.

The fourth degree Taylor expansion of the nonlinear model is

$$\begin{aligned}
\ddot{\theta}_r &\approx 566V_r - 22\varphi - 52\dot{\theta}_r + 29V_r\psi^2 - 3.6\varphi\psi^2 - 2.7\psi^2\dot{\theta}_r + 3.7\varphi^3 - 1.1\dot{\varphi}\psi\dot{\psi}, \\
\ddot{\varphi} &\approx 22\varphi - 55V_r + 5.1\dot{\theta}_r - 29V_r\psi^2 + 3.6\varphi\psi^2 + 2.7\psi^2\dot{\theta}_r - 3.7\varphi^3 + 1.1\dot{\varphi}\psi\dot{\psi}, \\
\ddot{\theta}_w &\approx 400V_w - 155\psi + 45\dot{\psi} - 68\dot{\theta}_w - 477V_w\psi^2 + 76\varphi^2\psi + 5\dot{\varphi}^2\psi \ldots \\
&\quad +5.5\psi\dot{\psi}^2 - 53\psi^2\dot{\psi} + 80\psi^2\dot{\theta}_w + 277\psi^3, \\
\ddot{\psi} &\approx 58\psi - 93.0V_w - 10.0\dot{\psi} + 16.0\dot{\theta}_w + 144.0V_w\psi^2 - 29\varphi^2\psi - 1.9\dot{\varphi}^2\psi \ldots \\
&\quad -1.1\psi\dot{\psi}^2 + 15\psi^2\dot{\psi} - 23\psi^2\dot{\theta}_w - 74\psi^3.
\end{aligned}$$

This system has two LPV variables (φ and ψ). The other variables are assumed to be linear around the operation point. These considerations lead to the following model

$$\ddot{\theta}_r \approx 566V_r - 22\varphi - 52\dot{\theta}_r + 29V_r\psi^2 - 3.6\varphi\psi^2 - 2.7\psi^2\dot{\theta}_r + 3.7\varphi^3, \tag{2.13}$$

$$\ddot{\varphi} \approx 22\varphi - 55V_r + 5.1\dot{\theta}_r - 29V_r\psi^2 + 3.6\varphi\psi^2 + 2.7\psi^2\dot{\theta}_r - 3.7\varphi^3, \tag{2.14}$$

$$\begin{aligned}
\ddot{\theta}_w &\approx 400V_w - 155\psi + 45\dot{\psi} - 68\dot{\theta}_w - 477V_w\psi^2 + 76\varphi^2\psi \ldots \\
&\quad -53\psi^2\dot{\psi} + 80\psi^2\dot{\theta}_w + 277\psi^3,
\end{aligned} \tag{2.15}$$

$$\begin{aligned}
\ddot{\psi} &\approx 58\psi - 93.0V_w - 10.0\dot{\psi} + 16.0\dot{\theta}_w + 144.0V_w\psi^2 - 29\varphi^2\psi \ldots \\
&\quad +15\psi^2\dot{\psi} - 23\psi^2\dot{\theta}_w - 74\psi^3,
\end{aligned} \tag{2.16}$$

Defining $\rho = \{\varphi, \psi\}$, the quasi-LPV model is given by

$$\dot{x}(t) = A(\varphi, \psi)x(t) + B(\varphi, \psi)u(t),$$

where

$$
\begin{aligned}
u &= \begin{bmatrix} V_r & V_w \end{bmatrix}^\top, \\
x &= \begin{bmatrix} \theta_r & \varphi & \theta_w & \psi & \dot{\theta}_r & \dot{\varphi} & \dot{\theta}_w & \dot{\psi} \end{bmatrix}^\top, \\
A(\varphi,\psi) &= \begin{bmatrix} 0 & I \\ \mathbf{A_1^1} & \mathbf{A_2^1} \end{bmatrix} + \varphi^2 \begin{bmatrix} 0 & I \\ \mathbf{A_1^2} & 0 \end{bmatrix} + \psi^2 \begin{bmatrix} 0 & I \\ \mathbf{A_1^3} & \mathbf{A_2^3} \end{bmatrix}, \\
B(\varphi,\psi) &= \begin{bmatrix} 0 \\ \mathbf{B^1} \end{bmatrix} + \psi^2 \begin{bmatrix} 0 \\ \mathbf{B^2} \end{bmatrix},
\end{aligned}
$$

with

$$
\begin{aligned}
\mathbf{A_1^1} &= \begin{bmatrix} 0 & -22 & 0 & 0 \\ 0 & 22 & 0 & 0 \\ 0 & 0 & 0 & -155 \\ 0 & 0 & 0 & 58 \end{bmatrix}, \ \mathbf{A_2^1} = \begin{bmatrix} -52 & 0 & 0 & 0 \\ 5.1 & 0 & 0 & 0 \\ 0 & 0 & -68 & 45 \\ 0 & 0 & 16 & -10 \end{bmatrix}, \ \mathbf{A_1^2} = \begin{bmatrix} 0 & -3.7 & 0 & 0 \\ 0 & 3.7 & 0 & 0 \\ 0 & 0 & 0 & 76 \\ 0 & 0 & 0 & -29 \end{bmatrix}, \\
\mathbf{A_1^3} &= \begin{bmatrix} 0 & -3.6 & 0 & 0 \\ 0 & 3.6 & 0 & 0 \\ 0 & 0 & 0 & 277 \\ 0 & 0 & 0 & -74 \end{bmatrix}, \ \mathbf{A_2^3} = \begin{bmatrix} -2.7 & -3.6 & 0 & 0 \\ 2.7 & 3.6 & 0 & 0 \\ 0 & 0 & 80 & -53 \\ 0 & 0 & -23 & 15 \end{bmatrix}, \ \mathbf{B^1} = \begin{bmatrix} 566 & 0 \\ -55 & 0 \\ 0 & 400 \\ 0 & -93 \end{bmatrix}, \\
\mathbf{B^2} &= \begin{bmatrix} 29 & 0 \\ -29 & 0 \\ 0 & -477 \\ 0 & 144 \end{bmatrix}.
\end{aligned}
$$

To evaluate the accuracy of the quasi-LPV model of the unicycle, a simulation was performed considering a Taylor expansion of degree four (Taylor$_4$), the associated quasi-LPV model (qLPV$_4$), and the nonlinear and linear models. Using the initial condition $x = \begin{bmatrix} 0 & -0.1\frac{\pi}{180}\text{rad} & 0 & 0.1\frac{\pi}{180}\text{rad} & 0 & 0 & 0 & 0 \end{bmatrix}^\top$, the results are shown in Figure 5, where, for simplicity, only φ and ψ are shown. Similarly to the Furuta pendulum, the differences between quasi-LPV and linear models are visible only at very high angles.

Considering now null initial condition, but with pulses in the inputs

$$
V_r = \begin{cases} 0.3, & 0.2 \le t \le 0.3 \\ 0, & \text{otherwise} \end{cases}, \tag{2.17}
$$

$$
V_w = \begin{cases} -0.3, & 0.9 \le t \le 1 \\ 0, & \text{otherwise} \end{cases}, \tag{2.18}
$$

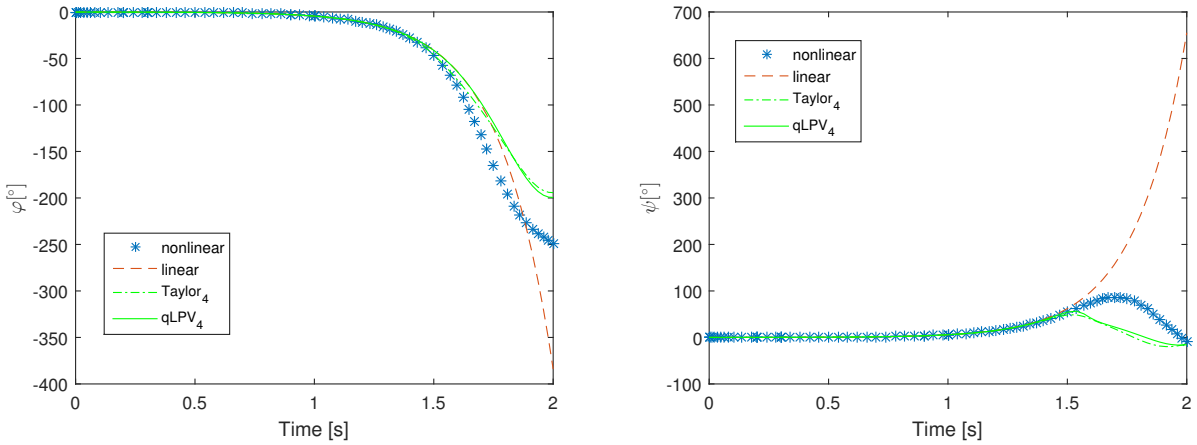

(a) φ (b) ψ

Figure 5: Angular positions of the unicycle simulation considering the initial condition $\varphi = -0.1°$, $\psi = 0.1°$ and without input.

the outputs of this simulation are shown in the Figure 6. Clearly, it is possible to see a significant difference between the linear and quasi-LPV models.

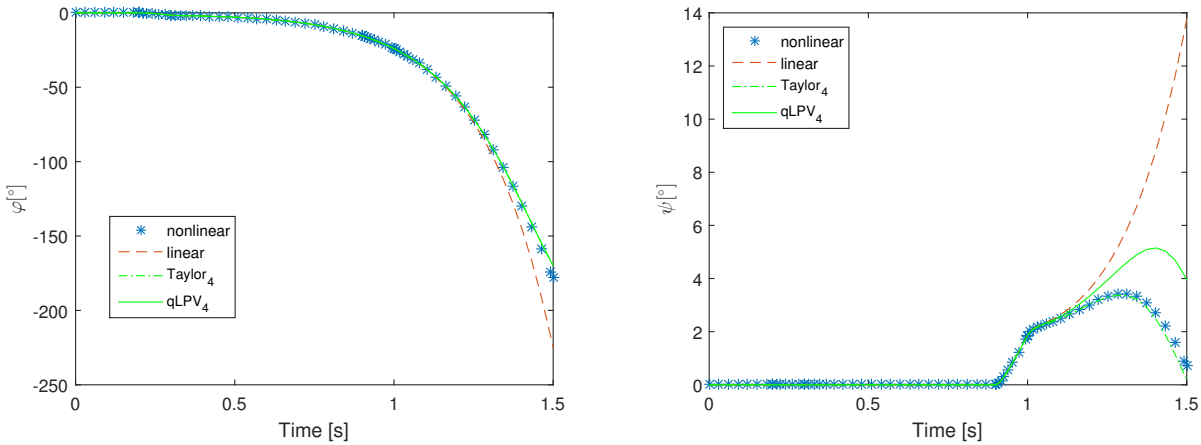

(a) φ (b) ψ

Figure 6: Angular positions of the unicycle simulation considering the inputs given in (2.17) and (2.18).

2.4 Modeling based on the Jacobian matrix with a polynomial regression

The strategy proposed in the previous section is specially suitable to address the regulation problem, where it is expected that trajectories of the states remain close to the operation point. However, although the LPV and quasi-LPV models can represent the dynamics with better accuracy than the standard linear model around the operating point,

all models will deviate significantly from the original nonlinear system as the trajectories move away from the operating condition. Aiming to tackle this problem, which occurs naturally in the case of designing controllers for reference tracking, this section proposes a new technique to design LPV and quasi-LPV models. The strategy relies on producing LPV and quasi-LPV models to approximate not a single but a family of operating conditions. In other words, for each value of the LPV (or quasi-LPV) variables, the resulting linear model is associated to a different operation point.

The approach proposed in this section is capable to design polynomial models of any order with an arbitrary number of variables. The goal is to devise an algorithm that can be used for any continuous nonlinear model structured as (2.1). This approach is somewhat similar to the LPV identification technique, as presented in (DE CAIGNY et al., 2010; DE CAIGNY; CAMINO; SWEVERS, 2011), where the main strategy is the interpolation of linear models.

The first step consists in computing linear approximations in n operations points[1]

$$A_k = J(\dot{x}, x)|_{x_{0k}},$$

where $k = 1, \ldots, n$ is the operation point. The strategy is to end up with a regression problem for each term of A (SEBER; WILD, 1989), such that

$$V(i,j)p(i,j) = b_A(i,j),$$

where $b_A(i,j)$ is the vector with the values of the entry (i,j) of matrix A_k, $p(i,j)$ is the vector of polynomial parameters for the entry (i,j) and $V(i,j)$ is a type of Vandermonde matrix (SEBER; WILD, 1989), here called generic Vandermonde matrix, for the entry (i,j). For ease of notation, all steps hereafter are considered for the entry (i,j).

The vector b_A is obtained by vectorization of the observations (values of each operation point)

$$b_A = \begin{bmatrix} a_1 \\ a_2 \\ \vdots \\ a_k \end{bmatrix}_{n\times 1}.$$

Vector p is the vector of parameters, whose dimension depends on the number of

[1]All analysis and demonstrations are done only for matrix A since the procedure for matrix B is similar.

variables and on the degree of each variable. For instance, consider a polynomial $\hat{f}$ with variables $(x,\, y)$ of degrees 2 and 1, respectively, given by

$$\begin{aligned} \hat{f} &= p_0 + p_1 x + p_2 x^2 + p_3 y + p_4 xy + p_5 x^2 y, \\ p &= \begin{bmatrix} p_0 & p_1 & p_2 & p_3 & p_4 & p_5 \end{bmatrix}^\top . \end{aligned}$$

In this case the dimension of p is given by the number of terms (monomials) n_p, which can be computed through

$$n_p = \prod_{l=1}^{n_v} (g_l + 1),$$

where n_v is the number of variables and g_l is the degree associated to the variable l.

The generic Vandermonde matrix can be generically expressed using vectors of the polynomials and by calculating a predetermined sequence of Kronecker products in a desired order. For example, let us consider a polynomial of three variables x, y and z with degrees two, two and one,

$$\begin{aligned} p_x &= \begin{bmatrix} 1 & x & x^2 \end{bmatrix}, \\ p_y &= \begin{bmatrix} 1 & y & y^2 \end{bmatrix}, \\ p_z &= \begin{bmatrix} 1 & z \end{bmatrix}. \end{aligned}$$

Hence, the combination of these vectors is represented as

$$\begin{aligned} p_{xy} = p_y \otimes p_x &= \begin{bmatrix} 1 & x & x^2 & y & yx & yx^2 & y^2 & y^2x & y^2x^2 \end{bmatrix}, \\ p_{xyz} = p_z \otimes p_{xy} &= \Big[\ 1 \quad x \quad x^2 \quad y \quad yx \quad yx^2 \quad y^2 \quad y^2x \quad y^2x^2 \quad \dots \\ &\quad \dots \quad z \quad zx \quad zx^2 \quad zy \quad zyx \quad zyx^2 \quad zy^2 \quad zy^2x \quad zy^2x^2\ \Big]. \end{aligned}$$

Then, the generic Vandermonde matrix is

$$V = \begin{bmatrix} 1 & x_1 & x_1^2 & y_1 & y_1x_1 & y_1x_1^2 & \dots & z_1y_1^2 & z_1y_1^2x_1 & z_1y_1^2x_1^2 \\ 1 & x_2 & x_2^2 & y_2 & y_2x_2 & y_2x_2^2 & \dots & z_2y_2^2 & z_2y_2^2x_2 & z_2y_2^2x_2^2 \\ \vdots & \vdots & \vdots & \vdots & \vdots & \vdots & \ddots & \vdots & \vdots & \vdots \\ 1 & x_n & x_n^2 & y_n & y_nx_n & y_nx_n^2 & \dots & z_ny_n^2 & z_ny_n^2x_n & z_ny_n^2x_n^2 \end{bmatrix}.$$

The last step consists in solving the resulting linear system of equations

$$Vp = b_A,$$

which can be performed considering the least squares approach,

$$\hat{p} = V^{+} b_A + z,$$

where z belongs to the null space of V and V^{+} is the pseudoinverse of V. Thus, considering the minimum norm result, the solution is calculated as

$$\hat{p} = V^{+} b_A.$$

The steps previously described can be summarized in terms of an algorithm, as presented in what follows.

Algorithm 1. *Considering the nonlinear model described as in* (2.1)*, the polynomial matrices $A(\rho)$ and $B(\rho)$ associated to model* (2.8) *are obtained through the following steps:*

1. *Define a vector of LPV variables $\rho = [\rho_1, \ldots, \rho_{n_v}]$ and choose the operation points x_k, $k = 1, \ldots, n$;*

2. *Compute linear models at each operation point*

$$A_k = J(f, x_k)|_{x_k}, \; k = 1, \ldots, n;$$

3. *For each entry (i, j) of A_k, build the observation vector b_A,*

$$b_A = \begin{bmatrix} A(i,j)_1 \\ A(i,j)_2 \\ \vdots \\ A(i,j)_k \end{bmatrix};$$

4. *Construct the vectors v_i, $i = 1, \ldots, n_v$, each one containing the monomials up to degree g_i of the LPV variable ρ_i, that is*

$$\begin{aligned} v_1 &= \begin{bmatrix} 1 & \rho_1 & \rho_1^2 & \ldots & \rho_1^{g_1} \end{bmatrix}, \\ v_2 &= \begin{bmatrix} 1 & \rho_2 & \rho_2^2 & \ldots & \rho_2^{g_2} \end{bmatrix}, \\ &\vdots \\ v_{n_v} &= \begin{bmatrix} 1 & \rho_{n_v} & \rho_{n_v}^2 & \ldots & \rho_{n_v}^{g_{n_v}} \end{bmatrix}; \end{aligned}$$

5. *Calculate the generic Vandermonde matrix using the Kronecker product applied to*

each operation point

$$V = \begin{bmatrix} v_{n_v} \otimes \cdots \otimes v_2 \otimes v_1\big|_{x_1} \\ v_{n_v} \otimes \cdots \otimes v_2 \otimes v_1\big|_{x_2} \\ \vdots \\ v_{n_v} \otimes \cdots \otimes v_2 \otimes v_i\big|_{x_k} \end{bmatrix};$$

6. *Solve the least square problem*

$$p = V^{+} b_A;$$

7. *Save the vector p of the previous step, return to step 3 and use the next value of the pair (i, j). Repeat the procedure for all elements of A_k. The combination of all entries $p(i, j)$ results in the polynomial matrix $A(\rho)$.*

8. *Finally, apply the algorithm for the input matrix.*

As a result of the algorithm one has the matrices $A(\rho)$ and $B(\rho)$ associated to the following LPV (or quasi-LPV) system

$$\dot{x}(t) = A(\rho)(x(t) - x_{op}(t)) + B(\rho)(u(t) - u_{op}(t)). \tag{2.19}$$

Particularly for quasi-LPV models, the substitution of a given value of ρ in the matrices $A(\rho)$ and $B(\rho)$ provides a linear model around an operating point defined by ρ. As a consequence, it is important to consider the variables $x_{op}(t)$ and $u_{op}(t)$ (that are time-varying). This topic is further discussed later.

To demonstrate the applicability of the algorithm, consider a gyroscope actuator (TORIUMI; ANGéLICO; TANNURI, 2018), with nonlinear model presented in Appendix D. This system was chosen because it presents a great complexity. The system can be of minimum or non-minimum phase and even the direction of the actuators depends on the value of the state variables. In addition, it is also an under-actuated system (TORIUMI; ANGELICO, 2020).

For this system, two LPV variables are considered: θ_B and θ_C, with the following operation limits

$$-75^\circ \leq \theta_B \leq 75^\circ,$$
$$-50^\circ \leq \theta_C \leq 50^\circ.$$

A grid with resolution of 5° is considered for each variable, resulting in

$$\begin{aligned}\mathrm{vec}_{\theta_B} &= \begin{bmatrix}-75^\circ & -70^\circ & \dots & 70^\circ & 75^\circ\end{bmatrix},\\ \mathrm{vec}_{\theta_c} &= \begin{bmatrix}-40^\circ & -35^\circ & \dots & 35^\circ & 40^\circ\end{bmatrix}.\end{aligned}$$

Second and third degree polynomials with respect to θ_B and θ_C are chosen. Because the matrices of the gyroscope model are very large and more complex than the models seen so far in this work, the algorithm is not shown step-by-step. The second degree model designed by the algorithm is

$$\begin{aligned}\dot{x} &= A(\theta_B,\theta_C)(x - x_0(\theta_B,\theta_C)) + B(\theta_B,\theta_C)(u - u_0),\\ A(\theta_B,\theta_C) &= A_1 + \theta_B A_2 + \theta_B^2 A_3 + \theta_C A_4 + \theta_B\theta_C A_5 \dots\\ &\quad + \theta_B^2\theta_C A_6 + \theta_C^2 A_7 + \theta_B\theta_C^2 A_7 + \theta_B^2\theta_C^2 A_9,\\ B(\theta_B,\theta_C) &= B_1 + \theta_B B_2 + \theta_B^2 B_3 + \theta_C B_4 + \theta_B\theta_C B_5 \dots\\ &\quad + \theta_B^2\theta_C B_6 + \theta_C^2 B_7 + \theta_B\theta_C^2 B_7 + \theta_B^2\theta_C^2 B_9,\end{aligned}$$

where the matrices $A_i,\ i = 1,\dots,9$, are given by

$$A_1 = \begin{bmatrix}0 & 0 & 1 & 0 & 0\\ 0 & 0 & 0 & 1 & 0\\ 0 & 0 & -0.02 & 0 & -8.78\\ 0 & 0 & 0 & -0.06 & 0\\ 0 & 0 & 42.41 & 0 & -0.44\end{bmatrix},\quad A_2 = \begin{bmatrix}0 & 0 & 0 & 0 & 0\\ 0 & 0 & 0 & 0 & 0\\ 0 & 0 & 5.94 & 0 & -0.1\\ 0 & 0 & 0 & 0 & 0\\ 0 & 0 & -0.02 & 0 & -5.94\end{bmatrix},$$

$$A_3 = \begin{bmatrix}0 & 0 & 0 & 0 & 0\\ 0 & 0 & 0 & 0 & 0\\ 0 & 0 & -0.01 & 0 & 2.42\\ 0 & 0 & 0 & 0 & 0\\ 0 & 0 & -15.22 & 0 & -0.09\end{bmatrix},\quad A_4 = \begin{bmatrix}0 & 0 & 0 & 0 & 0\\ 0 & 0 & 0 & 0 & 0\\ 0 & 0 & 0 & -0.002 & 22.59\\ 0 & 0 & -0.002 & 0 & 0\\ 0 & 0.07 & 0 & -40.29 & -0.44\end{bmatrix},$$

$$A_5 = \begin{bmatrix}0 & 0 & 0 & 0 & 0\\ 0 & 0 & 0 & 0 & 0\\ 0 & -0.04 & 0 & 0 & 0\\ 0 & 0 & -19.93 & 0 & -0.01\\ 0 & 0 & 0 & -0.002 & 0\end{bmatrix},\quad A_6 = \begin{bmatrix}0 & 0 & 0 & 0 & 0\\ 0 & 0 & 0 & 0 & 0\\ 0 & 0 & 0 & 0.001 & 0\\ 0 & 0 & 0.001 & 0 & 0.46\\ 0 & -0.08 & 0 & 0 & 0\end{bmatrix},$$

$$A_7 = \begin{bmatrix} 0 & 0 & 0 & 0 & 0 \\ 0 & 0 & 0 & 0 & 0 \\ 0 & 0 & -0.001 & 0 & 4.77 \\ 0 & 0 & 0 & 0.01 & 0 \\ 0 & 0 & -20.62 & 0 & 0 \end{bmatrix}, \quad A_8 = \begin{bmatrix} 0 & 0 & 0 & 0 & 0 \\ 0 & 0 & 0 & 0 & 0 \\ 0 & 0 & -3.31 & 0 & -0.002 \\ 0 & -0.01 & 0 & 0 & 0 \\ 0 & 0 & -0.001 & 0 & 3.31 \end{bmatrix},$$

$$A_9 = \begin{bmatrix} 0 & 0 & 0 & 0 & 0 \\ 0 & 0 & 0 & 0 & 0 \\ 0 & 0 & 0 & 0 & -1.2 \\ 0 & 0 & 0 & 0 & 0 \\ 0 & 0 & 7.08 & 0 & -0.001 \end{bmatrix},$$

and $B_i,\ i = 1, \ldots, 9$ are given by

$$B_1 = \begin{bmatrix} 0 & 0 \\ 0 & 0 \\ 0 & 0 \\ 0 & -21.9 \\ 36.85 & 0 \end{bmatrix}, \quad B_2 = \begin{bmatrix} 0 & 0 \\ 0 & 0 \\ 8.5 & 0 \\ 0 & 0 \\ 0 & 0 \end{bmatrix}, \quad B_3 = \begin{bmatrix} 0 & 0 \\ 0 & 0 \\ 0 & 0 \\ 0 & 0.01 \\ 7.17 & 0 \end{bmatrix}, \quad B_4 = \begin{bmatrix} 0 & 0 \\ 0 & 0 \\ 0 & -8.16 \\ 0 & 0 \\ 0 & 0 \end{bmatrix},$$

$$B_5 = \begin{bmatrix} 0 & 0 \\ 0 & 0 \\ 0 & 0 \\ 0.54 & 0 \\ 0 & -5.49 \end{bmatrix}, \quad B_6 = \begin{bmatrix} 0 & 0 \\ 0 & 0 \\ 0 & 2.28 \\ 0 & 0 \\ 0 & 0 \end{bmatrix}, \quad B_7 = \begin{bmatrix} 0 & 0 \\ 0 & 0 \\ 0 & 0 \\ 0 & 11.86 \\ 0.03 & 0 \end{bmatrix}, \quad B_8 = \begin{bmatrix} 0 & 0 \\ 0 & 0 \\ 0.18 & 0 \\ 0 & 0 \\ 0 & 0 \end{bmatrix},$$

$$B_9 = \begin{bmatrix} 0 & 0 \\ 0 & 0 \\ 0 & 0 \\ 0 & 0.43 \\ 0.09 & 0 \end{bmatrix}.$$

To evaluate the accuracy of the two designed polynomial LPV models (denoted by x_{qLPV2} and x_{qLPV3}), simulations are performed comparing the open-loop responses with the nonlinear dynamics ($x_{nlinear}$) given in Appendix D and, for completeness, with a linearized model (x_{linear}). The input signals are presented in Figure 7. As mentioned before, the proposed algorithm produces models structured as in (2.19), which are dependent on $(x - x_{op})$. In a closed-loop operation, x_{op} is treated as a reference, and, in the open-loop simulation, performed in this section, it is considered a grid with resolution of 5°. For instance, within the interval $0° \leq \theta_B < 5°$, the corresponding x_{op} is set to 0, but within

$5° \leq \theta_B < 10°$, it is set to $5°$, and so on. We stress that this approach is just considered in the open-loop simulation to verify how close the polynomial LPV representation is from the nonlinear model.

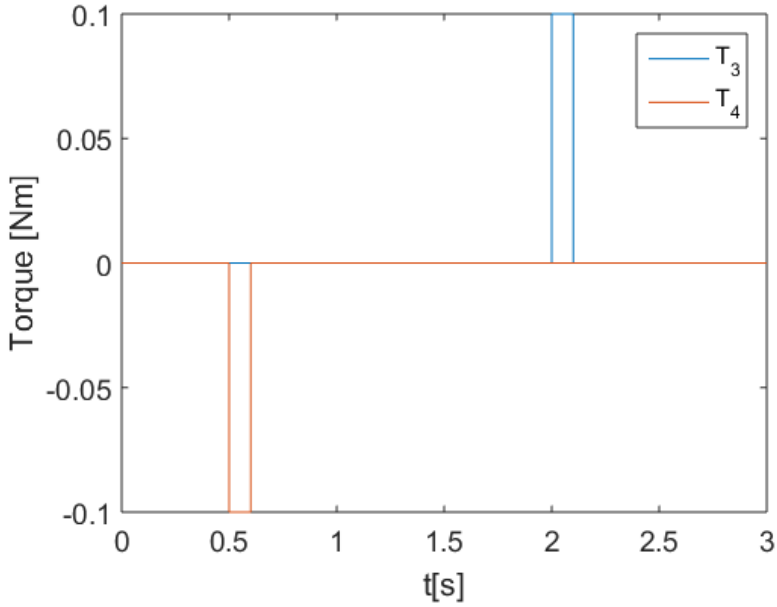

Figure 7: Inputs applied to validate the quasi-LPV model associated to the gyroscope system.

Regarding the linear model, it is obtained around the operating point[2]

$$\begin{aligned} x_{op} &= \begin{bmatrix} 0 & 0 & 0 & 0 & 400 \text{ rpm} \end{bmatrix}, \\ \theta_C &= 0, \end{aligned} \tag{2.20}$$

and, considering the initial condition given by

$$\begin{aligned} x_{ic} &= \begin{bmatrix} 0 & 20° & 0 & 0 & 400 \text{ rpm} \end{bmatrix}, \\ \theta_C &= -20°. \end{aligned} \tag{2.21}$$

The trajectories of θ_A and θ_B are shown in Figure 8. As can be seen, the linear model does not represent the nonlinear model well. On the other hand, the proposed quasi-LPV models, whose trajectories are also shown in Figure 8, are more accurate, specially model x_{qLPV3}.

The simulations presented in Figure 9 consider that the linear model was linearized

[2]The models investigated in this work assume the units of all variables in the international system. However, in some cases the units are explicitly presented to facilitate the reading.

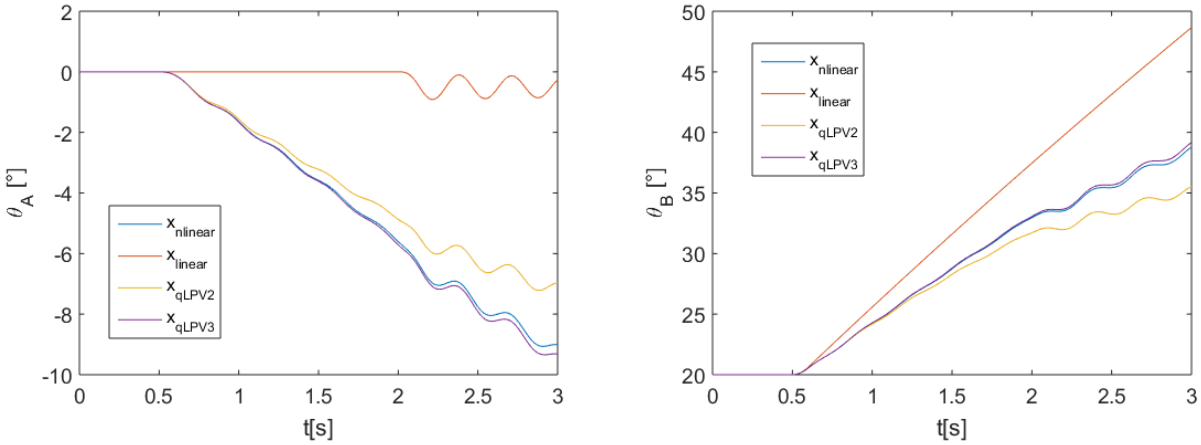

(a) θ_A (b) θ_B

Figure 8: Outputs of the nonlinear, second degree quasi-LPV, third degree quasi-LPV and the linear model obtained around $\theta_B = 0$ and $\theta_C = 0$, and initial conditions given in (2.21).

at the same point as the initial condition, i.e.,

$$\begin{aligned} x_{op} &= x_{ic} = \begin{bmatrix} 0 & 20^\circ & 0 & 0 & 400 \text{ rpm} \end{bmatrix}, \\ \theta_C &= -20^\circ, \end{aligned} \tag{2.22}$$

In this case the results show that the linear model represents the nonlinear model very well, but the third-degree quasi-LPV model does even better.

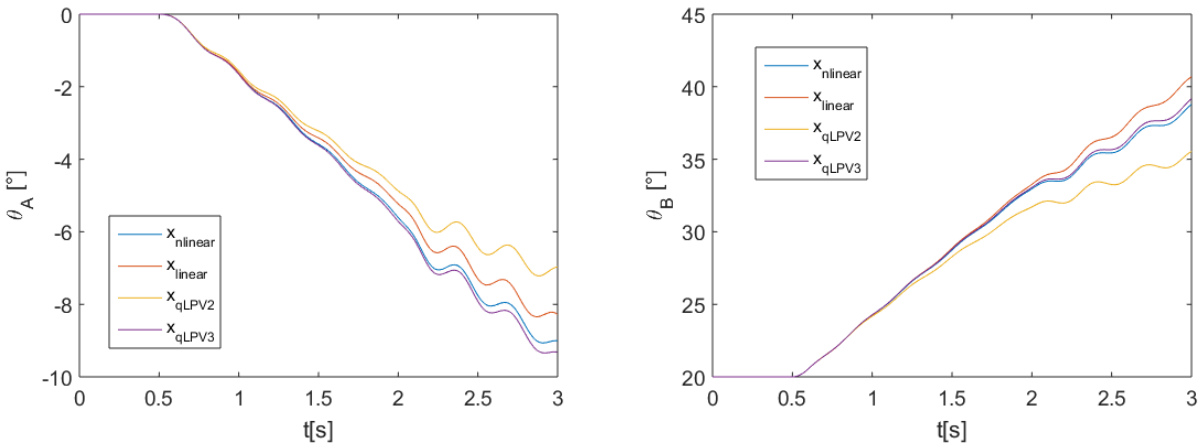

(a) θ_A (b) θ_B

Figure 9: Outputs of the nonlinear, second degree quasi-LPV, third degree quasi-LPV and the linear model obtained around $\theta_B = 20^\circ$ and $\theta_C = -20^\circ$, and initial conditions given in (2.22).

Let us consider now that, for some reason, the initial condition of the linear model has completely reversed (a situation that can naturally happen during the operation of

the system), i.e.,

$$\begin{aligned} x_{ic} &= \begin{bmatrix} 0 & -20^\circ & 0 & 0 & 400 \text{ rpm} \end{bmatrix}, \\ \theta_C &= 20^\circ, \end{aligned} \tag{2.23}$$

but the model is still linearized around the same point considered in previous simulation. The new results are presented in Figure 10.

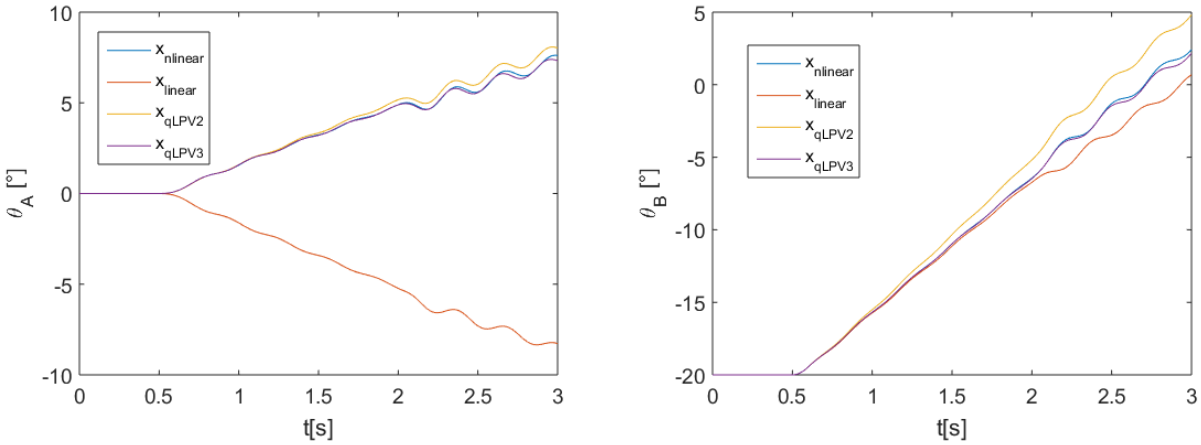

(a) θ_A (b) θ_B

Figure 10: Outputs of the nonlinear, second degree quasi-LPV, third degree quasi-LPV and the linear model obtained around $\theta_B = 20°0$ and $\theta_C = -20°$, and initial conditions given in (2.23).

As conclusion, the proposed quasi-LPV models can represent the nonlinear dynamics in all analyzed operating points, while the linear model loses representativeness when it is far from the linearization point, as expected. These results validate the ability of Algorithm 1 of providing accurate polynomial LPV representations for a nonlinear CMG model around a range of operation.

3 CONTROLLER DESIGN

In this chapter, synthesis conditions formulated in terms of parameter-dependent LMIs are provided for the design of gain-scheduled controllers for LPV (or quasi-LPV) systems. The approach addresses stabilization, $\mathcal{H}_2$ and $\mathcal{H}_\infty$ control, allowing the controllers to depend polynomially on the time-varying parameters. The results are split in three main topics: state feedback, static output feedback and dynamic output feedback control.

3.1 State-feedback control

This section presents synthesis procedures for the design of gain-scheduled state-feedback controllers. As a first step, the stabilization problem is presented in details to make clear the proposed technical contributions, which is a new strategy to deal with the time-derivative of the Lyapunov matrix, extending the conditions of (RODRIGUES; OLIVEIRA; CAMINO, 2018) to cope with time-varying parameters. A numerical example based on a simulation performed on a database of uncertain systems is given to illustrate the application of the proposed conditions and to evaluate the conservativeness when compared to similar conditions from the literature. After that, conditions for the synthesis of $\mathcal{H}_2$ and $\mathcal{H}_\infty$ controllers are presented.

Consider the LPV system

$$G = \begin{cases} \dot{x} = A(\rho(t))x + B(\rho(t))u + B_w(\rho(t))w \\ z = C_z(\rho(t))x + D(\rho(t))u + D_w(\rho(t))w \\ y = C(\rho(t))x + D_{wy}(\rho(t))w, \end{cases} \tag{3.1}$$

where $x(t) \in \mathbb{R}^{n_x}$, $u(t) \in \mathbb{R}^{n_u}$, $y(t) \in \mathbb{R}^{n_y}$, $w(t) \in \mathbb{R}^{n_w}$ and $z(t) \in \mathbb{R}^{n_z}$ are the state, control input, measured output, exogenous input and controlled output vectors[1], respectively. Matrices $A(\rho(t))$, $B(\rho(t))$, $B_w(\rho(t))$, $C_z(\rho(t))$, $D(\rho(t))$, $D_w(\rho(t))$, $C(\rho(t))$ and $D_{wy}(\rho)$ have appropriate dimensions and depend polynomially on $\rho(t)$. The parameters $\rho(t) =$

[1]The measured output vector y is used only the in output-feedback problem.

$[\rho_1(t), \ldots, \rho_N(t)]$ and their time-derivatives are assumed to be bounded in the form

$$\begin{aligned} \underline{a}_i \leq \rho_i(t) \leq \overline{a}_i, \\ \underline{b}_i \leq \dot{\rho}_i(t) \leq \overline{b}_i, \\ 0 \in [\underline{b}_i,\ \overline{b}_i], \end{aligned}$$

such that $\rho(t)$ belongs to the hyperrectangle Θ and $\dot{\rho}(t)$ belongs to the hyperrectangle Γ for all $t \geq 0$ (APKARIAN; ADAMS, 1998).

The aim is to design the gain-scheduled state-feedback control law $u(t) = K(\rho(t))x(t)$ to stabilize the system, possibly also ensuring attenuation levels from the input w to the output z in terms of the $\mathcal{H}_2$ and $\mathcal{H}_\infty$ norms. To make feasible the implementation of this control law, it is assumed that the vector of parameters $\rho(t)$ and states $x(t)$ are available in real-time. The closed-loop system is given by

$$\begin{aligned} \dot{x}(t) &= A_{cl}(\rho(t))x(t) + B_w(\rho(t))w(t), \\ z(t) &= C_{cl}(\rho(t))x(t) + D_w(\rho(t))w(t), \end{aligned}$$

where $A_{cl}(\rho(t)) = A(\rho(t)) + B(\rho(t))K(\rho(t))$ and $C_{cl}(\rho(t)) = C_z(\rho(t)) + D(\rho(t))K(\rho(t))$. As the parameters $\rho(t)$ and $\dot{\rho}(t)$ are assumed to belong to hyperrectangles for all $t \geq 0$, from this point the explicit dependence of these parameters on t is only presented if it is relevant for the context. In general this option streamlines the notation and shorten formulas.

As a final important remark, all synthesis conditions presented in this chapter consider an LPV system, assuring that all designed controllers are globally stabilizing. On the other hand, if the conditions are applied to quasi-LPV systems, the controllers are only locally stabilizing.

3.1.1 Stabilization

The next theorem presents a synthesis condition to design the gain $K(\rho)$ such that the closed-loop system is asymptotically stable.

Theorem 1. *Let $\epsilon \neq 0$ and $\xi \in (-1, 1)$ be given scalars. If there exist matrices $W(\rho) =$*

$W(\rho)^\top$, $Y(\rho)$, $X(\rho)$ and $Z(\rho)$ that satisfy[2]

$$W(\rho) > 0,$$
$$\begin{bmatrix} \Xi(1,1)(\rho) & \Xi(1,2)(\rho) & \bar{V}(\rho) \\ \star & \Xi(2,2)(\rho) & -\bar{V}(\rho) \\ \star & \star & -\mathrm{He}(X(\rho)) \end{bmatrix} < 0, \tag{3.2}$$

where

$$\begin{aligned}
\Xi(1,1)(\rho) &= W(\rho) + \mathrm{He}(\tilde{A}(\rho)Y(\rho) + \bar{B}(\rho)Z(\rho)), \\
\Xi(1,2)(\rho) &= \xi(\tilde{A}(\rho)Y(\rho) + \bar{B}(\rho)Z(\rho)) - Y(\rho)^\top \hat{A}(\rho)^\top - Z(\rho)^\top \bar{B}(\rho)^\top, \\
\Xi(2,2)(\rho) &= -W(\rho) - \xi\mathrm{He}(\hat{A}Y(\rho) + \bar{B}Z(\rho)), \\
\hat{A}(\rho) &= \epsilon A(\rho) + \frac{1}{2\epsilon}I, && (3.3) \\
\tilde{A}(\rho) &= \epsilon A(\rho) - \frac{1}{2\epsilon}I, && (3.4) \\
\bar{B}(\rho) &= \epsilon B(\rho), && (3.5) \\
\bar{V}(\rho) &= \epsilon\left(-\dot{W}(\rho) + \frac{1}{2}X(\rho)\right), && (3.6)
\end{aligned}$$

for all $\rho \in \Theta$ and $\dot{\rho} \in \Gamma$, then the gain-scheduled state-feedback gain $K(\rho) = Z(\rho)Y(\rho)^{-1}$ stabilizes the system (3.1).

Proof. First, we show that matrix $Y(\rho)$ is invertible. Note that the feasibility of inequality (3.2) ensures that

$$\begin{bmatrix} \Xi(1,1) & \Xi(1,2) \\ \star & \Xi(2,2) \end{bmatrix} < 0$$

Multiplying this inequality on the left by $T = \begin{bmatrix} I & I \end{bmatrix}$ and on the right by $T^\top$, yields

$$-\left(\frac{1}{\epsilon}\right)(1+\xi)(Y(\rho) + Y(\rho)^\top) < 0,$$

which ensures that $Y(\rho)$ is full rank, since $\xi \in (-1,1)$ and $\epsilon \neq 0$.

The next step is to prove that ξ belongs to a bounded interval. Applying the following transformation on (3.2)

$$\begin{bmatrix} \xi I & -I & 0 \\ 0 & 0 & I \end{bmatrix} \begin{bmatrix} \Xi(1,1)(\rho) & \Xi(1,2)(\rho) & \bar{V}(\rho) \\ \star & \Xi(2,2)(\rho) & -\bar{V}(\rho) \\ \star & \star & -\mathrm{He}(X(\rho)) \end{bmatrix} \begin{bmatrix} \xi I & 0 \\ -I & 0 \\ 0 & I \end{bmatrix} < 0,$$

[2] $\dot{W}(\rho)$ is used to denote $\frac{\partial W}{\partial \rho}\frac{d\rho}{dt}$ and $\mathrm{He}(A)$ denotes $A + A^\top$.

results in

$$\begin{bmatrix} (\xi^2-1)W(\rho) & (\xi-1)\bar{V}(\rho) \\ \bar{V}(\rho)^\top(\xi-1) & -X(\rho)-X(\rho)^\top \end{bmatrix} < 0, \tag{3.7}$$

which, to be feasible, requires that $(\xi^2-1)W(\rho) < 0$. As $W(\rho) > 0$, we conclude that $-1 < \xi < 1$.

Next, we prove that the feasibility of (3.2) is sufficient to guarantee closed-loop stability. Considering the transformation $K(\rho)Y(\rho) = Z(\rho)$ and the following transformation applied on (3.2)

$$\begin{bmatrix} \hat{A}_{cl}(\rho) & \tilde{A}_{cl}(\rho) & 0 \\ 0 & 0 & I \end{bmatrix} \begin{bmatrix} \Xi(1,1)(\rho) & \Xi(1,2)(\rho) & \bar{V}(\rho) \\ \star & \Xi(2,2)(\rho) & -\bar{V}(\rho) \\ \star & \star & -\mathrm{He}(X(\rho)) \end{bmatrix} \begin{bmatrix} \hat{A}_{cl}(\rho)^\top & 0 \\ \tilde{A}_{cl}(\rho)^\top & 0 \\ 0 & I \end{bmatrix} < 0,$$

where

$$\begin{aligned} \hat{A}_{cl}(\rho) &= \epsilon A_{cl}(\rho) + \frac{1}{2\epsilon} I, && (3.8) \\ \tilde{A}_{cl}(\rho) &= \epsilon A_{cl}(\rho) - \frac{1}{2\epsilon} I, && (3.9) \\ A_{cl}(\rho) &= A(\rho) + B(\rho)K(\rho), \end{aligned}$$

one has

$$\begin{bmatrix} \hat{A}_{cl}(\rho)W(\rho)\hat{A}_{cl}(\rho)^\top - \tilde{A}_{cl}(\rho)W(\rho)\tilde{A}_{cl}(\rho)^\top & (\hat{A}_{cl}(\rho)-\tilde{A}_{cl}(\rho))\bar{V}(\rho) \\ \bar{V}(\rho)^\top(\hat{A}_{cl}(\rho)-\tilde{A}_{cl}(\rho))^\top & -X(\rho)-X(\rho)^\top \end{bmatrix} < 0. \tag{3.10}$$

Using the definitions given in (3.3)-(3.6), condition (3.10) can be rewritten as

$$\begin{bmatrix} W(\rho)A_{cl}(\rho)^\top + A_{cl}(\rho)W(\rho) & -\dot{W}(\rho) + \frac{1}{2}X(\rho) \\ -\dot{W}(\rho) + \frac{1}{2}X(\rho)^\top & -X(\rho)-X(\rho)^\top \end{bmatrix} < 0.$$

Finally, applying the transformation

$$\begin{bmatrix} I & \frac{1}{2}I \end{bmatrix} \begin{bmatrix} W(\rho)A_{cl}(\rho)^\top + A_{cl}(\rho)W(\rho) & -\dot{W}(\rho) + \frac{1}{2}X(\rho) \\ -\dot{W}(\rho) + \frac{1}{2}X(\rho)^\top & -X(\rho)-X(\rho)^\top \end{bmatrix} \begin{bmatrix} I \\ \frac{1}{2}I \end{bmatrix} < 0,$$

provides

$$W(\rho)A_{cl}(\rho)^\top + A_{cl}(\rho)W(\rho) - \dot{W}(\rho) < 0,$$

that assures the closed-loop stability through the existence of the parameter-dependent

quadratic in the state Lyapunov function $v(x) = x^\top P(\rho)x$ with $P(\rho) = W(\rho)^{-1}$ (MONTAGNER et al., 2009). $\square$

The advantage of the synthesis conditions of Theorem 1 with respect to previous approaches from the literature, that also employ a search for a scalar parameter to reduce the conservativeness of the results, is the bounds for the scalar ξ. This feature facilitates the implementation of an optimization procedure aiming to obtain improved guaranteed costs. To achieve the bounds for ξ, note that a special treatment for the time-derivative of the Lyapunov matrix was employed. Using an additional slack variable $X(\rho)$, the term $\dot{W}(\rho)$ was removed from block (1,1) of the left-hand side of (3.2) (note that $\dot{W}(\rho)$ appears only in blocks (1,3) and (2,3)), allowing to define the bounds for ξ in equation (3.7). This technical contribution can be useful in other contexts where the time-derivative of the Lyapunov matrix is also an issue, as in the dynamic output-feedback problem.

The next result (Corollary 1) is an extension of Theorem 1 to address the problem of robust stabilizing control, that is, the design of a fixed (ρ-independent) gain $K(\rho) = K$. This synthesis condition is specially suitable to address problems where the parameters $\rho(t)$ cannot be measured in real time.

Corollary 1. *Let $\epsilon \neq 0$ and $\xi \in (-1, 1)$ be given scalars. If there exist matrices $W(\rho) = W(\rho)^\top$, $X(\rho)$, Y and Z that satisfy*

$$W(\rho) > 0,$$
$$\begin{bmatrix} \Xi(1,1)(\rho) & \Xi(1,2)(\rho) & \bar{V}(\rho) \\ \star & \Xi(2,2)(\rho) & -\bar{V}(\rho) \\ \star & \star & -\mathrm{He}(X(\rho)) \end{bmatrix} < 0,$$

where

$$\begin{aligned} \Xi(1,1)(\rho) &= W(\rho) + \mathrm{He}(\tilde{A}(\rho)Y + \bar{B}(\rho)Z), \\ \Xi(1,2)(\rho) &= \xi(\tilde{A}(\rho)Y + \bar{B}(\rho)Z) - Y^\top \hat{A}(\rho)^\top - Z^\top \bar{B}(\rho)^\top, \\ \Xi(2,2)(\rho) &= -W(\rho) - \xi\mathrm{He}(\hat{A}(\rho)Y + \bar{B}(\rho)Z), \end{aligned}$$

with $\hat{A}(\rho)$, $\tilde{A}(\rho)$, $\bar{B}(\rho)$ and $\bar{V}(\rho)$ given in (3.3)-(3.6)*, for all $\rho \in \Theta$ and $\dot{\rho} \in \Gamma$, then the robust state-feedback gain $K = ZY^{-1}$ stabilizes the system* (3.1)*.*

One possibility to evaluate the conservatism of the proposed synthesis conditions is to perform a numerical comparison with conditions from the literature. With this purpose, we consider a comparison in the context of time-invariant uncertainty, employing

the database of unstable uncertain systems provided in (Oliveira; de Oliveira; Peres, 2011). The systems are guaranteedly stabilized by a robust (parameter-independent) state-feedback gain but not quadratically stabilized. The following variation rates are considered:

$$-\kappa \leq \dot{\rho}_i \leq \kappa,$$

where $\kappa \in \{10^{-3}, 10^{-1}, 1\}$. As the database was created for time-invariant uncertainty, the case $\kappa = 10^{-3}$ is specially suitable to evaluate the performance of Corollary 1 when compared to other conditions specialized in time-invariant uncertainty.

As shown in (Oliveira; de Oliveira; Peres, 2011), the least conservative condition (based on Finsler's Lemma) was given in (EBIHARA; HAGIWARA, 2004) (denoted by EH04) and we also consider the condition from (RODRIGUES; OLIVEIRA; CAMINO, 2015) (denoted by ROC15), that is the method from which our approach was derived. Table 1 shows the result of the simulation, where n is the number of states, N is the number of vertices of polytope and m is the number of inputs. As the main interest of Theorem 1 and Corollary 1 is to exploit the bounded parameter ξ, the parameter ϵ is fixed at 0.1 (as suggested in (RODRIGUES; OLIVEIRA; CAMINO, 2015)). Besides, the following set of values is considered for the parameter ξ when testing Corollary 1 (19 equally spaced values)

$$\xi = \begin{bmatrix} -0.9 & -0.8 & -0.7 & \dots & 0.7 & 0.8 & 0.9 \end{bmatrix}.$$

As expected, as κ grows, the effectiveness of Corollary 1 decreases. However, the important conclusion is that the results obtained for $\kappa = 10^{-3}$ are very close to the condition given in (RODRIGUES; OLIVEIRA; CAMINO, 2015) (ROC15 in Table 1). This fact shows that the extra slack variable $X(\rho)$, specially included to deal with the time-derivative of the Lyapunov matrix, does not generate conservativeness when imposing particular structures to the variables.

Motivated by the results obtained in the case of stabilization, the extensions to cope with $\mathcal{H}_2$ and $\mathcal{H}_\infty$ performance are presented in the next sections.

Table 1: Number of system (among 100) stabilized by a robust state-feedback gain.

(n,N,m)	EH04	ROC15	Corollary 1		
			$\kappa = 10^{-3}$	$\kappa = 10^{-1}$	$\kappa = 1$
(2,2,1)	100	82	82	65	40
(2,3,1)	58	56	54	35	25
(2,4,1)	50	52	51	42	26
(2,5,1)	60	63	62	56	31
(3,2,1)	82	78	78	70	48
(3,3,1)	49	52	52	46	26
(3,4,1)	38	40	39	37	31
(3,5,1)	33	38	38	35	27
(4,2,1)	75	74	74	73	53
(4,3,1)	49	54	54	51	36
(4,4,1)	41	43	43	41	34
(4,5,1)	28	32	32	30	20
(5,2,1)	77	78	78	76	60
(5,3,1)	54	62	62	61	49
(5,4,1)	39	47	47	43	33
(5,5,1)	26	29	29	29	22
Success m=1	53.7%	55%	54.7%	49.4%	35.1%
(3,2,2)	97	97	97	95	83
(3,3,2)	75	78	78	72	57
(3,4,2)	70	73	73	70	49
(3,5,2)	61	66	66	62	48
(4,2,2)	98	97	97	97	78
(4,3,2)	67	69	69	66	53
(4,4,2)	63	68	68	65	55
(4,5,2)	60	68	68	66	51
(5,2,2)	91	91	91	90	74
(5,3,2)	71	75	75	74	58
(5,4,2)	68	72	72	71	57
(5,5,2)	59	67	67	66	51
Success m=2	73.3%	76.8%	76.8%	74.5%	59.5%

3.1.2 $\mathcal{H}_2$ control

Considering the system G given in (3.1) as asymptotically stable and assuming that $D_w(\rho) = 0$, the $\mathcal{H}_2$ norm of G is defined as

$$\|G\|_2^2 = \lim_{h\to\infty} \varepsilon \left\{ \frac{1}{h} \int_0^h z(t)^\top z(t) dt \right\}$$

when the input $w(t)$ is a stationary zero-mean white noise with power spectrum density matrix equal to identity (DE SOUZA; TROFINO, 2006). The symbol ε denotes the mathematical expectation.

Lemma 1. *(SZNAIER, 1999) Let $D_w(\rho) = 0$. If there exist parameter-dependent matrices $W(\rho) = W(\rho)^\top$ and $H(\rho) = H(\rho)^\top$ and a scalar $\mu > 0$ such that the parameter-dependent LMIs*

$$\mu > Tr(H(\rho)), \tag{3.11}$$

$$\begin{bmatrix} H(\rho) & B_w(\rho)^\top \\ \star & W(\rho) \end{bmatrix} > 0, \tag{3.12}$$

$$\begin{bmatrix} A(\rho)W(\rho) + W(\rho)A(\rho)^\top - \dot{W}(\rho) & W(\rho)C_z(\rho)^\top \\ \star & -I \end{bmatrix} < 0 \tag{3.13}$$

hold for all $\rho \in \Theta$ and $\dot{\rho} \in \Gamma$, then system (3.1) in open-loop is asymptotically stable and $\sqrt{\mu}$ is an $\mathcal{H}_2$ guaranteed cost, that is, $\|G\|_2 < \sqrt{\mu}$.

Next theorem is the extension of Theorem 1 to cope with the $\mathcal{H}_2$ norm as performance criterion. As a result, one can design a gain-scheduled stabilizing controller that guarantees an $\mathcal{H}_2$ guaranteed cost for the closed-loop system. As a necessary hypothesis, matrix $D_w(\rho)$ is considered null (to ensure the existence of the $\mathcal{H}_2$ norm).

Theorem 2. *Let $\xi \in (-1, 1)$ and $\epsilon \neq 0$ be given scalars. If there exist parameter-dependent matrices $W(\rho) = W(\rho)^\top$, $H(\rho) = H(\rho)^\top$, $Y(\rho)$, $X(\rho)$ and $Z(\rho)$, and a scalar $\mu > 0$ such that the following parameter-dependent LMIs*

$$\mu > \mathrm{Tr}(H(\rho)), \tag{3.14}$$

$$\begin{bmatrix} H(\rho) & B_w(\rho)^\top \\ \star & W(\rho) \end{bmatrix} > 0, \tag{3.15}$$

$$\begin{bmatrix} \Xi(1,1)(\rho) & \Xi(1,2)(\rho) & \Xi(1,3) & \bar{V}(\rho) \\ \star & \Xi(2,2)(\rho) & \xi\Xi(1,3)(\rho) & -\bar{V}(\rho) \\ \star & \star & -I & 0 \\ \star & \star & \star & -\mathrm{He}(X(\rho)) \end{bmatrix} < 0, \tag{3.16}$$

where

$$\begin{aligned}
\Xi(1,1)(\rho) &= W(\rho) + \mathrm{He}\left(\tilde{A}(\rho)Y(\rho) + \bar{B}(\rho)Z(\rho)\right), \\
\Xi(1,2)(\rho) &= \xi(\tilde{A}(\rho)Y(\rho) + B(\rho)Z(\rho)) - Y(\rho)^\top\hat{A}(\rho)^\top - Z(\rho)^\top B(\rho)^\top, \\
\Xi(1,3)(\rho) &= Y(\rho)^\top C_z(\rho)^\top + Z(\rho)^\top D(\rho)^\top \\
\Xi(2,2)(\rho) &= -W(\rho) - \xi\mathrm{He}\left(\hat{A}(\rho)Y(\rho) + B(\rho)Z(\rho)\right),
\end{aligned}$$

with $\hat{A}(\rho)$, $\tilde{A}(\rho)$, $\bar{B}(\rho)$ and $\bar{V}(\rho)$ given in (3.3)-(3.6), hold for all $\rho \in \Theta$ and $\dot{\rho} \in \Gamma$, then

$K(\rho(t)) = Z(\rho)Y(\rho)^{-1}$ is a robustly stabilizing parameter-dependent state-feedback gain and $\sqrt{\mu}$ is an $\mathcal{H}_2$ guaranteed cost for the system (3.1) *in closed-loop, that is, $\|G\|_2 < \sqrt{\mu}$.*

Proof. First, we show that ξ can be constrained to the range $(-1, 1)$ without loss of generality. To see this, multiply (3.16) on the left by $\mathcal{B}_\perp^\top$ and on the right by $\mathcal{B}_\perp$, where

$$\mathcal{B}_\perp = \begin{bmatrix} \xi I & 0 & 0 \\ -I & 0 & 0 \\ 0 & I & 0 \\ 0 & 0 & I \end{bmatrix}, \tag{3.17}$$

yielding

$$\begin{bmatrix} (\xi^2 - 1)W(\rho) & 0 & (\xi + 1)\bar{V}(\rho) \\ 0 & -I & 0 \\ (\xi + 1)\bar{V}(\rho)^\top & 0 & -X(\rho) - X(\rho)^\top \end{bmatrix} < 0, \tag{3.18}$$

which is feasible only if $(\xi^2 - 1)W(\rho)$ is negative definite. As $W(\rho)$ is positive definite, then it is necessary that $-1 < \xi < 1$.

Multiplying (3.16) on the left by $\mathcal{A}_\perp^\top$ and on the right by $\mathcal{A}_\perp$, with

$$\mathcal{A}_\perp = \begin{bmatrix} \hat{A}(\rho)^\top + K(\rho)^\top B(\rho)^\top & C_z(\rho)^\top + K(\rho)^\top D(\rho)^\top & 0 \\ \tilde{A}(\rho)^\top + K(\rho)^\top B(\rho)^\top & C_z(\rho)^\top + K(\rho)^\top D(\rho)^\top & 0 \\ 0 & I & 0 \\ 0 & 0 & I \end{bmatrix},$$

and considering the change of variable $Z(\rho) = K(\rho)Y(\rho)$, results in

$$\begin{bmatrix} \hat{A}_{cl}(\rho)W(\rho)\hat{A}_{cl}(\rho)^\top - \tilde{A}_{cl}(\rho)W(\rho)\tilde{A}_{cl}(\rho)^\top & \star & \star \\ \bar{C}_{cl}(\rho)W(\rho)(\hat{A}_{cl}(\rho) - \tilde{A}_{cl}(\rho))^\top & -I & \star \\ \bar{V}(\rho)^\top(\hat{A}_{cl}(\rho) - \tilde{A}_{cl}(\rho))^\top & 0 & -\mathrm{He}(X(\rho)) \end{bmatrix} < 0,$$

where $\hat{A}_{cl}(\rho)$ and $\tilde{A}_{cl}(\rho)$ are given in (3.8) and (3.9), respectively, and $\bar{C}_{cl}(\rho) = \epsilon C_{cl}(\rho)$.

Using the definitions given in (3.3)-(3.6), the previous inequality can be rewritten in

the form

$$\begin{bmatrix} W(\rho)A_{cl}(\rho)^\top + A_{cl}(\rho)W(\rho) & W(\rho)C_{cl}(\rho)^\top & -\dot{W}(\rho) + \frac{1}{2}X(\rho) \\ C_{cl}(\rho)W(\rho) & -I & 0 \\ -\dot{W}(\rho) + \frac{1}{2}X(\rho)^\top & 0 & -X(\rho) - X(\rho)^\top \end{bmatrix} < 0,$$

where $A_{cl}(\rho) = A(\rho) + B(\rho)K(\rho)$ and $C_{cl}(\rho) = C_z(\rho) + D(\rho)K(\rho)$.

Finally, multiplying the last inequality on the left by $\mathcal{C}_\perp^\top$ and on the right by $\mathcal{C}_\perp$, with

$$\mathcal{C}_\perp = \begin{bmatrix} I & 0 \\ 0 & I \\ \frac{1}{2}I & 0 \end{bmatrix}, \tag{3.19}$$

provides

$$\begin{bmatrix} W(\rho)A_{cl}(\rho)^\top + A_{cl}(\rho)W(\rho) - \dot{W}(\rho) & W(\rho)C_{cl}(\rho)^\top \\ C_{cl}(\rho)W(\rho) & -I \end{bmatrix} < 0. \tag{3.20}$$

Conditions (3.20), (3.14) and (3.15) are precisely the ones given in Lemma 1, assuring that $K(\rho) = Z(\rho)Y(\rho)^{-1}$ is a stabilizing gain and $\sqrt{\mu}$ is an $\mathcal{H}_2$ guaranteed cost for the closed-loop system. The proof of the invertibility of $Y(\rho)$ is similar to the one presented for Theorem 1. □

A controller $K(\rho(t))$ designed using the conditions of Theorem 2 is identified throughout this work as an $\mathcal{H}_2$ gain-scheduled state-feedback controller. In the next chapter, some simulations and practical results obtained using this technique are presented.

3.1.3 $\mathcal{H}_\infty$ control

Considering the system G given in (3.1) is asymptotically stable, the $\mathcal{H}_\infty$ norm of the system is defined as (also known as the $\mathcal{L}_2$ gain of the system)

$$\|G\|_\infty = \sup_{w \neq 0} \frac{\|z\|_2}{\|w\|_2}.$$

This performance criterion assures an attenuation level for the output z when finite energy disturbances are applied in the input $w(t)$. Moreover, an upper bound for this performance level can be computed using LMIs.

As extension of Theorem 1 to deal with the $\mathcal{H}_\infty$ norm as performance criterion is also

possible, as shown in the next theorem.

Theorem 3. *Let $\xi \in (-1,1)$ and $\epsilon \neq 0$ be given scalars. If there exist matrices $W(\rho) = W(\rho)^\top > 0$, $Y(\rho)$, $X(\rho)$, $Z(\rho)$ and a scalar $\gamma > 0$ such that the following parameter-dependent LMI*

$$\begin{bmatrix} \Xi(1,1) & \Xi(1,2) & \epsilon B_w(\rho) & \Xi(1,4) & \bar{V}(\rho) \\ \star & \Xi(2,2) & -\epsilon B_w(\rho) & \xi\Xi(1,4) & -\bar{V}(\rho) \\ \star & \star & -I & D_w(\rho)^\top & 0 \\ \star & \star & \star & -\gamma I & 0 \\ \star & \star & \star & \star & -\mathrm{He}(X(\rho)) \end{bmatrix} < 0, \tag{3.21}$$

holds for all $(\rho, \dot{\rho}) \in \Theta \times \Gamma$, where

$$\begin{aligned} \Xi(1,1)(\rho) &= W(\rho) + \mathrm{He}(\tilde{A}(\rho)Y(\rho) + \bar{B}(\rho)Z(\rho)), \\ \Xi(1,2)(\rho) &= \xi(\tilde{A}(\rho)Y(\rho) + \bar{B}(\rho)Z(\rho)) - Y(\rho)^\top \hat{A}(\rho)^\top - Z(\rho)^\top \bar{B}(\rho)^\top, \\ \Xi(2,2)(\rho) &= -W(\rho) - \xi\mathrm{He}(\hat{A}(\rho)Y(\rho) + \bar{B}(\rho)Z(\rho)), \\ \Xi(1,4)(\rho) &= Y(\rho)^\top C_z(\rho)^\top + Z(\rho)^\top D(\rho)^\top, \end{aligned}$$

with $\hat{A}(\rho)$, $\tilde{A}(\rho)$, $\bar{B}(\rho)$ and $\bar{V}(\rho)$ given in (3.3)-(3.6)*, then $K(\rho) = Z(\rho)Y(\rho)^{-1}$ is an $\mathcal{H}_\infty$ gain-scheduled state-feedback controller that stabilizes the system with an $\mathcal{H}_\infty$ guaranteed cost given by $\sqrt{\gamma}$.*

Proof. First, it is shown that ξ is contained in a limited interval. For this, multiplying (3.21) on the left by $B_\perp^\top$ and on the right by $B_\perp$, with

$$\mathcal{B}_\perp = \begin{bmatrix} \xi I & 0 & 0 & 0 \\ -I & 0 & 0 & 0 \\ 0 & I & 0 & 0 \\ 0 & 0 & I & 0 \\ 0 & 0 & 0 & I \end{bmatrix},$$

results in

$$\begin{bmatrix} (\xi^2 - 1)W(\rho) & (\xi+1)\epsilon B_w(\rho) & 0 & (\xi+1)\bar{V}(\rho) \\ \star & -I & D_w(\rho)^\top & 0 \\ \star & \star & -\gamma I & 0 \\ \star & \star & \star & -X(\rho) - X(\rho)^\top \end{bmatrix} < 0. \tag{3.22}$$

As $W(\rho)$ is positive definite, it is clear that (3.22) has a solution only if

$$-1 < \xi < 1. \tag{3.23}$$

To show the invertibility of $Y(\rho)$, note that the feasibility of (3.21) ensures that

$$\begin{bmatrix} \Xi(1,1)(\rho) & \Xi(1,2)(\rho) \\ \star & \Xi(2,2)(\rho) \end{bmatrix} < 0,$$

which, multiplied on the left by $T = \begin{bmatrix} I & I \end{bmatrix}$ and on the right by $T^\top$, provides

$$-\left(\frac{1}{\epsilon}\right)(1+\xi)(Y(\rho)+Y(\rho)^\top) < 0,$$

that assures that $Y(\rho)$ is full rank since $\xi \in (-1,1)$.

Next, considering the change of variable $Z(\rho) = K(\rho)Y(\rho)$ and multiplying (3.21) by $\mathcal{A}_\perp^\top$ on the left and by $\mathcal{A}_\perp$ on the right, where

$$\mathcal{A}_\perp = \begin{bmatrix} \hat{A}(\rho)^\top + K(\rho)^\top \bar{B}(\rho)^\top & 0 & \xi(C_z(\rho)^\top + K(\rho)^\top D(\rho)^\top) & 0 \\ \tilde{A}(\rho)^\top + K(\rho)^\top \bar{B}(\rho)^\top & 0 & \xi(C_z(\rho)^\top + K(\rho)^\top D(\rho)^\top) & 0 \\ 0 & I & 0 & 0 \\ 0 & 0 & I & 0 \\ 0 & 0 & 0 & I \end{bmatrix},$$

one has

$$\begin{bmatrix} \hat{A}_{cl}(\rho)W(\rho)\hat{A}_{cl}(\rho)^\top - \tilde{A}_{cl}(\rho)W(\rho)\tilde{A}_{cl}(\rho)^\top & \star & \star & \star \\ \bar{B}_w(\rho)(\hat{A}_{cl}(\rho) - \tilde{A}_{cl}(\rho))^\top & -I & \star & \star \\ \bar{C}_{cl}(\rho)W(\rho)(\hat{A}_{cl}(\rho) - \tilde{A}_{cl}(\rho))^\top & D_w(\rho) & -\gamma I & \star \\ \bar{V}(\rho)^\top(\hat{A}_{cl}(\rho) - \tilde{A}_{cl}(\rho))^\top & 0 & 0 & -\mathrm{He}(X(\rho)) \end{bmatrix} < 0, \tag{3.24}$$

where $\hat{A}_{cl}(\rho)$ and $\tilde{A}_{cl}(\rho)$ are given in (3.8) and (3.9), respectively, and $\bar{C}_{cl}(\rho) = \epsilon C_{cl}(\rho)$. By substituting the expressions given in (3.3)-(3.6), it is possible to rewrite (3.24) as

$$\begin{bmatrix} \mathrm{He}(A_{cl}(\rho)W(\rho)) & B_w(\rho) & W(\rho)C_{cl}(\rho)^\top & -\dot{W}(\rho) + \frac{1}{2}X(\rho) \\ \star & -I & D_w(\rho)^\top & 0 \\ \star & \star & -\gamma I & 0 \\ \star & \star & \star & -\mathrm{He}(X(\rho)) \end{bmatrix} < 0, \tag{3.25}$$

where $A_{cl}(\rho) = A(\rho) + B(\rho)K(\rho)$ and $C_{cl}(\rho) = C_z(\rho) + D(\rho)K(\rho)$.

Finally, the inequality in (3.25) is pre- and post-multiplied by $\mathcal{C}_\perp^\top$ and $\mathcal{C}_\perp$, respectively, where

$$\mathcal{C}_\perp = \begin{bmatrix} I & 0 \\ 0 & I \\ \frac{1}{2}I & 0 \end{bmatrix},$$

yielding

$$\begin{bmatrix} W(\rho)A_{cl}(\rho)^\top + A_{cl}(\rho)W(\rho) - \dot{W}(\rho) & B_w(\rho) & W(\rho)C_{cl}(\rho)^\top \\ \star & -I & D_w(\rho)^\top \\ \star & \star & -\gamma I \end{bmatrix} < 0, \tag{3.26}$$

which can be recognized as the *bounded real lemma* for continuous-time LPV systems (WU et al., 1996). As a consequence, Theorem 3 guarantees that $K(\rho(t))$ is a stabilizing gain-scheduled state-feedback gain and $\sqrt{\gamma}$ is an $\mathcal{H}_\infty$ guaranteed cost for the closed-loop system. □

As a final comment regarding the proposed $\mathcal{H}_2$ and $\mathcal{H}_2$ control techniques, note that the design of parameter-independent controllers can be immediately obtained by fixing the variables $Z(\rho) = Z$ and $Y(\rho) = Y$ in both Theorems 2 and 3.

3.2 Output-feedback control

This section addresses the more challenging problem of output-feedback control. The strategy relies on using a given state-feedback controller as a starting point to design both static and dynamic output-feedback controllers. Next section presents the static case, whereas the dynamic case is given in Section 3.3.

3.2.1 $\mathcal{H}_2$ static output-feedback

Consider the gain-scheduled static output-feedback control law

$$u(t) = L(\rho)y(t)$$

where $L(\rho)$ is a design variable. Applying this feedback control law in system (3.1) with $D_w(\rho) = D_{wy}(\rho) = 0$ provides the following closed-loop dynamics

$$\begin{aligned} \dot{x} &= (A(\rho) + B(\rho)L(\rho)C(\rho))x + B_w(\rho)w \\ z &= (C_z(\rho) + D(\rho)L(\rho)C(\rho))x. \end{aligned} \tag{3.27}$$

The next theorem presents conditions to compute $L(\rho)$ once a stabilizing state-feedback gain $K(\rho)$ is available.

Theorem 4. *Let $\xi \in (-1, 1)$ and $\epsilon \neq 0$ be given scalars, and $K(\rho)$ a given stabilizing state-feedback gain. If there exist parameter-dependent matrices $W(\rho) = W(\rho)^\top$, $M(\rho) = M(\rho)^\top$, $Y(\rho)$, $X(\rho)$, $H(\rho)$ and $J(\rho)$, and a scalar $\mu > 0$ such that the following parameter-dependent LMIs*

$$\mu > \mathrm{Tr}(H(\rho)),$$

$$\begin{bmatrix} M(\rho) & B_w(\rho)^\top W(\rho) \\ \star & W(\rho) \end{bmatrix} > 0, \tag{3.28}$$

$$\begin{bmatrix} \Xi(1,1)(\rho) & \Xi(1,2)(\rho) & \bar{C}_z(\rho)^\top + K(\rho)^\top \bar{D}(\rho)^\top & \bar{V}(\rho) & \Xi(1,5)(\rho) \\ \star & \Xi(2,2)(\rho) & -\bar{C}_z(\rho)^\top - K(\rho)^\top \bar{D}(\rho)^\top & -\bar{V}(\rho) & \Xi(2,5)(\rho) \\ \star & \star & -I & 0 & \bar{D}(\rho) \\ \star & \star & \star & -\mathrm{He}(X(\rho)) & 0 \\ \star & \star & \star & \star & -\mathrm{He}(H(\rho)) \end{bmatrix} < 0, \tag{3.29}$$

where

$$\begin{aligned} \Xi(1,1)(\rho) &= W(\rho) + \mathrm{He}\left(Y(\rho)^\top(\tilde{A}(\rho) + \bar{B}(\rho)K(\rho))\right), \\ \Xi(1,2)(\rho) &= \xi(\tilde{A}(\rho)^\top + K(\rho)^\top \bar{B}(\rho)^\top)Y(\rho) - Y(\rho)^\top(\hat{A}(\rho) + \bar{B}(\rho)K(\rho)), \\ \Xi(1,5)(\rho) &= Y(\rho)^\top \bar{B}(\rho) + C(\rho)^\top J(\rho)^\top - K(\rho)^\top H(\rho)^\top, \\ \Xi(2,2)(\rho) &= -W(\rho) - \xi\mathrm{He}\left(\hat{A}(\rho)Y(\rho) + B(\rho)Z(\rho)\right), \\ \Xi(2,5)(\rho) &= \xi Y(\rho)^\top \bar{B}(\rho) - C(\rho)^\top J(\rho)^\top + K(\rho)^\top H(\rho)^\top, \\ \bar{C}_z(\rho) &= \epsilon C_z(\rho), \\ \bar{D}(\rho) &= \epsilon D(\rho), \end{aligned}$$

with $\hat{A}(\rho)$, $\tilde{A}(\rho)$, $\bar{B}(\rho)$ and $\bar{V}(\rho)$ given in (3.3)-(3.6)*, hold for all $\rho \in \Theta$ and $\dot{\rho} \in \Gamma$, then $L(\rho) = H(\rho)^{-1}J(\rho)$ is a robustly stabilizing parameter-dependent static output-feedback*

gain and $\sqrt{\mu}$ is an $\mathcal{H}_2$ guaranteed cost for the system (3.27).

Proof. The proof that $H(\rho)$ is invertible is trivial, because as $\mathrm{He}(H(\rho))$ appears at the diagonal of (3.29), we have that $H(\rho)$ is nonsingular.

Considering the change of variable $J(\rho) = H(\rho)L(\rho)$ and multiplying (3.29) on the left by $V_\perp^\top$ and on the right by $V_\perp$, where

$$V_\perp = \begin{bmatrix} I & 0 & 0 & 0 \\ 0 & I & 0 & 0 \\ 0 & 0 & I & 0 \\ 0 & 0 & 0 & I \\ L(\rho)C(\rho) - K(\rho) & -L(\rho)C(\rho) + K(\rho) & 0 & 0 \end{bmatrix},$$

results in

$$\begin{bmatrix} W(\rho) + \mathrm{He}(Y(\rho)^\top \tilde{A}_{cl}(\rho)) & \xi \tilde{A}_{cl}(\rho)^\top Y(\rho) - Y(\rho)^\top \hat{A}_{cl}(\rho) & \bar{C}_{cl}(\rho)^\top & \bar{V}(\rho) \\ \star & -W(\rho) - \xi \mathrm{He}(Y(\rho)^\top \hat{A}_{cl}(\rho)) & -\bar{C}_{cl}(\rho)^\top & -\bar{V}(\rho) \\ \star & \star & -I & 0 \\ \star & \star & \star & -\mathrm{He}(X(\rho)) \end{bmatrix} < 0, \tag{3.30}$$

where $\tilde{A}_{cl}(\rho) = \tilde{A}(\rho) + \bar{B}(\rho)L(\rho)C(\rho)$, $\hat{A}_{cl}(\rho) = \hat{A}(\rho) + \bar{B}(\rho)L(\rho)C(\rho)$ and $\bar{C}_{cl}(\rho) = \bar{C}_z(\rho) + D(\rho)L(\rho)$.

Multiplying (3.30) by $\mathcal{A}_\perp^\top$ on the left and by $\mathcal{A}_\perp$ on the right, where

$$\mathcal{A} = \begin{bmatrix} \hat{A}_{cl}(\rho) & 0 & 0 \\ \tilde{A}_{cl}(\rho) & 0 & 0 \\ 0 & I & 0 \\ 0 & 0 & I \end{bmatrix},$$

results in

$$\begin{bmatrix} \hat{A}_{cl}(\rho)^\top W(\rho) \hat{A}_{cl}(\rho) - \tilde{A}_{cl}(\rho)^\top W(\rho) \tilde{A}_{cl}(\rho) & \star & \star \\ \bar{C}_{cl}(\rho)(\hat{A}_{cl}(\rho) - \tilde{A}_{cl}(\rho)) & -I & \star \\ \bar{V}(\rho)^\top (\hat{A}_{cl}(\rho) - \tilde{A}_{cl}(\rho)) & 0 & -\mathrm{He}(X(\rho)) \end{bmatrix} < 0,$$

that, applying the definitions given in (3.3)-(3.6), provides

$$\begin{bmatrix} A_{cl}(\rho)^\top W(\rho) + W(\rho)A_{cl}(\rho) & C_{cl}(\rho)^\top & -\dot{W}(\rho) + \frac{1}{2}X(\rho) \\ \star & -I & 0 \\ \star & \star & -\mathrm{He}(X(\rho)) \end{bmatrix} < 0.$$

Next, multiplying last inequality on the left by $C_\perp^\top$ and on the right by $C_\perp$, with $C_\perp$ given in (3.19), one has

$$\begin{bmatrix} A_{cl}(\rho)^\top W(\rho) + W(\rho)A_{cl}(\rho) + \dot{W}(\rho) & C_{cl}(\rho)^\top \\ \star & -I \end{bmatrix} < 0.$$

Consider the following congruence transformation

$$\begin{bmatrix} W(\rho)^{-1} & 0 \\ 0 & I \end{bmatrix} \begin{bmatrix} A_{cl}(\rho)^\top W(\rho) + W(\rho)A_{cl}(\rho)^\top + \dot{W}(\rho) & C_{cl}(\rho)^\top \\ \star & -I \end{bmatrix} \begin{bmatrix} W(\rho)^{-1} & 0 \\ 0 & I \end{bmatrix} < 0 \Rightarrow$$
$$\begin{bmatrix} W(\rho)^{-1}A_{cl}^\top(\rho) + A_{cl}(\rho)W(\rho)^{-1} + W(\rho)^{-1}\dot{W}(\rho)W(\rho)^{-1} & W(\rho)^{-1}C_{cl}(\rho)^\top \\ \star & -I \end{bmatrix} < 0.$$

Taking the time-derivative of the relation $W(\rho)W(\rho)^{-1} = I$ on both sides, yields

$$\dot{W}(\rho)W(\rho)^{-1} + W(\rho)\dot{W}(\rho)^{-1} = 0 \Rightarrow W(\rho)^{-1}\dot{W}(\rho)W(\rho)^{-1} = -\dot{W}(\rho)^{-1}$$

. Using this relation in the previous inequality, provides

$$\begin{bmatrix} W(\rho)^{-1}A_{cl}(\rho)^\top + A_{cl}(\rho)W(\rho)^{-1} - \dot{W}(\rho)^{-1} & W(\rho)^{-1}C_{cl}(\rho)^\top \\ \star & -I \end{bmatrix} < 0.$$

Adopting the changing $W(\rho)^{-1} = P(\rho)$, one has

$$\begin{bmatrix} P(\rho)A_{cl}(\rho)^\top + A_{cl}(\rho)P(\rho) - \dot{P}(\rho) & P(\rho)C_{cl}(\rho)^\top \\ \star & -I \end{bmatrix} < 0. \tag{3.31}$$

Next, applying the congruence transformation on (3.28)

$$\begin{bmatrix} I & 0 \\ 0 & W(\rho)^{-1} \end{bmatrix} \begin{bmatrix} H(\rho) & B_w(\rho)^\top W(\rho) \\ \star & W(\rho) \end{bmatrix} \begin{bmatrix} I & 0 \\ 0 & W(\rho)^{-1} \end{bmatrix} > 0,$$

one has

$$\begin{bmatrix} H(\rho) & B_w(\rho)^\top \\ \star & W(\rho)^{-1} \end{bmatrix} = \begin{bmatrix} H(\rho) & B_w(\rho)^\top \\ \star & P(\rho) \end{bmatrix} > 0. \tag{3.32}$$

Conditions $\mu > H(\rho)$, (3.31) and (3.32) are equivalent to the ones of Lemma 1 (with $W(\rho) = P(\rho)^{-1}$).

The proof that $-1 < \xi < 1$ is similar to the one given in the proof of Theorem 2. □

The synthesis conditions of Theorem 4 belong to the class of techniques from the literature known as *two-stage methods* (PEAUCELLE; ARZELIER, 2001; ARZELIER; PEAUCELLE; SALHI, 2003; MOREIRA; OLIVEIRA; PERES, 2011; AGULHARI; OLIVEIRA; PERES, 2012), since the approach requires the design of a state-feedback gain as a preliminary step. For instance, any state-feedback gain designed with Theorem 1, 2 or 3 can be used.

Note that Theorem 4 can also be used to design a gain-scheduled state-feedback controller simply considering $C(\rho) = I$. In this case Theorem 4 can be seen as an alternative design condition to Theorem 2 (whenever a stabilizing state-feedback gain is available).

3.3 Dynamic output feedback control

The problems $\mathcal{H}_2$ and $\mathcal{H}_\infty$ full-order dynamic control are investigated in this section. As in the case of static controllers, the strategy proposed to design full-order dynamic controllers also starts from a stabilizing state-feedback gain. However, to role of this gain is slightly different, being used as one of the gains of the dynamic controller. Moreover, differently from the case of static output-feedback control synthesis, the input state-feedback gain is considered in the form $K(\rho) = Z(\rho)Y(\rho)^{-1}$, which is the structure provided by the synthesis conditions of Theorems 1, 2 and 3. This approach was proposed in (DE OLIVEIRA; GEROMEL; BERNUSSOU, 2000) to discrete-time systems and here it is extended to cope with continuous-time LPV (or quasi-LPV) systems.

Next section investigates the problem of $\mathcal{H}_2$ full-order gain-scheduled dynamic output-feedback, requiring as input parameter a stabilizing state-feedback gain.

3.3.1 $\mathcal{H}_2$ dynamic output-feedback

The aim is to design the full-order dynamic output-feedback controller

$$\begin{aligned} \dot{x}_c &= A_c(\rho)x_c + B_c(\rho)y, \\ u &= C_c(\rho)x_c. \end{aligned} \tag{3.33}$$

where $x_c \in \mathbb{R}^n$ is the vector of states of the controller and $A_c(\rho)$, $B_c(\rho)$ and $C_c(\rho)$ are parameter-dependent gains to be designed. Connecting the controller (3.33) with the plant given in (3.1), one has the closed-loop system

$$\begin{aligned}
\begin{bmatrix} \dot{x} \\ \dot{x}_c \end{bmatrix} &= \underbrace{\begin{bmatrix} A(\rho) & B(\rho)C_c(\rho) \\ B_c(\rho)C(\rho) & A_c(\rho) \end{bmatrix}}_{A_{cl}(\rho)} \begin{bmatrix} x \\ x_c \end{bmatrix} + \underbrace{\begin{bmatrix} B_w(\rho) \\ B_c(\rho)D_{wy}(\rho) \end{bmatrix}}_{B_{cl}(\rho)} w, \\
z &= \underbrace{\begin{bmatrix} C_z(\rho) & D(\rho)C_c(\rho) \end{bmatrix}}_{C_{cl}(\rho)} \begin{bmatrix} x \\ x_c \end{bmatrix}.
\end{aligned} \tag{3.34}$$

Next theorem presents a sufficient condition to compute an $\mathcal{H}_2$ full-order dynamic output-feedback controller.

Theorem 5. *Let $\xi \in (-1, 1)$ and $\epsilon \neq 0$ be given scalars, and $Z(\rho)$ and $G(\rho)$ matrices such that $K(\rho) = Z(\rho)G(\rho)^{-1}$ is a state-feedback stabilizing gain. If there exist parameter-dependent matrices $R(\rho) = R(\rho)^\top$, $M(\rho) = M(\rho)^\top$, $X(\rho)$, $P(\rho)$, $Q(\rho)$, Y_1, V_1 and V_3, and a scalar $\mu > 0$ such that the following parameter-dependent LMIs*

$$\begin{gathered}
\mu > \mathrm{Tr}(H(\rho)) \\
\begin{bmatrix} M(\rho) & B_{\mathcal{T}2}(\rho)^\top \\ \star & R(\rho) \end{bmatrix} > 0,
\end{gathered} \tag{3.35}$$

$$\begin{bmatrix}
G_c(\rho)^\top R(\rho) G_c(\rho) + \mathrm{He}(\tilde{\mathcal{A}}_{\mathcal{T}}(\rho)) & \xi\tilde{\mathcal{A}}_{\mathcal{T}}(\rho) - \hat{\mathcal{A}}_{\mathcal{T}}(\rho)^\top & C_{\mathcal{T}}(\rho) & \mathcal{V}_{\mathcal{T}}(\rho) \\
\star & -G_c(\rho)^\top R(\rho) G_c(\rho) - \mathrm{He}(\hat{\mathcal{A}}_{\mathcal{T}}(\rho)) & \xi C_{\mathcal{T}}(\rho) & -\mathcal{V}_{\mathcal{T}}(\rho) \\
\star & \star & -I & 0 \\
\star & \star & \star & -\mathrm{He}(X(\rho))
\end{bmatrix} < 0, \tag{3.36}$$

where

$$\begin{aligned}
G_c(\rho) &= \begin{bmatrix} G(\rho) & 0 \\ 0 & I \end{bmatrix}, \\
J(\rho) &= \begin{bmatrix} Y_1 & Y_1 \\ V_1 + V_3 & I \end{bmatrix}, \\
\tilde{\mathcal{A}}_{\mathcal{T}}(\rho) &= \epsilon \begin{bmatrix} \Xi(\rho)_1 & G(\rho)^\top Y_1 A(\rho) \\ \Xi(\rho)_2 & V_1(A(\rho) + Q(\rho)C(\rho) \end{bmatrix} - \frac{1}{2\epsilon} G_c(\rho)^\top J(\rho) G_c(\rho), \\
\hat{\mathcal{A}}_{\mathcal{T}}(\rho) &= \epsilon \begin{bmatrix} \Xi(\rho)_1 & G(\rho)^\top Y_1 A(\rho) \\ \Xi(\rho)_2 & V_1(A(\rho) + Q(\rho)C(\rho) \end{bmatrix} + \frac{1}{2\epsilon} G_c(\rho)^\top J(\rho) G_c(\rho),
\end{aligned}$$

$$
\begin{aligned}
\Xi(\rho)_1 &= G(\rho)^\top Y_1(A(\rho)G(\rho)+B(\rho)Z(\rho)),\\
\Xi(\rho)_2 &= V_1(A(\rho)G(\rho)+B(\rho)Z(\rho))+Q(\rho)C(\rho)G(\rho)+P(\rho)G(\rho),\\
B_{\mathcal{T}2}(\rho) &= \begin{bmatrix} Y_1B_w(\rho) \\ V_1B_w(\rho)+Q(\rho)D_{wy}(\rho)\end{bmatrix},\\
C_{\mathcal{T}}(\rho) &= \begin{bmatrix} C_z(\rho)G(\rho)+D(\rho)Z(\rho) & C_z(\rho)\end{bmatrix},\\
\mathcal{V}_{\mathcal{T}} &= \epsilon G_c(\rho)^\top \dot{R}(\rho)+\frac{\epsilon}{2}G_c(\rho)^\top X,
\end{aligned}
$$

hold for all $\rho \in \Theta$ *and* $\dot{\rho} \in \Gamma$*, then* $A_c(\rho) = V_3^{-1}P(\rho)$*,* $B_c(\rho) = V_3^{-1}Q(\rho)$ *and* $C_c(\rho) = Z(\rho)G(\rho)^{-1}$ *are parameter-dependent matrices of the controller* (3.33) *and* $\sqrt{\mu}$ *is an* $\mathcal{H}_2$ *guaranteed cost for the system* (3.34)*.*

Proof. Initially, it is defined the following structures for the slack variable matrix Y and its inverse

$$
Y = \begin{bmatrix} Y_1^{-1^\top} & Y_3 \\ Y_1^{-1^\top} & Y_4 \end{bmatrix} \text{ and } Y^{-1} = \begin{bmatrix} V_1^\top & V_2^\top \\ V_3^\top & V_4^\top \end{bmatrix}. \tag{3.37}
$$

Next, defining

$$
\begin{aligned}
T &= \begin{bmatrix} Y_1^\top & V_1^\top \\ 0 & V_3^\top \end{bmatrix},\\
R(\rho) &= T^\top W(\rho) T,
\end{aligned} \tag{3.38}
$$

the condition (3.35) can be rewritten as

$$
\begin{bmatrix} I & 0 \\ 0 & T^\top \end{bmatrix} \begin{bmatrix} M(\rho) & B_{cl}(\rho)^\top \\ B_{cl}(\rho) & W(\rho) \end{bmatrix} \begin{bmatrix} I & 0 \\ 0 & T \end{bmatrix} < 0.
$$

As a consequence, if the condition (3.35) is feasible, then

$$
\begin{bmatrix} M(\rho) & B_{cl}(\rho)^\top \\ B_{cl}(\rho) & W(\rho) \end{bmatrix} < 0,
$$

assuring that (3.12) holds.

Defining now the matrix

$$\bar{T}(\rho) = \begin{bmatrix} TG_c(\rho) & 0 & 0 & 0 \\ 0 & TG_c(\rho) & 0 & 0 \\ 0 & 0 & I & 0 \\ 0 & 0 & 0 & T \end{bmatrix},$$

and considering the change of variables $P(\rho) = V_3 A_c(\rho)$ and $Q(\rho) = V_3 B_c(\rho)$, condition (3.36) can be rewritten as $\bar{T}(\rho)\Phi(\rho)\bar{T}(\rho) < 0$ with

$$\Phi(\rho) = \begin{bmatrix} W(\rho) + \mathrm{He}(\tilde{A}_{cl}(\rho)Y) & \xi\tilde{A}_{cl}(\rho)Y - Y^\top \hat{A}_{cl}(\rho)^\top & Y^\top C_{cl}(\rho)^\top & \bar{V}(\rho) \\ \star & -W(\rho) - \mathrm{He}(\hat{A}_{cl}(\rho)Y) & \xi Y^\top C_{cl}(\rho)^\top & -\bar{V}(\rho) \\ \star & \star & -I & 0 \\ \star & \star & \star & -\mathrm{He}(X(\rho)) \end{bmatrix},$$

where

$$\hat{A}_{cl}(\rho) = \epsilon A_{cl}(\rho) + \frac{1}{2\epsilon} I, \tag{3.39}$$

$$\tilde{A}_{cl}(\rho) = \epsilon A_{cl}(\rho) - \frac{1}{2\epsilon} I, \tag{3.40}$$

and matrices $A_{cl}(\rho)$ e $C_{cl}(\rho)$ are presented in (3.34).

As a consequence, the feasibility of (3.36) implies that $\Phi(\rho) < 0$. The proof that $\Phi(\rho) < 0$ implies (3.13) and $-1 < \xi < 1$ follows the same steps presented in the proof of Theorem 2, concluding the demonstration. □

An important comment about Theorem 5 is the consideration of the slack variable Y as ρ-independent. This constraint, although conservative, is important in order to treat the term $\dot{W}(\rho)$, which would be more involved to deal in the case of $Y(\rho)$.

As a general comment about the proposed condition, note that the controller matrix $C_c(\rho)$ is fixed as the given stabilizing state-feedback gain. Clearly, different stabilizing gains will provide distinct results.

3.3.2 $\mathcal{H}_\infty$ dynamic output-feedback

Considering system (3.1) fed back by the full-order dynamic output-feedback controller given in (3.33), one has the closed-loop system

$$\begin{aligned}\begin{bmatrix}\dot{x}\\ \dot{x}_c\end{bmatrix} &= \begin{bmatrix}A(\rho) & B(\rho)C_c(\rho)\\ B_c(\rho)C(\rho) & A_c(\rho)\end{bmatrix}\begin{bmatrix}x\\ x_c\end{bmatrix}+\begin{bmatrix}B_w(\rho)\\ B_c(\rho)D_{wy}(\rho)\end{bmatrix}w,\\ z &= \begin{bmatrix}C_z(\rho) & D(\rho)C_c(\rho)\end{bmatrix}\begin{bmatrix}x\\ x_c\end{bmatrix}+D_w(\rho)w.\end{aligned} \tag{3.41}$$

The next theorem presents a sufficient condition to compute the full-order dynamic output-feedback controller (3.33) considering the $\mathcal{H}_\infty$ norm as performance criterion. As in the $\mathcal{H}_2$ case, a stabilizing state-feedback gain is required as input data.

Theorem 6. *Let $\xi \in (-1,1)$ and $\epsilon \neq 0$ be given scalars, and $Z(\rho)$ and $G(\rho)$ matrices such that $K(\rho) = Z(\rho)G(\rho)^{-1}$ is a stabilizing state-feedback controller. If there exist parameter-dependent matrices $R(\rho) = R(\rho)^\top$, $X(\rho)$, $P(\rho)$, $Q(\rho)$, Y_1, V_1 and V_3, and a scalar $\gamma > 0$ such that the following parameter-dependent LMI*

$$\begin{bmatrix}\Xi(1,1)(\rho) & \xi\tilde{\mathcal{A}}_{\mathcal{T}}(\rho)-\hat{\mathcal{A}}_{\mathcal{T}}(\rho)^\top & B_{\mathcal{T}}(\rho) & C_{\mathcal{T}}(\rho)^\top & \mathcal{V}_{\mathcal{T}}(\rho)\\ \star & \Xi(2,2)(\rho) & -B_{\mathcal{T}}(\rho) & \xi C_{\mathcal{T}}(\rho)^\top & -\mathcal{V}_{\mathcal{T}}(\rho)\\ \star & \star & -\gamma I & D_w(\rho)^\top & 0\\ \star & \star & \star & \star & -\mathrm{He}(X(\rho))\end{bmatrix} < 0, \tag{3.42}$$

where

$$\begin{aligned}\Xi(1,1)(\rho) &= G_c(\rho)^\top R(\rho)G_c(\rho)+\mathrm{He}(\tilde{\mathcal{A}}_{\mathcal{T}}(\rho)),\\ \Xi(2,2)(\rho) &= -G_c(\rho)^\top R(\rho)G_c(\rho)-\mathrm{He}(\hat{\mathcal{A}}_{\mathcal{T}}(\rho)),\\ G_c(\rho) &= \begin{bmatrix}G(\rho) & 0\\ 0 & I\end{bmatrix},\\ J(\rho) &= \begin{bmatrix}Y_1 & Y_1\\ V_1+V_3 & I\end{bmatrix},\\ \tilde{\mathcal{A}}_{\mathcal{T}}(\rho) &= \epsilon\begin{bmatrix}\Xi(\rho)_1 & G(\rho)^\top Y_1 A(\rho)\\ \Xi(\rho)_2 & V_1(A(\rho)+Q(\rho)C(\rho)\end{bmatrix}-\frac{1}{2\epsilon}G_c(\rho)^\top J(\rho)G_c(\rho),\\ \hat{\mathcal{A}}_{\mathcal{T}}(\rho) &= \epsilon\begin{bmatrix}\Xi(\rho)_1 & G(\rho)^\top Y_1 A(\rho)\\ \Xi(\rho)_2 & V_1(A(\rho)+Q(\rho)C(\rho)\end{bmatrix}+\frac{1}{2\epsilon}G_c(\rho)^\top J(\rho)G_c(\rho),\end{aligned}$$

$$
\begin{aligned}
\Xi(\rho)_1 &= G(\rho)^\top Y_1(A(\rho)G(\rho)+B(\rho)Z(\rho)),\\
\Xi(\rho)_2 &= V_1(A(\rho)G(\rho)+B(\rho)Z(\rho))+Q(\rho)C(\rho)G(\rho)+P(\rho)G(\rho),\\
B_{\mathcal{T}}(\rho) &= \begin{bmatrix} G(\rho)^\top Y_1 B_w(\rho) \\ V_1 B_w(\rho)+Q(\rho)D_{wy}(\rho)\end{bmatrix},\\
C_{\mathcal{T}}(\rho) &= \begin{bmatrix} C_z(\rho)G(\rho)+D(\rho)Z(\rho) & C_z(\rho)\end{bmatrix},\\
\mathcal{V}_{\mathcal{T}} &= \epsilon G_c(\rho)^\top \dot{R}(\rho)+\frac{\epsilon}{2}G_c(\rho)^\top X(\rho),
\end{aligned}
$$

hold for all $\rho \in \Theta$ *and* $\dot{\rho} \in \Gamma$*, then* $A_c(\rho) = V_3^{-1}P(\rho)$*,* $B_c(\rho) = V_3^{-1}Q(\rho)$ *and* $C_c(\rho) = Z(\rho)G(\rho)^{-1}$ *are parameter-dependent matrices of the controller* (3.33) *and* $\sqrt{\gamma}$ *is an* $\mathcal{H}_\infty$ *guaranteed cost for the system* (3.41)*.*

Proof. The proof of this theorem is very similar to that of Theorem 5. Considering the same structures for Y and Y^{-1} given in (3.37), define the transformation matrix

$$
\bar{T}(\rho) = \begin{bmatrix} TG_c(\rho) & 0 & 0 & 0 & 0\\ 0 & TG_c(\rho) & 0 & 0 & 0\\ 0 & 0 & I & 0 & 0\\ 0 & 0 & 0 & I & 0\\ 0 & 0 & 0 & 0 & T\end{bmatrix},
$$

with T given in (3.38). Next, adopting the change of variables $P(\rho) = V_3A_c(\rho)$, $Q(\rho) = V_3B_c(\rho)$, condition (3.42) can be rewritten as $\bar{T}(\rho)\Psi(\rho)\bar{T}(\rho) < 0$ with

$$
\Psi(\rho) = \begin{bmatrix} W(\rho)+\mathrm{He}(\tilde{A}_{cl}(\rho)Y) & \xi\tilde{A}_{cl}(\rho)Y - Y^\top\hat{A}_{cl}(\rho) & \bar{B}_w(\rho) & YC_{cl}(\rho)^\top & \bar{V}(\rho)\\ \star & -W(\rho)-\xi\mathrm{He}(\hat{A}_{cl}(\rho)Y) & -\bar{B}_w(\rho) & \xi YC_{cl}(\rho)^\top & -\bar{V}(\rho)\\ \star & \star & -I & D_w(\rho)^\top & 0\\ \star & \star & \star & -\gamma I & 0\\ \star & \star & \star & \star & -\mathrm{He}(X(\rho))\end{bmatrix},
$$

with $\hat{A}_{cl}(\rho)$ and $\tilde{A}_{cl}(\rho)$ presented in (3.39) and (3.40) and matrices $A_{cl}(\rho)$ e $C_{cl}(\rho)$ given in (3.34). As a consequence, the feasibility of (3.42) implies that $\Psi(\rho) < 0$. The proof that $\Psi(\rho) < 0$ implies (3.26) and $-1 < \xi < 1$ follows similar steps presented in the proof of Theorem 3, concluding the demonstration. □

3.4 Programming and Final Remarks

Motivated by the results proposed in the modeling chapter, all control design techniques presented in this chapter were established considering that the matrices of the system have arbitrary polynomial dependence on ρ. However, no particular structure was imposed to any optimization variable, including the ones used to construct the control gains. This latter feature characterizes all synthesis conditions as *infinite-dimensional* optimization problems, which are not numerically tractable. To obtain solvable conditions in terms of LMIs, first it is necessary to impose a *fixed structure* (with respect to ρ) for the optimization variables. Motivated by the polynomial structures of the system matrices and also by polynomial approximation techniques for parameter-dependent LMIs (OLIVEIRA; PERES, 2007), all proposed conditions can be solved by considering the optimization variables as polynomials with fixed degrees. Concretely, the conditions are programmed with the aid of the Robust LMI Parser (ROLMIP) (AGULHARI et al., 2019), which provides a high level programming interface in which the user only needs to define the inequalities and the degrees of the variables. The task of converting the positivity (or negativity) test of polynomial matrix inequalities into a finite set of LMIs (through relaxations techniques) is performed automatically by the parser.

As a consequence of the chosen polynomial structures, the control gains associated with the controllers are also *polynomial* or *rational*. In this context, it is important to mention that the degrees associated with the gains have a direct impact on the computational burden required to implement the gains in practice, since matrix-valued polynomials expressions need to be evaluated in real-time from the values of the time-varying parameters $\rho(t)$. Since the inversion of a matrix is a costly operation, one possibility to alleviate the computational complexity is to fix the matrix as parameter-independent (for instance, matrix Y in Theorems 1, 2 and 3). However, this option tends to increase the conservatism (worst performance).

Finally, thanks to the employment of slack variables to design state- and output-feedback controllers, the treatment of the more involved mixed $\mathcal{H}_2/\mathcal{H}_\infty$ gain-scheduled control problem can be done in a straightforward way. Basically, the $\mathcal{H}_2$ and $\mathcal{H}_\infty$ conditions can be put together and distinct Lyapunov matrices (one for each performance criterion) can be used to reduce the conservatism.

In the next section, some applications and simulations are presented to validate the proposed control techniques. Regarding the implementation of the synthesis conditions, besides the ROLMIP parser (AGULHARI et al., 2019), the semidefinite programming

solver Mosek (ANDERSEN; ANDERSEN, 2000) was used to solve the LMIs. All the scripts were programmed in Matlab version 2015 64bit, Windows 10 64bit, in a PC equipped with Core i5 processor, 8GB of memory.

4 SIMULATIONS AND EXPERIMENTAL VALIDATIONS

This chapter presents simulations and experimental validations considering the proposed modeling and control approaches. As in the previous chapter, it is firstly considered the results for the state-feedback controller, then for the static output-feedback, and finally for the dynamic controller.

4.1 State-feedback

To illustrate the proposed modeling and the synthesis conditions for gain-scheduled state-feedback controllers, three examples are considered: The reaction wheel inverted pendulum; Unicycle and the CMG. The first two examples deal with regulatory control, in which the aim is to keep the trajectories close to the equilibrium point. In these cases, the quasi-LPV modeling is considered with the purpose of increasing the accuracy of the representation region around the operation point. The CMG example consists in a pure LPV system (time-varying parameters are not state variables) and it is either considered a regulatory mode application (keep the trajectories at equilibrium) and a tracking application using an augmented model with integrators.

4.1.1 Reaction Wheel Inverted Pendulum

The nonlinear model and a brief description of this system can be found in the Appendix A. The purpose is to stabilize the system using an $\mathcal{H}_2$ gain-scheduled state-feedback controller.

First, regarding the synthesis of the quasi-LPV model, it is considered that θ_1 is an LPV variable (observe that the nonlinear model depends on $\sin(\theta_1)$). Besides, the control objective is to stabilize the system in the upright position, being impossible to stabilize it in any other position (not considering the stable equilibrium point, vertical position downwards). Therefore, to obtain the quasi-LPV model, the high-order Taylor series

expansion method is employed.

Applying the method presented in Section 2.3.2 considering a third-order expansion, we have the following model

$$\begin{bmatrix}\ddot{\theta}_1\\ \ddot{\theta}_2\end{bmatrix} = A(\theta_1)\begin{bmatrix}\theta_1\\ \theta_2\end{bmatrix} + \begin{bmatrix}0\\ -70.405\\ 382.9616\end{bmatrix}u + \begin{bmatrix}1 & 0 & 0\\ 0 & 1 & 0\\ 0 & 0 & 1\end{bmatrix}w,$$

where

$$A(\theta_1) = \left(\begin{bmatrix}0 & 1 & 0\\ 66.7479 & 0 & 1.0774\\ -66.7479 & 0 & -5.8606\end{bmatrix} + \theta_1^2\begin{bmatrix}0 & 0 & 0\\ -11.1247 & 0 & 0\\ 11.1247 & 0 & 0\end{bmatrix}\right).$$

Observe that in this case the matrix $B(\theta_1)$ has order zero and $A(\theta_1)$ has order two. As discussed in Chapter 2, this is not an issue since the proposed approach can deal with matrices of different degrees on the time-varying parameters. Concerning the controlled output

$$z = \underbrace{\begin{bmatrix}0.0757 & 0 & 0\\ 0 & 0.0633 & 0\\ 0 & 0 & 0.0109\\ 0 & 0 & 0\end{bmatrix}}_{C_z}\begin{bmatrix}\theta_1\\ \theta_2\end{bmatrix} + \underbrace{\begin{bmatrix}0\\ 0\\ 0\\ 0.3742\end{bmatrix}}_{D}u,$$

where the matrices C_z and D were obtained after some trials, considering the Bryson's rule (HESPANHA, 2018).

Before applying the synthesis condition to compute the gain-scheduled state-feedback controller, it is necessary to set, choose the bounds for the LPV variable and its associated time-derivative. We set

$$\begin{aligned} -30^\circ \leq\ & \theta_1 \leq 30^\circ,\\ -1 \text{ rad/s} \leq\ & \dot{\theta}_1 \leq 1 \text{ rad/s}. \end{aligned}$$

These values were chosen based on previous practical experiments with the pendulum.

Theorem 2 is then applied considering the parameters[1] of Table 2. Note that in

[1]Whenever $\mathrm{Deg}(K(\rho))$ is presented, it means that the two polynomial matrices used to compute the

this example, both ξ and ϵ are considered in the linear scalar search to find the lowest guaranteed cost. In a generic case, to perform a search on two scalars can be time-consuming and for this reason the preference is always to perform a search on ξ, which has a bounded domain. The value of ϵ is suggested to be fixed in 0.1 (as indicated in (RODRIGUES; OLIVEIRA; CAMINO, 2018)). However, we present the guaranteed costs for each value of ξ and ϵ (in the Table 3), just to show how the search would work.

Table 2: Parameters employed in the design of the $\mathcal{H}_2$ state-feedback gain for the reaction wheel pendulum. Deg$(\cdot)$ is the polynomial degree of the associated variable with respect to ρ.

Deg$(W(\rho))$	Deg$(K(\rho))$	ξ	ϵ
2	2	$\{-0.8, -0.6, \ldots, 0.6, 0.8\}$	$\{0.1, 1, 10\}$

Table 3: $\mathcal{H}_2$ guaranteed-costs of the reaction wheel pendulum in terms of ξ and ϵ.

		ξ								
		-0.8	-0.6	-0.4	-0.2	0	0.2	0.4	0.6	0.8
	0.1	0.4562	0.4561	0.4561	0.4560	0.4560	0.4560	0.4560	0.4560	0.4560
ϵ	1	0.4560	0.4560	0.4560	0.4560	0.4560	0.4561	0.4561	0.4562	0.4563
	10	0.4564	0.4568	0.4571	0.4572	0.4573	0.4574	0.4575	0.4576	0.4582

Note that the guaranteed costs slightly vary with the scalar variables but all controllers are robustly stabilizing[2]. Also, note that $\epsilon = 10$ provided the worst guaranteed costs.

Table 4 shows the values of the scalars that provided the lowest guaranteed cost and the associated numerical complexity given in terms of the number of LMI rows and optimization variables.

Table 4: Result of the $\mathcal{H}_2$ state-feedback applied to reaction wheel pendulum.

LMI rows	variables	$\sqrt{\mu}$	ξ_{min}	ϵ_{min}
151	100	0.4560	0.8	0.1

Then, the simulation of the closed-loop system with the $\mathcal{H}_2$ state-feedback controller is presented in Figure 11. For the sake of comparison, an LQR controller designed for the linearized model at the unstable equilibrium point ($\theta_1 = 0$) is also presented in Figure 11 and labeled as "linear". The LQR controller was designed considering the same performance specification

$$Q = C_z^\top C_z,$$
$$R = D^\top D,$$

feedback gains ($Z(\rho)$ and $Y(\rho)$) have the same degree and equal to Deg$(K(\rho))$.

[2]The numbers were truncated considering four decimal digits for the sake of presentation.

where Q and R are the weighting matrices for state and input, respectively.

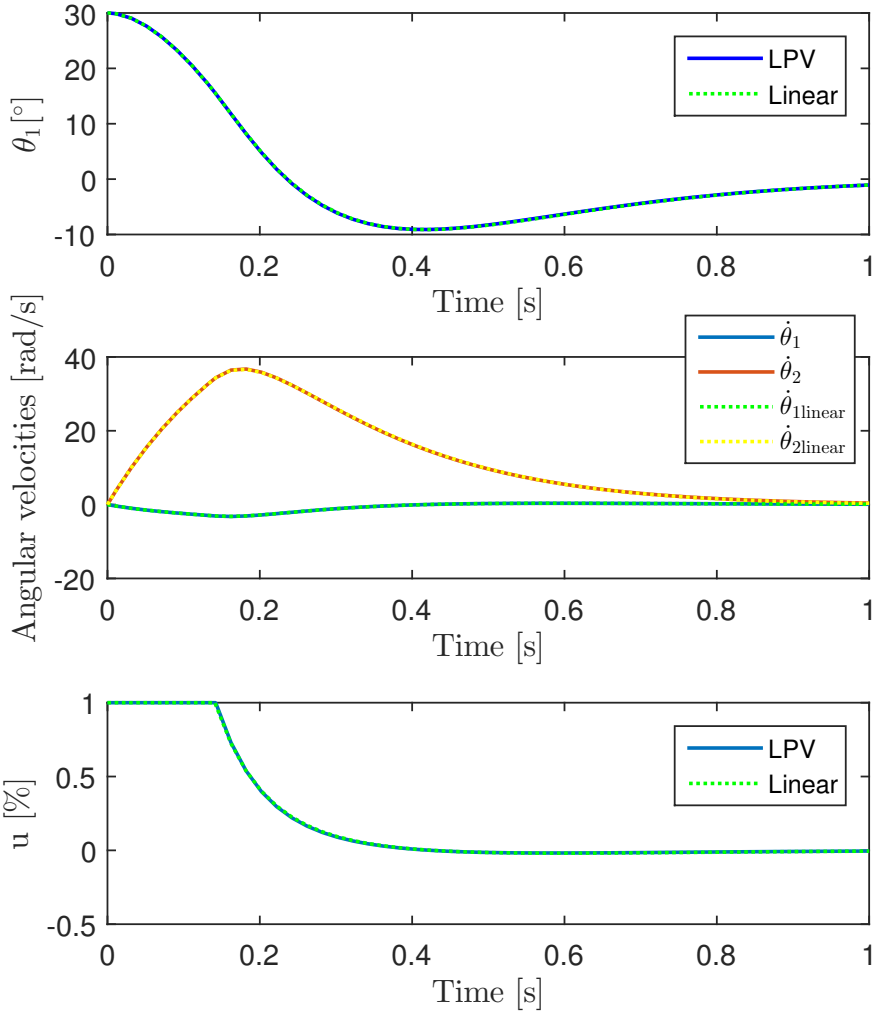

Figure 11: Simulation result of the $\mathcal{H}_2$ gain-scheduled and LQR controllers applied in the pendulum reaction wheel.

Note that the LPV controller did not present an improvement in relation to the linear control, since the linear model represents quite well the reaction wheel inverted pendulum dynamics within the considered range. Such a difference would be more evident with a larger angle variation, as observed in the Furuta pendulum presented in Section 2.3.2.

However, this result validates the proposed technique. In this example, the controller stabilized the system with a performance similar to the LQR approach. The controller was then implemented in a prototype to visualize its performance in a practical application.

Figure 12 shows the result of the practical implementation where it is possible to see that the controller stabilizes the system with a small variation around the equilibrium

point (variation caused mainly by the dead-zone and backlash of the actuator not considered in the modeling procedure). Figure 13 shows the response when a perturbation[3] in θ_1 of $\approx 10°$ at $t = 7$s. The controller was able to reject the disturbance and maintain the stability of the system.

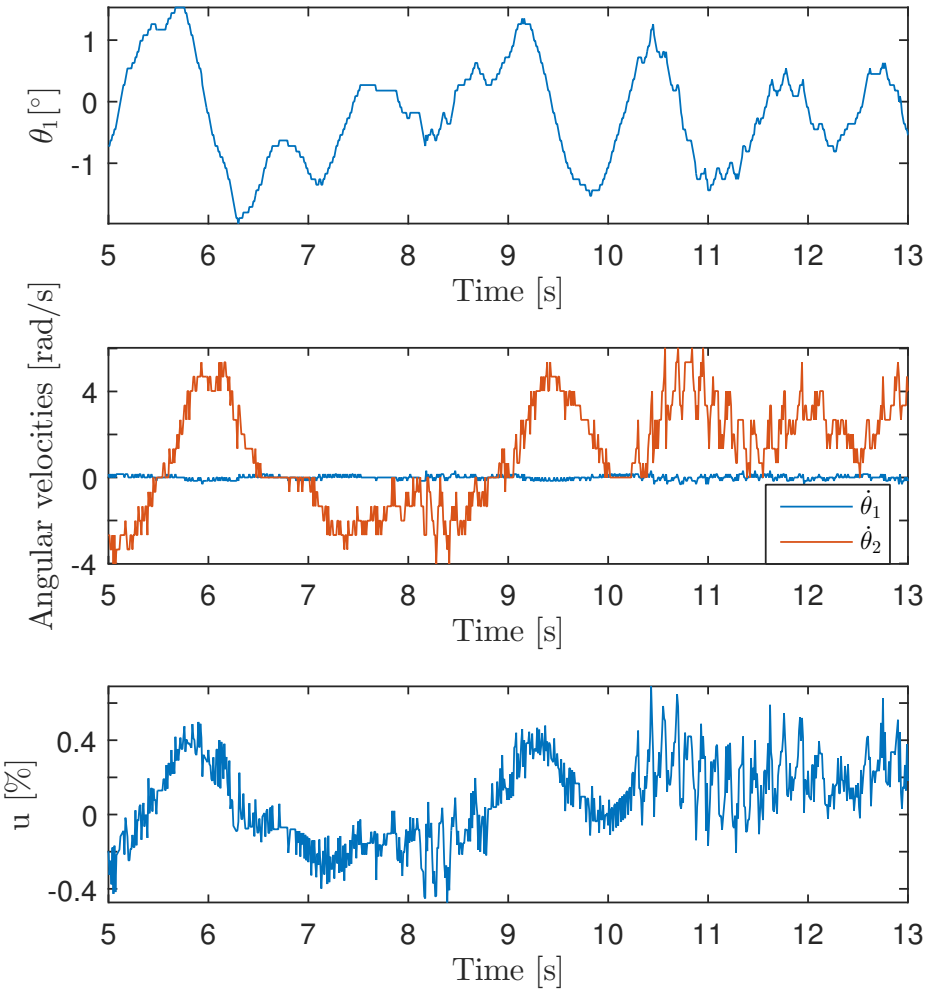

Figure 12: Practical result of $\mathcal{H}_2$ controller applied to the reaction wheel pendulum.

[3]The perturbation was artificially considered by adding this value to the angle measurement in the software for 0.5 seconds.

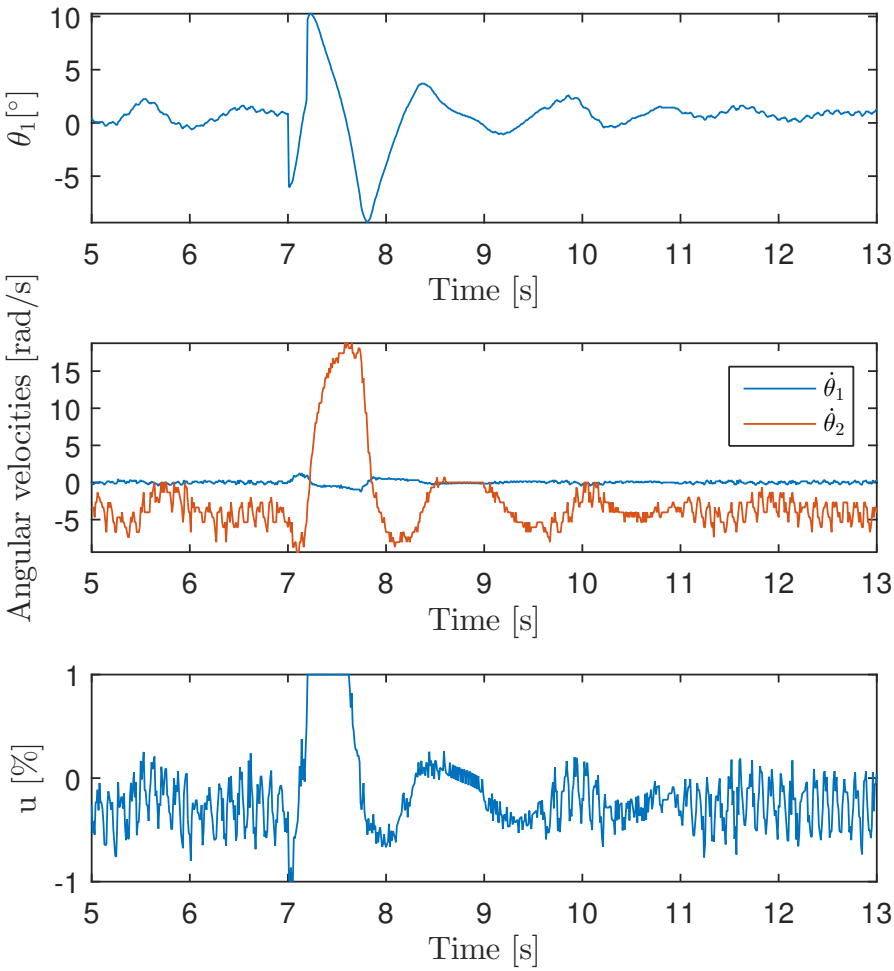

Figure 13: Practical result of $\mathcal{H}_2$ controller applied to the reaction wheel pendulum considering a disturbance in θ_1 applied at $t = 7$s.

4.1.2 Unicycle

The second example is the unicycle presented in Appendix C. The LPV model is considered to represent the dynamics aiming to increase the representability region around the operating point when compared to the linear model. Thus, the technique used is Taylor's high order expansion.

In this example, it is used a model similar to the one presented in (2.13)-(2.16), but considering fourth order expansion rather than second order. For the controlled output

we set

$$z = \underbrace{\begin{bmatrix} 0.0316 & 0 & 0 & 0 & 0 & 0 & 0 & 0 \\ 0 & 3.8197 & 0 & 0 & 0 & 0 & 0 & 0 \\ 0 & 0 & 0.3162 & 0 & 0 & 0 & 0 & 0 \\ 0 & 0 & 0 & 3.8197 & 0 & 0 & 0 & 0 \\ 0 & 0 & 0 & 0 & 0.0809 & 0 & 0 & 0 \\ 0 & 0 & 0 & 0 & 0 & 3.1623 & 0 & 0 \\ 0 & 0 & 0 & 0 & 0 & 0 & 0.0809 & 0 \\ 0 & 0 & 0 & 0 & 0 & 0 & 0 & 1 \\ 0 & 0 & 0 & 0 & 0 & 0 & 0 & 0 \\ 0 & 0 & 0 & 0 & 0 & 0 & 0 & 0 \end{bmatrix}}_{C_z} x + \underbrace{\begin{bmatrix} 0 & 0 \\ 0 & 0 \\ 0 & 0 \\ 0 & 0 \\ 0 & 0 \\ 0 & 0 \\ 0 & 0 \\ 0 & 0 \\ 1 & 0 \\ 0 & 2 \end{bmatrix}}_{D} u,$$

and the exogenous input matrix is chosen as $B_w = \begin{bmatrix} 0 & 1 & 1 & 1 & 0 & 1 & 1 & 1 \end{bmatrix}^\top$.

The bounds for ϕ and ψ and for their associated time-derivatives are set to

$$-10^\circ \leq \varphi \leq 10^\circ \quad \text{and} \quad -10^\circ \leq \psi \leq 10^\circ$$
$$-1 \ \text{rad/s} \leq \dot{\varphi} \leq 1 \ \text{rad/s} \quad \text{and} \quad -1 \ \text{rad/s} \leq \dot{\psi} \leq 1 \ \text{rad/s}.$$

Theorem 2 is then applied considering the parameters shown in Table 5, providing stabilizing controllers with $\mathcal{H}_2$ guaranteed costs given in Table 6. Observe that both $\text{Deg}(W(\rho))$ and $\text{Deg}(K(\rho))$ require two degrees (in this case {2,2}), because the unicycle model was derived with two LPV variables. As a consequence, the controller can be scheduled with polynomial dependence on both variables.

Table 5: Parameters employed in the design of the $\mathcal{H}_2$ state-feedback gain for the unicycle. $\text{Deg}(\cdot)$ is the polynomial degree of the associated variable with respect to $\rho = [\phi, \psi]$.

$\text{Deg}(W(\rho))$	$\text{Deg}(K(\rho))$	ξ	ϵ
{2,2}	{2,2}	$\{-0.9, -0.7, \ldots, -0.1, 0, 0.1, \ldots, 0.7, 0.9\}$	$\{0.1, 1, 10\}$

Table 6: $\mathcal{H}_2$ guaranteed-costs of the unicycle in terms of ξ and ϵ.

		ξ								
		-0.9	-0.7	-0.5	-0.3	0	0.3	0.5	0.7	0.9
	0.1	12.4899	12.4886	12.4878	12.4873	12.4868	12.4866	12.4868	12.4876	12.4917
ϵ	1	12.4874	12.4914	12.4950	12.4993	12.5068	12.5154	12.5214	12.5275	12.5343
	10	-	-	12.5403	-	12.5529	12.5878	12.6268	12.7175	-

Observe that some combinations of (ξ, ϵ) did not provided feasible solutions, that is, stabilizing controllers. Besides, as in the reaction wheel pendulum case, $\epsilon = 0.1$ presents

better guaranteed costs in most cases. Choosing the pair (ξ, ϵ) that provided the lowest guaranteed cost, we have the results shown in Table 7, which includes the numerical complexity.

Table 7: Result of the $\mathcal{H}_2$ state-feedback applied to unicycle.

LMI rows	variables	$\sqrt{\mu}$	ξ_{min}	ϵ_{min}
4904	1630	12.4866	0.3	0.1

Figure 14 shows the closed-loop simulations considering the $\mathcal{H}_2$ gain-scheduled controller. We set an initial condition for the pitch angle of $\varphi_{IC} = 10°$ and roll angle of $\psi_{IC} = -10°$. Besides, to further evaluate the quality of the model and the robustness of the controller, exogenous disturbances are considered. For the pitch angle, it is a pulse of $7°$ that starts at $t = 2$s with 2 seconds of duration, and for the roll angle it is a pulse of $-7°$ that starts at the same instant and with the same duration.

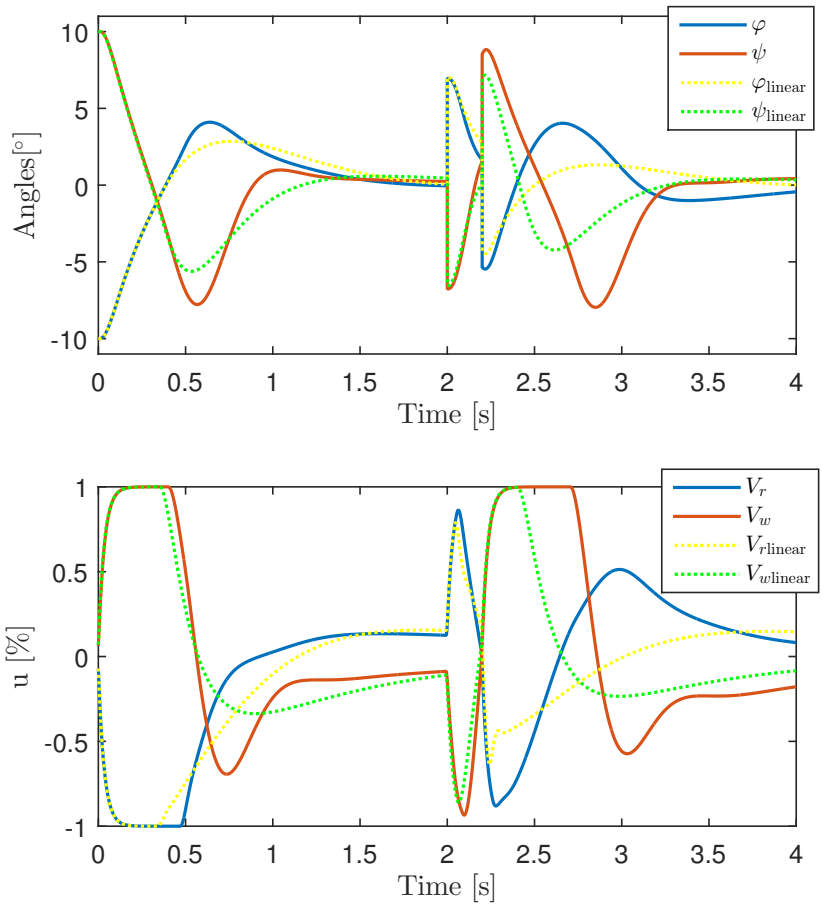

Figure 14: Closed-loop simulation with the $\mathcal{H}_2$ controller applied in the unicycle.

Observe that in this simulation the gain-scheduled controller presented a slightly worse result than the linear controller, especially in disturbance rejection test. The pitch and

roll angles, when considering the LPV controller, present a larger overshooting that the LQR. However, note that the control signal of the gain-scheduled controller saturated for a longer time. As the actuator saturation is an issue not addressed by the proposed synthesis conditions, the simulations are performed again to evaluate the performance of the gain-scheduled controller in the absence of saturation[4], and the results are depicted in Figure 15.

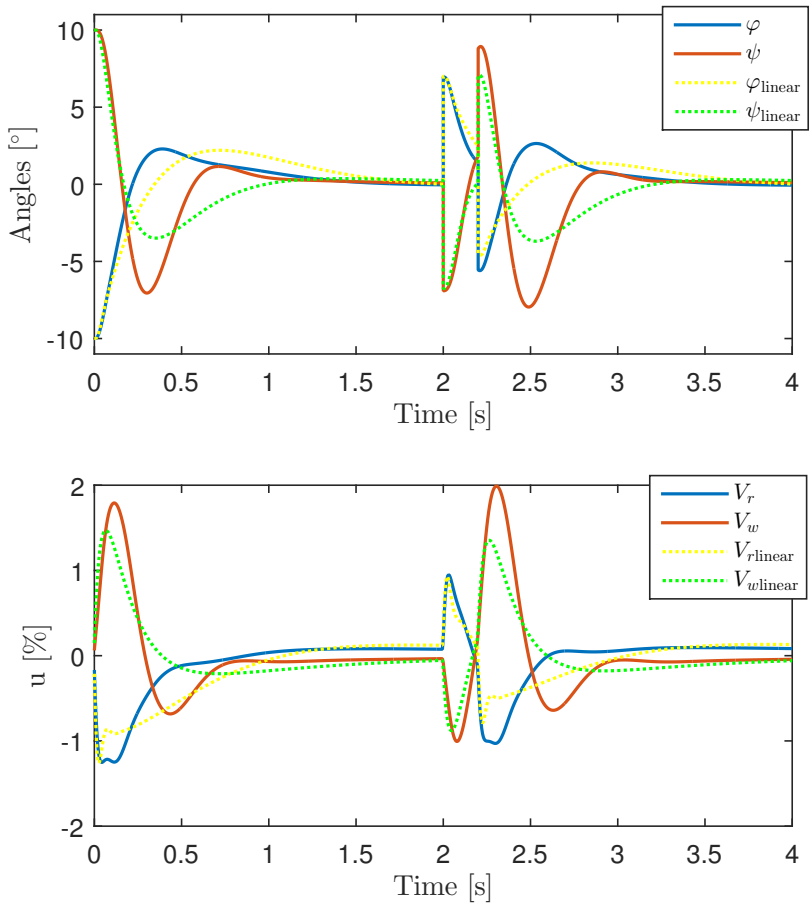

Figure 15: Closed-loop simulation with the $\mathcal{H}_2$ controller applied in the unicycle but not considering the input saturation.

Observe now that, despite the bigger overshooting, the gain-scheduled controller yields a faster response, which is consistent, as it is observed that the quasi-LPV model can represent the coupling that appears in a position other than the unstable equilibrium point, but the linear model does not.

Another important point to highlight is the computational complexity. The unicycle

[4]The control effort is given as the percentage of the PWM duty cycle, which is calculated as a constant multiplying the supply voltage. As a consequence, $u > 1$ means an unrealistic situation where the control effort is greater than the maximum allowed.

has eight states and two LPV variables. Considering a gain-scheduled state-feedback controller with polynomial dependence of degree two, the computational complexity is significantly larger when compared to the reaction wheel pendulum (that have four states and one LPV variable).

The proposed approach can increase the region of representability when compared to a linear controller. However, depending on the polynomial degrees of the model and controller, the computational complexity can be an issue, and the actuator saturation will have to be addressed. For instance, one can restrict the norm of $K(\rho)$ or combine the proposed synthesis conditions with some LMI methods capable to treat the input saturation (TARBOURIECH et al., 2011).

4.1.3 CMG

The two previous examples, despite verifying the functionality of gain-scheduled controller designed with the proposed conditions, were not capable to show a significant advantage when compared to time-invariant modeling and control. Motivated by this fact, we apply the proposed techniques in a control moment gyroscope (CMG) plant aiming both regulatory and tracking control. The nonlinear model can be found in Appendix D.

Two approaches are considered: in the first one we model the CMG as a pure LPV model (where the dependent variables do not represent any state) and apply an $\mathcal{H}_2$ gain-scheduled controller. In the second case, the CMG is modeled as a quasi-LPV model and an $\mathcal{H}_\infty$ gain-scheduled controller is applied.

4.1.3.1 LPV model

Consider the LPV model of the CMG given in (2.5) and (2.6). Recall that this model depends on the variables θ_C and $\dot{\theta}_D$, which are not state variables.

Two different control strategies are considered in this example. The first one is the tracking mode, where two integrators were included in the model. In this case, the coefficient matrices given in (2.5) are redefined as

$$A_0 = \begin{bmatrix} A_0 & 0 \\ -C_{int} & 0 \end{bmatrix}, \quad A_i = \begin{bmatrix} A_i & 0 \\ 0 & 0 \end{bmatrix}, \; i = 1, \ldots, 5,$$

$$B_j = \begin{bmatrix} B_j \\ 0 \end{bmatrix}, \; j = 0, \ldots, 2, \quad C_{int} = \begin{bmatrix} 1 & 0 & 0 & 0 & 0 \\ 0 & 1 & 0 & 0 & 0 \end{bmatrix}.$$

With this strategy, the error concerning the tracking of a trajectory is considered in the augmented system, thus allowing to solve the tracking problem. The second strategy is the regulatory mode, where integrators are unnecessary.

To implement and solve the synthesis conditions, it is necessary to define the limits of the time-varying parameters. The limits of θ_C and $\dot{\theta}_D$ are chosen according to the operating range, and their derivatives are calculated considering the actuator saturation limits divided by 10, approximately. Thus, the LPV parameters are constrained to the ranges

$$\begin{gathered} -40^\circ \leq \theta_C \leq 40^\circ, \\ 200 \text{ rpm} \leq \dot{\theta}_D \leq 600 \text{ rpm}, \\ -2 \text{ rad/s} \leq \dot{\theta}_C \leq 2 \text{ rad/s}, \\ -10 \text{ rad/s}^2 \leq \ddot{\theta}_D \leq 10 \text{ rad/s}^2. \end{gathered}$$

Matrices C_z and D are chosen according to Bryson's rule (HESPANHA, 2018), which represents a normalization of the weighting matrices. The resulting matrices (parameter-independent) for the regulatory mode are

$$\begin{aligned} C_a &= \text{diag}(11.4548, 11.4548, 1, 1, 1), \; C_z = \begin{bmatrix} C_a & 0 \end{bmatrix}^\top, \\ D_a &= \text{diag}(2.8329, 0.6831), \; D = \begin{bmatrix} 0 & D_a \end{bmatrix}^\top, \end{aligned}$$

assuring that $C_z^\top D = 0$. For the tracking mode matrix C_a is chosen as (D_a is the same)

$$C_a = \text{diag}(11.4548, 11.4548, 1, 1, 1, 14.1421, 14.1421).$$

Finally, the input disturbance matrix is fixed as $B_w(\rho) = I$.

The synthesis conditions of Theorem 2 were tested considering

$$\xi \in \{-0.9, -0.8, \ldots, -0.1, 0, 0.1, \ldots, 0.8, 0.9\},$$

and polynomial degrees from zero to two for the optimization variables that define the controller in terms of the parameters θ_C and $\dot{\theta}_D$. Regarding the value of ϵ, only two values were considered $\{0.1, 1\}$, as suggested in (RODRIGUES; OLIVEIRA; CAMINO, 2018). Other values could lead to improved results, at the price of a larger computational effort

necessary to implement a search procedure. In general, the best results were obtained with $\epsilon = 0.1$ for the regulatory mode and $\epsilon = 1$ for the tracking mode. Table 8 shows the guaranteed costs provided by the best value of ξ for each pair of polynomial degrees for both regulatory and tracking modes. As can be seen, in the regulatory mode, gain-scheduled controllers present a good improvement in terms of $\mathcal{H}_2$ performance over the robust controller (degree zero for both θ_C and $\dot{\theta}_D$). A general observation is that the higher the degrees, the better is the guaranteed costs, but the improvements become insignificant for degrees higher than two, while the complexity of the controller increases a lot. Evaluating the trade-off between the guaranteed costs and the computational complexity to implement the control law, we chose degree two for θ_C and degree one for $\dot{\theta}_D$ for both regulatory and tracking modes, although the best guaranteed costs were obtained with degree two for both θ_C and $\dot{\theta}_D$.

Table 8: Guaranteed-costs provided by Theorem 2 considering different degrees for the time-varying parameters, $\epsilon = 0.1$ for regulatory mode, $\epsilon = 1$ for tracking mode and the values given in (4.1) for ξ.

Deg($K(\rho)$) of θ_C	Deg($K(\rho)$) of $\dot{\theta}_D$	Regulatory mode		Tracking mode	
		ξ	μ	ξ	μ
0	0	-0.9	13.0765	-0.9	26.4223
1	0	-0.1	11.7162	-0.7	26.3355
2	0	0.4	11.4216	-0.7	25.9741
0	1	-0.8	11.7355	-0.9	25.6902
1	1	0.1	10.9403	-0.4	24.9269
2	1	0.7	10.7208	-0.3	24.8199
0	2	-0.9	11.6552	-0.9	25.6878
1	2	0.8	10.9672	-0.2	25.0398
2	2	0.7	10.6916	-0.1	24.5809

Choosing the case where Deg($K(\rho)$) $= [2, 1]$, the results obtained with Theorem 2 are shown in Table 9. Regarding the linear controller used for a comparison reference, LQR controllers are considered in both cases.

Table 9: Result of the $\mathcal{H}_2$ state-feedback applied to CMG LPV model.

	LMI rows	variables	$\sqrt{\mu}$	ξ_{min}	ϵ_{min}
Regulatory mode	1419	706	10.6929	0.7	0.1
Tracking mode	2535	1513	24.8199	-0.3	1

The experimental setup is composed of two steps. First, a PI control is activated to bring the disk speed to 400 rpm, from 0 to 18 seconds. Then, in the second step, the PI is turned off and the state feedback control is activated. Beside that, the test is divided in two situations. The first considers the initial condition $\theta_C = 20°$, corresponding

to the linearization point of the LQR project. The second considers the initial condition $\theta_C = -20°$. The idea of testing with the initial condition away from the linearization point is to show the difficulty faced by time-invariant control strategies when these changes occur (which can happen naturally since these variables are not being controlled).

Figure 16 shows the practical results obtained considering that the initial conditions coincide with the linearization point in the Tracking mode. Note that the LPV and LQR controllers presented very similar responses, with small differences in the controlled variables. However, note that the values of θ_C and $\dot{\theta}_D$ start to drift away from the starting point. The explanation for this fact is because these variables are not being considered in the control design.

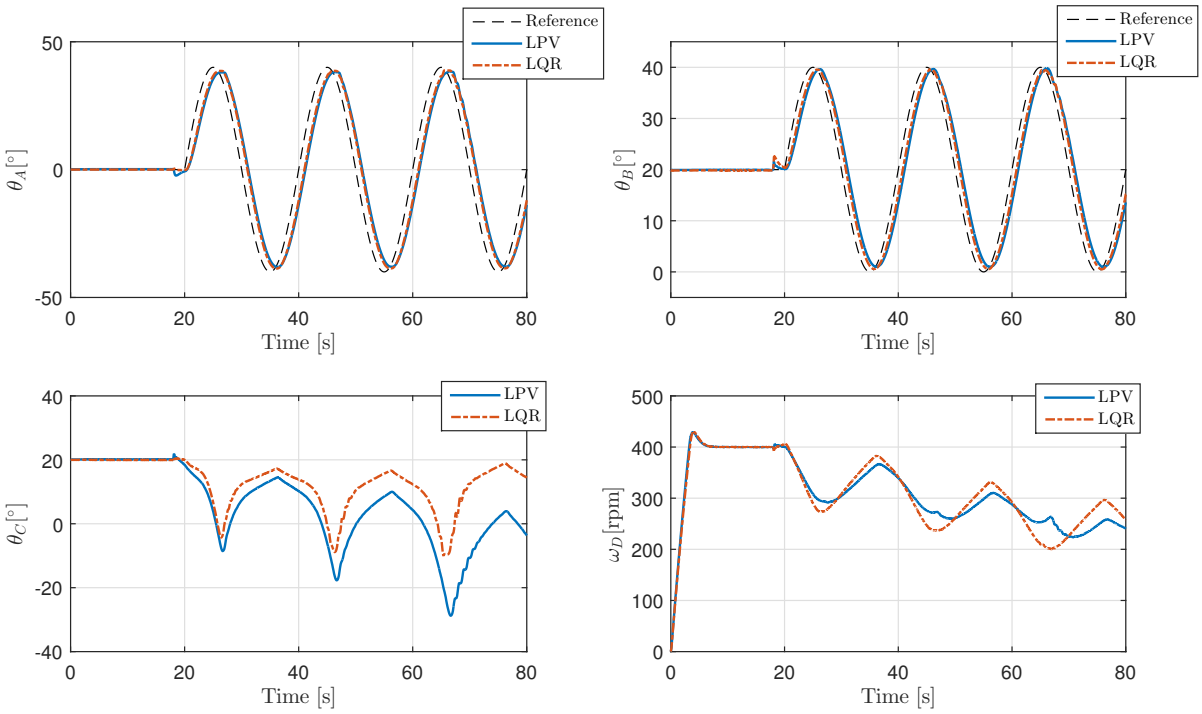

Figure 16: Sinusoidal tracking practical results of $\mathcal{H}_2$ gain-scheduled and LQR controller applied in the CMG considering the initial position $\theta_C = 20°$.

In the second case, shown in Figure 17, it is considered that the initial condition is different from the linearization point ($\theta_C = -20°$). Note that now the LQR was not able to stabilize the plant. At approximately $t = 70s$, the CMG became unstable and shut down the system.

To test the regulatory mode, a disturbance is considered in the output, as seen in Figure 18. The other conditions are the same of the previous experiment.

Figure 19 presents the results where the initial condition is the same of the operation

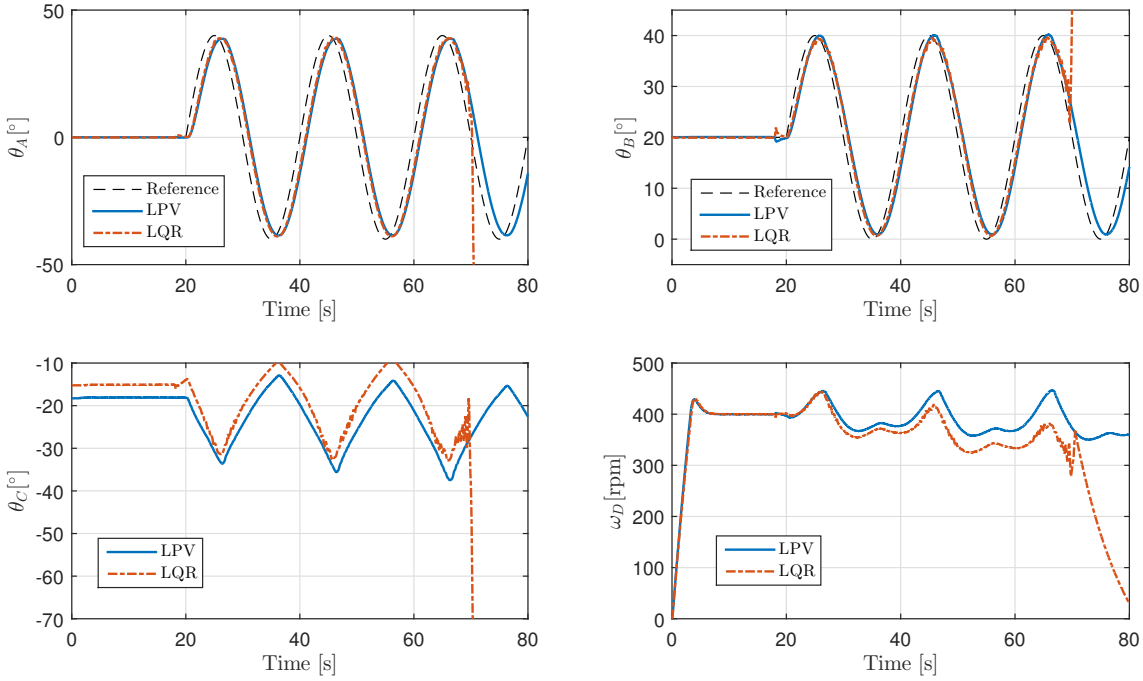

Figure 17: Sinusoidal tracking practical results of $\mathcal{H}_2$ gain-scheduled and LQR controller applied in the CMG considering the initial position $\theta_C = -20°$.

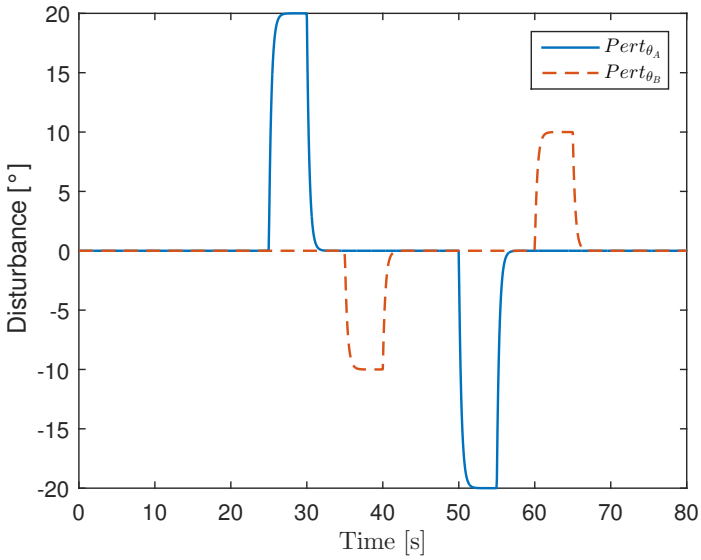

Figure 18: Disturbance considered in the output of the CMG.

point. Both controllers satisfactorily rejected the disturbances. The results associated to θ_A are quite similar. However, in θ_B it is possible to see some differences, but it is still difficult to classify which controller is better. At the instant $t = 25s$ the LPV controller had a larger overshoot, but at the instant $t = 50s$ the same occurred with the LQR. Overall, the two controllers presented similar behavior.

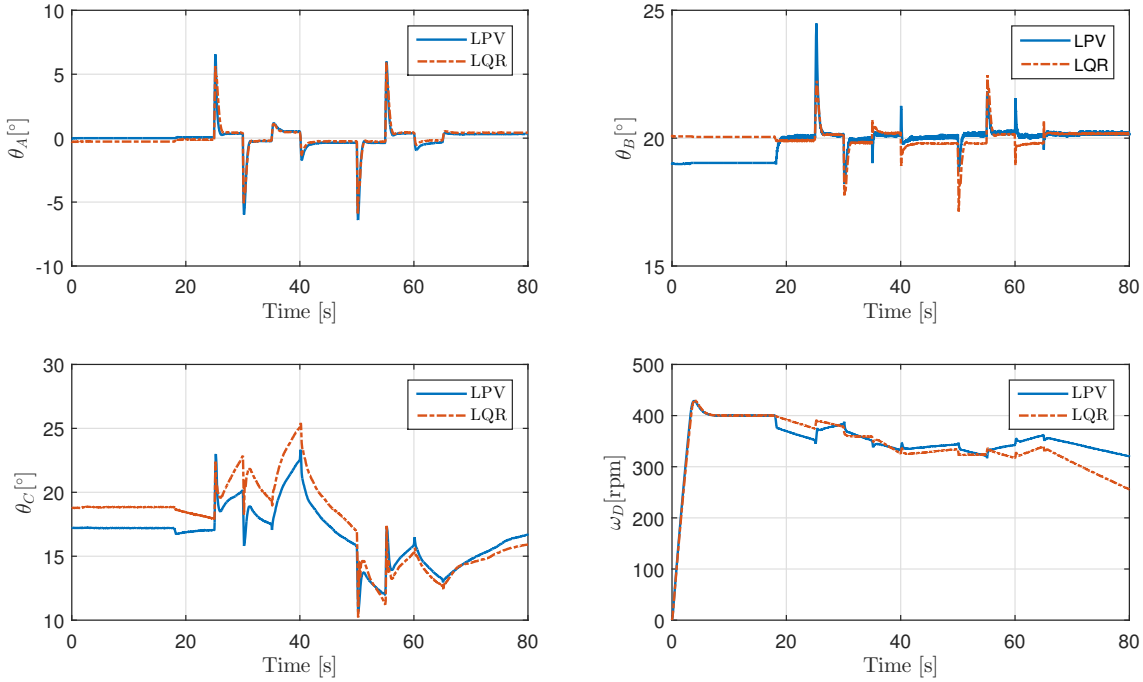

Figure 19: Disturbance rejection practical results of $\mathcal{H}_2$ gain-scheduled and LQR controller applied in the CMG considering the initial position $\theta_C = 20°$.

In the second case, the initial condition is different from the linearization point ($\theta_C = -20°$), and the results are shown in Figure 20. Once again, the LQR controller failed to maintain stability, while the LPV controller did it successfully. Moreover, even before losing stability, the LQR control already presented worse results.

Overall, the proposed $\mathcal{H}_2$ gain-scheduled controller showed superiority with respect to time-invariant control. There are other techniques that can handle this problem (nonlinear controllers, for example), but the proposed one is a state feedback.

4.1.3.2 quasi-LPV model

Consider the quasi-LPV model obtained by the proposed polynomial regression method (Algorithm 1) with both LPV variables with quadratic dependence. Although the third-order model better represents the plant, the higher the order, the greater the computational complexity. Furthermore, the second order model is already able to represent the change of direction of the control effort caused by the variation of θ_B and θ_C.

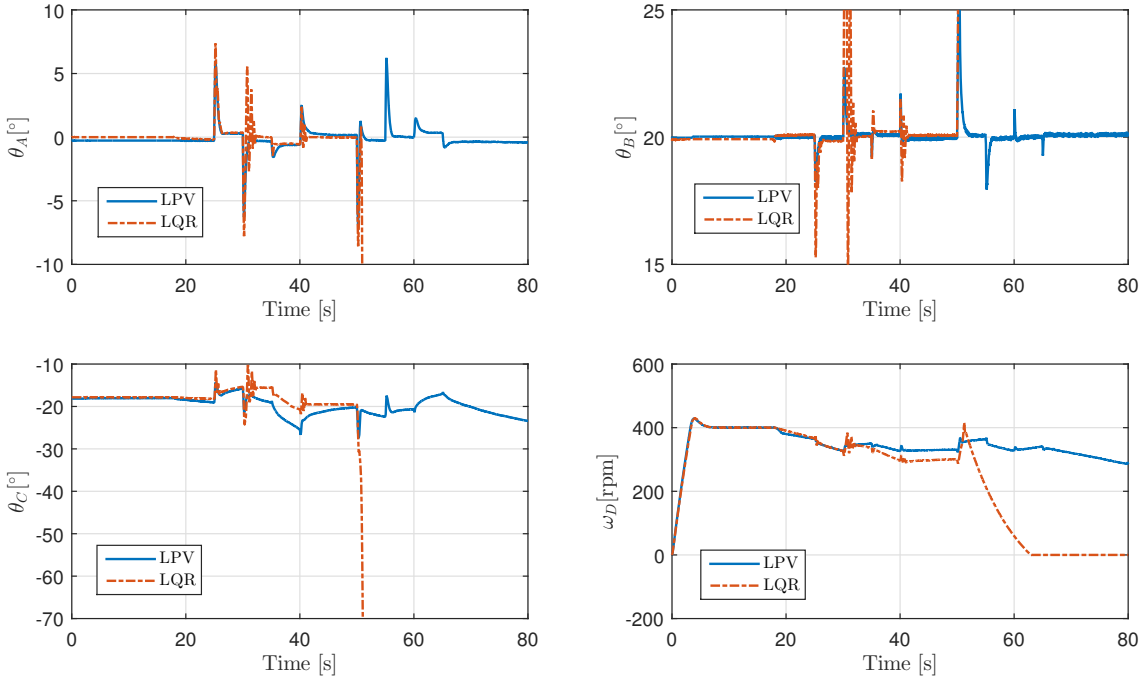

Figure 20: Disturbance rejection practical results of $\mathcal{H}_2$ gain-scheduled and LQR controller applied in the CMG considering the initial position $\theta_C = -20°$.

Regarding the controlled output (z), it is considered

$$z = \underbrace{\begin{bmatrix} 11.4548 & 0 & 0 & 0 & 0 \\ 0 & 11.4548 & 0 & 0 & 0 \\ 0 & 0 & 2.2361 & 0 & 0 \\ 0 & 0 & 0 & 2.2361 & 0 \\ 0 & 0 & 0 & 0 & 1 \\ 0 & 0 & 0 & 0 & 0 \\ 0 & 0 & 0 & 0 & 0 \end{bmatrix}}_{C_z} x + \underbrace{\begin{bmatrix} 0 & 0 \\ 0 & 0 \\ 0 & 0 \\ 0 & 0 \\ 0 & 0 \\ 155.1622 & 0 \\ 0 & 9.6599 \end{bmatrix}}_{D} u$$

$$+ \underbrace{\begin{bmatrix} 0.1 & 0 & 0 & 0 & 0 \\ 0 & 0.1 & 0 & 0 & 0 \\ 0 & 0 & 0.0032 & 0 & 0 \\ 0 & 0 & 0 & 0.0032 & 0 \\ 0 & 0 & 0 & 0 & 0.0032 \end{bmatrix}}_{D_w} w,$$

and the matrix associated the exogenous input (w) is chosen as $B_w = I_7$ (7×7 identity matrix).

This experiment considers the $\mathcal{H}_\infty$ gain-scheduled controller and the bounds for the LPV variables are chosen as follows

$$-75^\circ \leq \theta_B \leq 75^\circ \quad \text{and} \quad -35^\circ \leq \theta_C \leq 35^\circ,$$
$$-3 \ \text{ rad/s} \ \text{ rad/s} \leq \dot{\theta}_B \leq 3 \ \text{ rad/s} \quad \text{and} \quad -2 \ \text{ rad/s} \leq \dot{\theta}_C \leq 2 \ \text{ rad/s}.$$

Table 10 shows the parameters considered for the controller design.

Table 10: Parameters employed in the design of the $\mathcal{H}_\infty$ state-feedback gain for the CMG quasi-LPV model.

Deg($W(\rho)$)	Deg($K(\rho)$) of θ_B	Deg($K(\rho)$) of θ_C	ξ	ϵ
{2,2}	{0,1,2}	{0,1,2}	$\{-0.9, -0.8, \ldots, 0.8, 0.9\}$	0.1

Applying Theorem 3 and considering the parameters informed in Table 10, one has the results presented in Table 11, where only the best guaranteed cost for all values of the parameters ξ and ϵ was informed for each pair of the degrees associated to θ_B and θ_C. The symbol '–' means that no feasible solution was obtained.

Table 11: $\mathcal{H}_\infty$ Guaranteed-costs provided by Theorem 3 considering different degrees for the time-varying parameters, $\epsilon = 0.1$ and the values given in (4.1) for ξ.

Deg($K(\rho)$) of θ_B	Deg($K(\rho)$) of θ_C degree	ξ	$\mathcal{H}_\infty$ Guaranteed-cost
0	0	-	-
1	0	-	-
2	0	-0.7	404.3010
0	1	0	228.7062
1	1	-0.1	216.3027
2	1	0	216.1996
0	2	-0.5	228.6861
1	2	-0.7	216.0578
2	2	-0.7	216.0252

As can be seen, it is not possible to design a stabilizing robust (not scheduled, degree zero) controller, since the CMG reverses the direction of the gyroscopic precession due to the position of θ_B and θ_C (it changes from a minimum phase system to a non-minimum phase one). Controllers with degrees greater than or equal to one (for both scheduling parameters) present the best results. However, it is noted that Deg($K(\rho)$) $= \{2, 2\}$, showed a slight improvement with respect to Deg($K(\rho)$) $= \{1, 2\}$. As higher degree controllers demand a more complex implementation, we decided to consider a controller with degree two for both parameters. The results and numerical complexity associated

to this case are summarized in Table 12 and the resultant controller has the structure

$$u(t) = Z(\rho)Y(\rho)^{-1}(x(t) - x_{ref}(t)),$$

where $x_{ref} = \begin{bmatrix}\theta_{Aref} & \theta_{Bref} & 0 & 0 & 0\end{bmatrix}^\top$.

Table 12: Result of the $\mathcal{H}_\infty$ state-feedback applied to CMG quasi-LPV model.

LMI rows	variables	$\sqrt{\mu}$	ξ_{min}	ϵ_{min}
2700	676	216.0252	-0.7	0.1

Figure 21 shows a closed-loop simulation with the designed controller applied to the CMG system. As can be seen, the tracking problem was solved with good results. We stress that the designed gain-scheduled controller itself solves the tracking problem, that is, it is not necessary to include a pre-filter or an integrator as in (ABBAS et al., 2014).

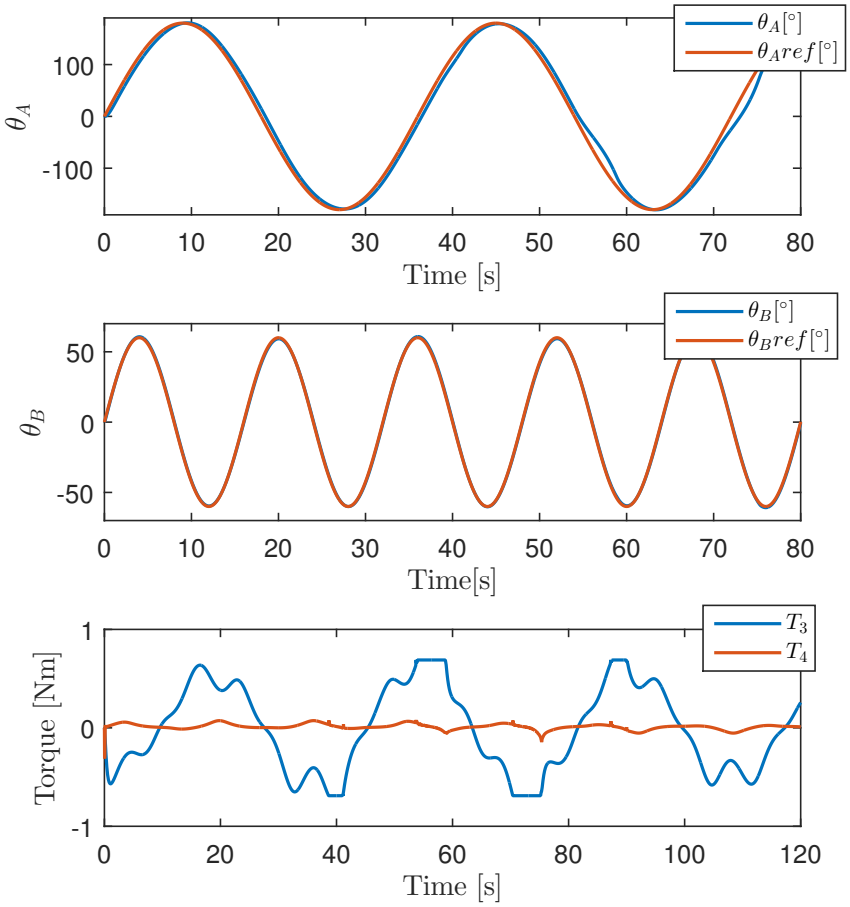

Figure 21: Simulation result with the $\mathcal{H}_\infty$ gain-scheduled controller applied in the CMG quasi-LPV model.

The results presented in the sequence were obtained through a practical validation. In

this experiment, the proposed control is compared to a linear control with the same performance specifications ($Q = C_z^\top C_z$, $R = D^\top D$, B_w and D_w). To enhance the comparisons, two linear control techniques are investigated: Standard $\mathcal{H}_\infty$ linear control ($\text{STD}_{\mathcal{H}_\infty}$) and $\mathcal{H}_\infty$ linear control with integrator insertion ($\text{INT}_{\mathcal{H}_\infty}$).

The $\text{STD}_{\mathcal{H}_\infty}$ is the standard $\mathcal{H}_\infty$ state feedback design using an LTI linearized model obtained at the operation point $x = 0$. The state and input matrices resulted of this linearization are

$$
\begin{aligned}
A_{LTI} &= A(\theta_A = 0, \theta_B = 0) = \begin{bmatrix} 0 & 0 & 1 & 0 & 0 \\ 0 & 0 & 0 & 1 & 0 \\ 0 & 0 & -0.0203 & 0 & -8.5916 \\ 0 & 0 & 0 & -0.0592 & 0 \\ 0 & 0 & 42.0419 & 0 & -0.4338 \end{bmatrix} \\
B_{LTI} &= B(\theta_A = 0, \theta_B = 0) = \begin{bmatrix} 0 & 0 \\ 0 & 0 \\ 0 & 0 \\ 0 & -21.9298 \\ 36.7647 & 0 \end{bmatrix}.
\end{aligned}
$$

As it is well known, a standard $\mathcal{H}_\infty$ state-feedback control law is not enough to ensure null steady-state error when performing tracking of trajectories. Thus, it also considered here the addition of one integrator for each state θ_A and θ_B (TORIUMI; ANGéLICO, 2020). The augmented system considering the integrators is given by[5]

$$
A_a = \begin{bmatrix} A_{LTI} & 0 \\ I_2 & 0 \end{bmatrix} \text{ and } B_a = \begin{bmatrix} B_{LTI} \\ 0 \end{bmatrix}. \tag{4.1}
$$

[5] I_2 indicates an identity matrix of dimension 2.

The augmented system has two more states, with the new matrices C_z and D_w given by

$$C_z = \begin{bmatrix} 11.4548 & 0 & 0 & 0 & 0 & 0 & 0 \\ 0 & 11.4548 & 0 & 0 & 0 & 0 & 0 \\ 0 & 0 & 2.2361 & 0 & 0 & 0 & 0 \\ 0 & 0 & 0 & 2.2361 & 0 & 0 & 0 \\ 0 & 0 & 0 & 0 & 1 & 0 & 0 \\ 0 & 0 & 0 & 0 & 0 & 500 & 0 \\ 0 & 0 & 0 & 0 & 0 & 0 & 500 \\ 0 & 0 & 0 & 0 & 0 & 0 & 0 \\ 0 & 0 & 0 & 0 & 0 & 0 & 0 \end{bmatrix}, \tag{4.2}$$

$$D_w = \begin{bmatrix} 0.1 & 0 & 0 & 0 & 0 & 0 & 0 \\ 0 & 0.1 & 0 & 0 & 0 & 0 & 0 \\ 0 & 0 & 0.0032 & 0 & 0 & 0 & 0 \\ 0 & 0 & 0 & 0.0032 & 0 & 0 & 0 \\ 0 & 0 & 0 & 0 & 0.0032 & 0 & 0 \\ 0 & 0 & 0 & 0 & 0 & 0 & 0 \\ 0 & 0 & 0 & 0 & 0 & 0 & 0 \end{bmatrix}. \tag{4.3}$$

The experiment relies on tracking a reference signal comprised of two pulses of amplitudes of 50° and -50° (10 seconds of duration each) for both variables θ_A and θ_B. The results are depicted in Figure 22 (θ_A at the top, θ_B at the bottom), where qLPV$_{\mathcal{H}_\infty}$ represents the proposed strategy. The associated trajectories of θ_C and the control signals (torques) are shown in Figure 23. As can be seen, the qLPV$_{\mathcal{H}_\infty}$ technique was able to guarantee the reference tracking. In addition, despite being slightly oscillatory, the control effort did not reach saturation at any time. Besides, it is possible to see that the other two strategies present far inferior results.

Depending on the position of θ_C, the system presents a different coupling. It is observed that, as the controller adapts itself to the variation in θ_C, the coupling does not significantly affect the output. This feature, on the other hand, does not occur with the fixed controllers (not scheduled), where it can be observed a much more accentuated coupling effect.

The second test consists in a sinusoidal reference tracking. The output response

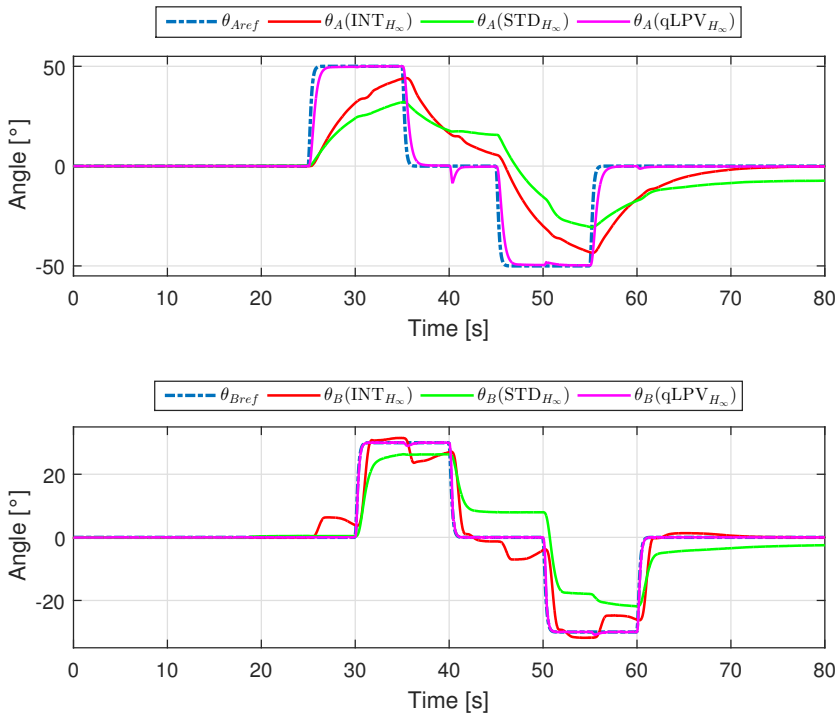

Figure 22: Responses of the CMG system (in terms of θ_A and θ_B) to input pulses considering different controllers.

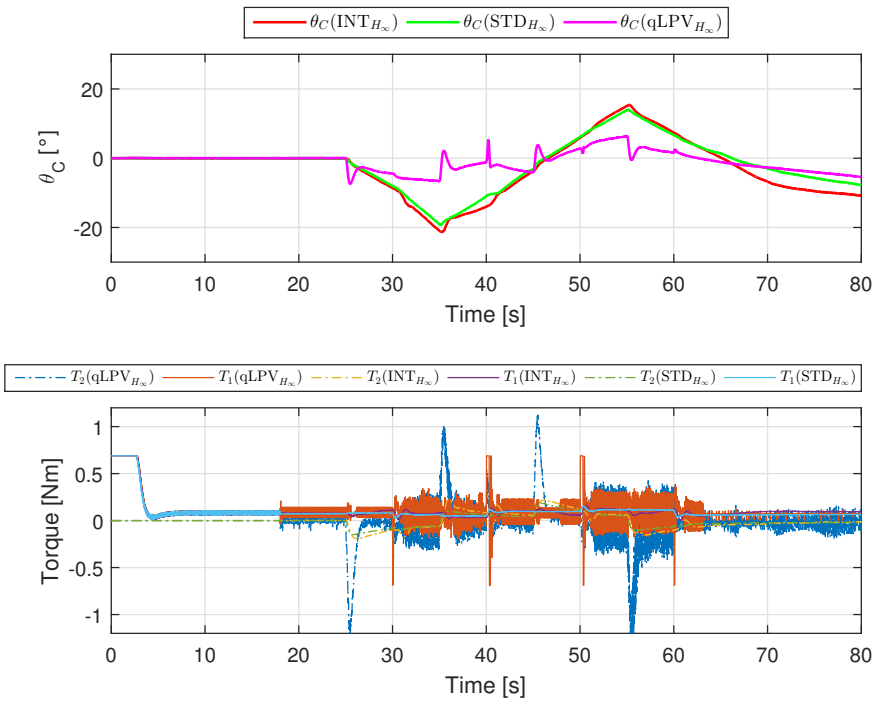

Figure 23: Pulses response: control effort and θ_C.

is shown in Figure 24, whereas the control effort and θ_C are presented in Figure 25. The proposed gain-scheduled controller was able to track a high amplitude reference. Despite the oscillatory behavior, the control effort is relatively low and does not reach the saturation limits. The controller $\text{STD}_{\mathcal{H}_\infty}$ was unable to track the reference, becoming unstable at 26 s. Differently, the $\text{INT}_{\mathcal{H}_\infty}$ maintained the stability, but the result was not satisfactory (even with quite high integrators gains). In addition, it was observed that with an additional slight increase in the weight of the integrators $C_z(6,6)$ and $C_z(7,7)$, the system becomes unstable.

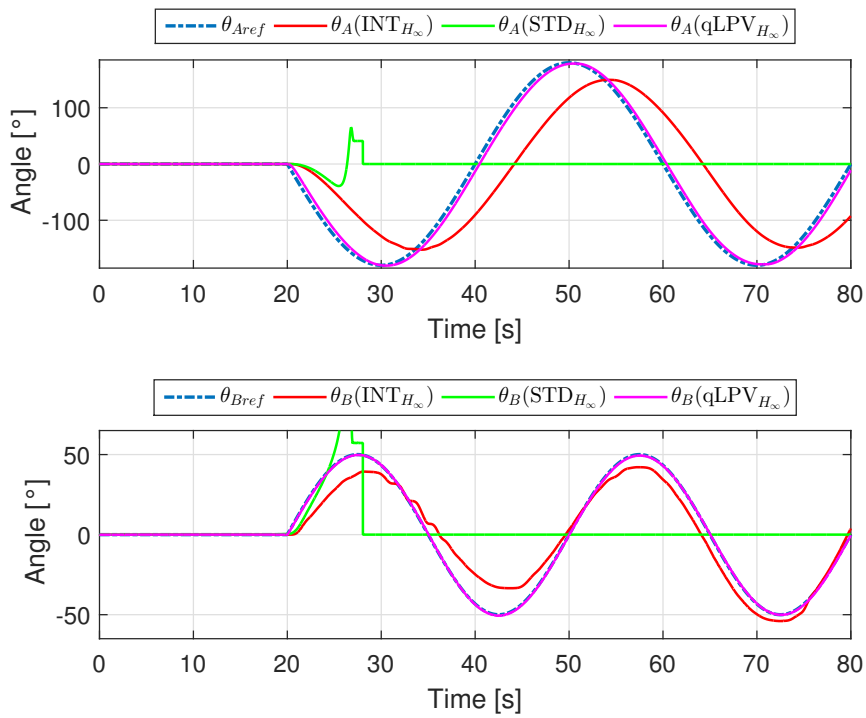

Figure 24: Sinusoidal reference tracking output of the $\mathcal{H}_\infty$ controller test.

To better show the differences among the three strategies, Table 13 shows the absolute errors (maximum and mean) observed in each test. As can be seen, the controller $\text{qLPV}_{\mathcal{H}_\infty}$ showed better results when compared to the other techniques. As a final comment, it is important to highlight that by using the proposed modeling, the synthesized state-feedback controller was able to deal with the reference tracking problem without needing a pre-filter or integration insertion.

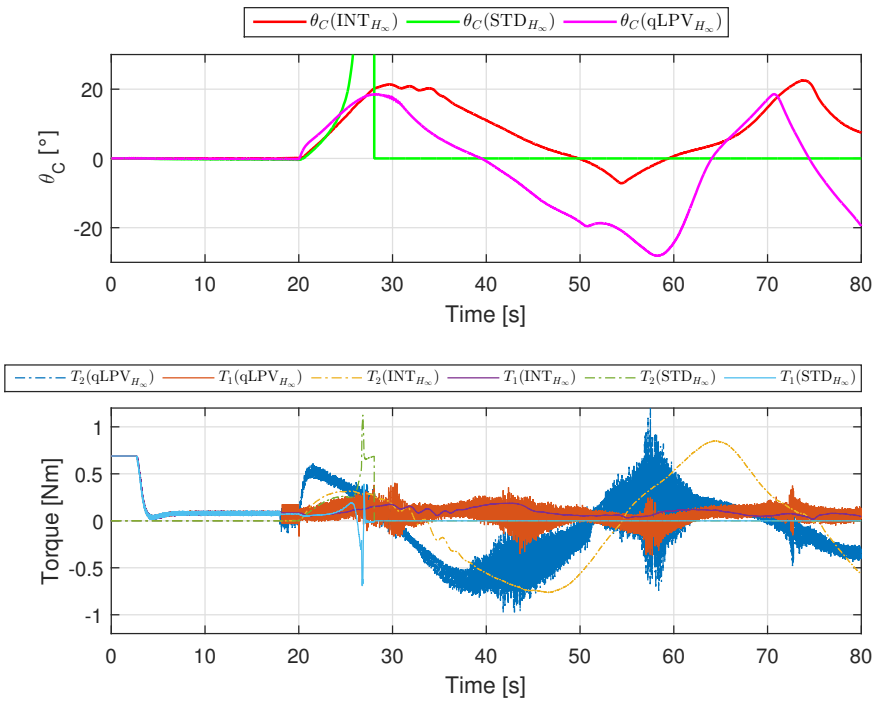

Figure 25: Sinusoidal reference tracking: control effort and θ_C.

Table 13: Mean and maximum values of absolute errors observed in practical results.

		Maximum		Mean	
	Controller	θ_A	θ_B	θ_A	θ_B
Pulses	STD_{H_∞}	59.36°	30.62°	14.01°	4.54°
	INT_{H_∞}	50.35°	22.66°	10.54°	2.34°
	qLPV_{H_∞}	27.22°	6.78°	1.31°	0.11°
Sine	STD_{H_∞}	-	-	-	-
	INT_{H_∞}	111.99°	18.59°	47.80°	6.30°
	qLPV_{H_∞}	13.24°	0.74°	6.11°	0.32°

4.2 Static output-feedback control

As a general observation regarding mechatronic systems, sometimes the static feedback of the outputs is not enough to stabilize the plant or assure a satisfactory performance. For instance, considering that the states variables are positions and velocities, a feedback control law without the velocities may not be feasible, specially when phase lead is necessary. This observation has been verified in all real plants investigated in this thesis.

As the conditions of Theorem 4 did not provide feasible solutions for any system treated in this work, a numerical test is presented to exemplify the proposed technique in

the design of static output-feedback controllers.

4.2.1 Numerical example

Consider the randomly generated LPV system described by

$$\begin{aligned}
\dot{x} &= A(\rho)x + B(\rho)u, \\
y &= C(\rho)x \\
z &= \begin{bmatrix} 1 & 0 & 0 \\ 0 & 1 & 0 \\ 0 & 0 & 1 \\ 0 & 0 & 0 \\ 0 & 0 & 0 \\ 0 & 0 & 0 \end{bmatrix} x + \begin{bmatrix} 0 & 0 \\ 0 & 0 \\ 0 & 0 \\ 1 & 0 \\ 0 & 1 \\ 0 & 0 \end{bmatrix} u,
\end{aligned}$$

where

$$\begin{aligned}
A(\rho) &= \begin{bmatrix} -1.0616 & 0.7481 & -0.7648 \\ 2.3505 & -0.1924 & -1.4023 \\ -0.6156 & 0.8886 & -1.4224 \end{bmatrix} + \rho \begin{bmatrix} 0.4882 & 1.4193 & 1.5877 \\ -0.1774 & 0.2916 & -0.8045 \\ -0.1961 & 0.1978 & 0.6966 \end{bmatrix}, \\
B(\rho) &= \begin{bmatrix} 0.7537 & 0.0759 \\ 0.3804 & 0.0540 \\ 0.5678 & 0.5308 \end{bmatrix} + \rho \begin{bmatrix} 0.7792 & 0.5688 \\ 0.9340 & 0.4694 \\ 0.1299 & 0.0119 \end{bmatrix}, \\
C(\rho) &= \begin{bmatrix} 0.3371 & 0.1622 & 0 \end{bmatrix} + \rho \begin{bmatrix} 0.7943 & 0.3112 & 0 \end{bmatrix}.
\end{aligned}$$

The time-varying parameter ρ has the following bounds

$$-1 \leq \rho \leq 1 \quad \text{and} \quad -0.5 \leq \dot{\rho} \leq 0.5.$$

Figure 26 shows the eigenvalues of matrix $A(\rho)$ for a set of values (frozen) of ρ. As can be clearly seen, there are eigenvalues with positive real part for several values of ρ (a fined grid was used). This is a proof of instability since the Hurwitz stability for all values of ρ is a necessary condition for the stability of the system ($\dot{\rho} = 0$ is particular case of the model).

Theorem 4 requires a state-feedback stabilizing gain (first stage) to calculate the output-feedback gain (second stage). In this case, the first stage is computed using the

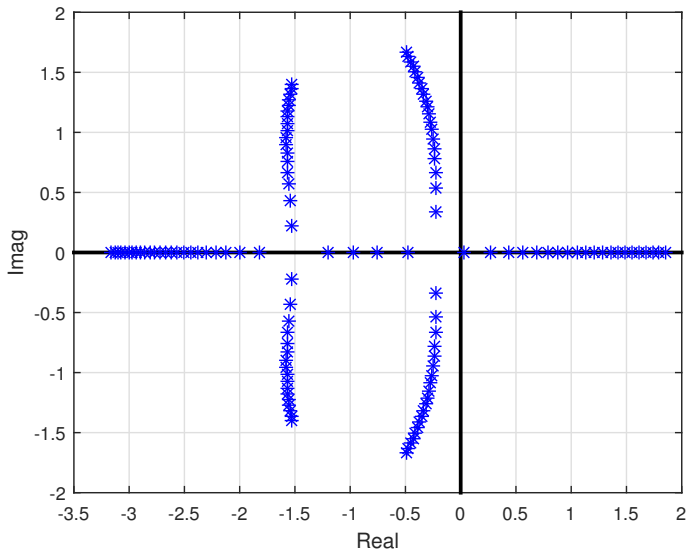

Figure 26: Open-loop poles of the numerical example considering several values of $\rho \in [-1, 1]$.

conditions of Theorem 2 with the parameters presented in Table 14.

Table 14: Parameters of the first stage (Theorem 2) of the output-feedback design.

$\text{Deg}(W(\rho))$	$\text{Deg}(Z(\rho))$	$\text{Deg}(Y)$	ξ	ϵ
1	1	Constant	$\{-0.9, -0.8, \ldots, 0.8, 0.9\}$	$\{0.1, 1, 10\}$

Note that variable Y was defined as ρ-independent because Theorem 4 requires a polynomial gain as input.

Table 15: Results of the first stage of the output-feedback design.

LMI rows	variables	$\sqrt{\mu}$	ξ_{min}	ϵ_{min}
104	64	2.7075	0.8	0.1

The state-feedback obtained in the first stage ($K(\rho) = Z(\rho)Y^{-1}$) is used in the second stage condition as well as the parameters presented in Table 16. A search on parameter ϵ is not performed again, and the value that presented the best result in the first stage is used.

Using Theorem 4 in the second stage one has the results presented in Table 17. Observe that the value of ξ that provided the best the guaranteed cost is different from

Table 16: Parameters of the second stage (Theorem 4) of the output-feedback design.

$\mathrm{Deg}(W(\rho))$	$\mathrm{Deg}(H(\rho))$	$\mathrm{Deg}(J)$	ξ	ϵ
1	1	1	$\{-0.9, -0.8, \ldots, 0.8, 0.9\}$	0.1

the one of the first stage. The resulting controller is

$$
\begin{aligned}
J(\rho) &= \begin{bmatrix} -0.0993 \\ -0.0767 \end{bmatrix} + \rho \begin{bmatrix} 0.00183 \\ 0.000543 \end{bmatrix}, \\
H(\rho) &= \begin{bmatrix} 0.0156 & 0.000892 \\ 0.0217 & 0.0313 \end{bmatrix} + \rho \begin{bmatrix} -0.00471 & 0.00362 \\ -0.0159 & -0.00752 \end{bmatrix}.
\end{aligned}
$$

Table 17: Results of the second stage of the output-feedback design.

LMI rows	variables	$\sqrt{\mu}$	ξ_{min}	ϵ_{min}
156	73	3.6482	0.6	0.1

4.3 Dynamic output-feedback control

To illustrate the results of the proposed dynamic full-order output-feedback design conditions, we consider two examples, the Furuta pendulum and the CMG.

4.3.1 Furuta Pendulum

In this example the $\mathcal{H}_2$ dynamic full-order gain-scheduled output-feedback control is applied to the Furuta pendulum. The quasi-LPV model considered in the design is the one presented in Section 2.3.2.

Consider the following bounds for θ_1 and $\dot{\theta}_1$

$$-20^\circ \leq \theta_1 \leq 20^\circ \quad \text{and} \quad -1 \text{ rad/s} \leq \dot{\theta}_1 \leq 1 \text{ rad/s}.$$

The exogenous input and controlled output matrices are defined as

$$
\begin{aligned}
C_z &= \begin{bmatrix} 17.1887 & 0 & 0 & 0 \\ 0 & 171.8873 & 0 & 0 \\ 0 & 0 & 5.7296 & 0 \\ 0 & 0 & 0 & 5.7296 \\ 0 & 0 & 0 & 0 \end{bmatrix}, \\
D &= \begin{bmatrix} 0 & 0 & 0 & 0 & 20 \end{bmatrix}^\top, \\
D_{wy} &= 0, \\
B_w &= I.
\end{aligned}
$$

Theorem 2 is used to compute the state-feedback stabilizing gain associated to the first stage ($Z(\rho)$ and $Y(\rho)$, where $K(\rho) = Z(\rho)Y(\rho)^{-1}$), which is then employed as initial condition ($K(\rho) = C_c(\rho)$) of Theorem 5 to compute the full-order dynamic output-feedback controller. The adopted parameters are shown in Table 18.

Table 18: Parameters used in the design of the dynamic controller for the Furuta pendulum.

Deg($W(\rho)$)	Deg($K(\rho)$), Deg($A_c(\rho)$) and Deg($B_c(\rho)$)	ξ	ϵ
2	{0,1,2,3}	$\{-0.9, -0.8, \ldots, 0.8, 0.9\}$	0.1

Table 19 presents the guaranteed costs obtained at each stage for all considered degrees as well as the associated numerical complexity. Note that the higher the degree, the lower the guaranteed cost. The second stage has a greater variation than the first one. Although the third-degree controller resulted in the lowest guaranteed-cost in both stages, it is still very close to the second-degree controller. Therefore, the second-degree controller was considered in the implementation of the control design of the Furuta pendulum.

Besides, observe that the guaranteed cost provided by the second stage is slightly larger than the one yielded by the first stage. This is expected, because in general state-feedback provides better performance than output-feedback.

Figure 27 shows a closed-loop simulation of the Furuta pendulum controlled by the designed dynamic gain-scheduled output-feedback controller. Note that the dynamic controller not only guarantees the stability of θ_1 but also the reference tracking of θ_0, which is referenced by a square wave of 90° amplitude.

Figure 28 shows the control effort and a comparison of the angular positions (θ_0 and θ_1) with the controller states (x_c). It is possible to observe that the controller state ended

Table 19: $\mathcal{H}_2$ guaranteed-costs of the Furuta pendulum associated to the degrees of θ_1.

	Controller degree	ξ	Guaranteed-cost	LMI Rows	variables
First stage	0	0.7	58.7435	129	129
	1	0.7	58.5777	163	149
	2	0.7	58.3648	197	169
	3	0.8	58.2859	231	189
Second stage	0	0.8	81.2409	213	403
	1	0.7	79.4788	329	427
	2	0.7	68.5166	445	451
	3	0.7	68.3023	561	475

up becoming a plant state observer. This is because the matrix $C_c(\rho)$ was defined as the states feedback of the first stage ($K(\rho) = Z(\rho)Y(\rho)^{-1}$).

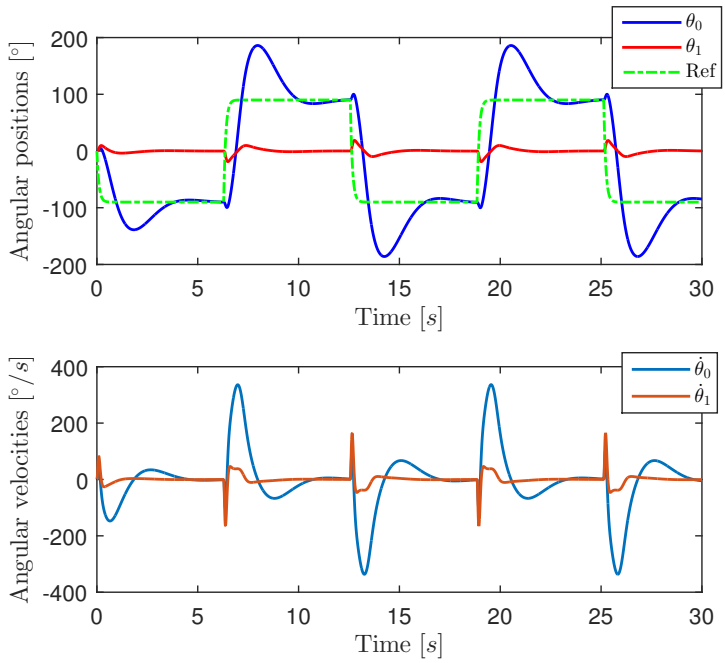

Figure 27: Simulation result of the $\mathcal{H}_2$ dynamic control applied to the Furuta pendulum.

4.3.2 CMG

In this example the same model that was considered in the $\mathcal{H}_\infty$ state-feedback design is used. The only difference is the range of the LPV variables, which are here defined as

$$-60^\circ \leq \theta_B \leq 60^\circ \quad \text{and} \quad -35^\circ \leq \theta_C \leq 35^\circ,$$
$$-3 \ \text{ rad/s} \leq \dot{\theta_B} \leq 3 \ \text{ rad/s} \quad \text{and} \quad -2 \ \text{ rad/s} \leq \dot{\theta_C} \leq 2 \ \text{ rad/s}.$$

Besides, it is considered that $D_{wy} = 0$.

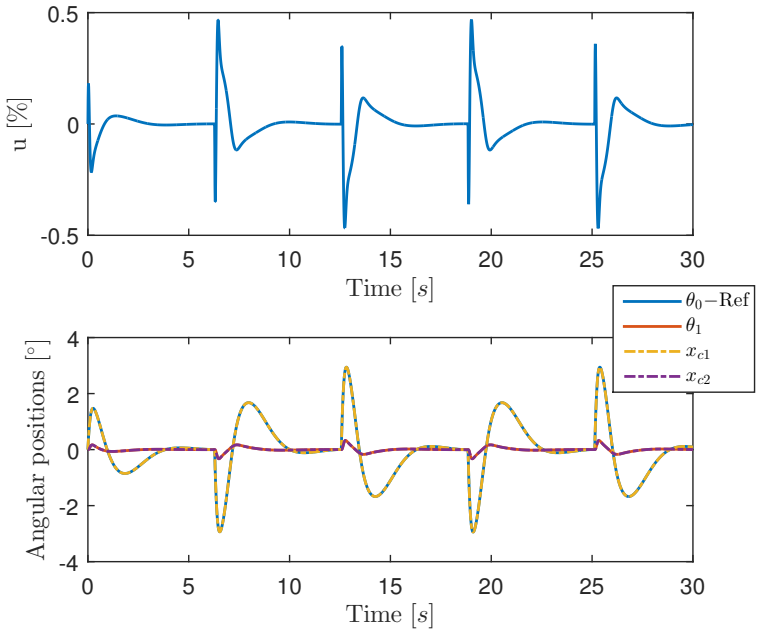

Figure 28: Control effort and controller states from the simulation of the $\mathcal{H}_2$ dynamic control applied to the Furuta pendulum.

We stress that when considering the previous limits, the controller calculation was relatively complex. For the few cases where feasible stabilizing controllers were found, the guaranteed costs were relatively high.

Initially, an $\mathcal{H}_2$ state-feedback controller is considered in the first stage with the design parameters presented in Table 20. Note that in the dynamic controller there are three polynomial (or rational) matrices in the controller ($A_c(\rho)$, $B_c(\rho)$ and $C_c(\rho)$), and the degree of each matrix is arbitrary and independent of the others. However, we arbitrarily consider the same degree for all polynomial matrices.

Table 20: Parameters of the $\mathcal{H}_2$ state-feedback design to the CMG quasi-LPV model in the first stage of the dynamic control.

$\text{Deg}(W(\rho))$	$\text{Deg}(C_c(\rho))$ of θ_B	$\text{Deg}(C_c(\rho))$ of θ_C	ξ	ϵ
2	2	2	$\{-0.9, -0.8, \ldots, 0.8, 0.9\}$	$\{0.1, 1, 10\}$

The results obtained with the application of Theorem 2 are shown in Table 21.

Table 21: Result of the first stage (Theorem 2) in the design of the dynamic controller for the CMG.

LMI rows	variables	$\sqrt{\mu}$	ξ_{min}	ϵ_{min}
2299	811	14.7703	-0.8	1

Next step is to use the state-feedback controller obtained in the first stage (in the form

of $Z(\rho)$ and $G\rho)$) as an input parameter for Theorem 5, also considering the parameters presented in Table 22. In this example, the scalar search is performed again as a strategy to obtain the lowest guaranteed cost in the second stage.

Table 22: Parameters of the $\mathcal{H}_2$ state-feedback design to the CMG quasi-LPV model in the second stage of the dynamic control.

$\text{Deg}(W(\rho))$	$\text{Deg}(A_c(\rho))$ and $\text{Deg}(B_c(\rho))$ of θ_B	$\text{Deg}(A_c(\rho))$ and $\text{Deg}(B_c(\rho))$ of θ_C	ξ	ϵ
2	2	2	$\{-0.9, -0.8, \ldots, 0.8, 0.9\}$	$\{0.1, 1, 10\}$

Finally, the result of the second stage is shown in Table 23. Note that the linear search of the scalars resulted in values different from the first stage, specially for ϵ. In addition, the computational complexity demanded by the second stage is higher than the one of the first stage.

As the output-feedback controller only requires the measurement of the outputs, it is expected a higher guaranteed cost when compared to the one obtained for state-feedback.

Table 23: Results of the second stage of the output-feedback design for the CMG.

LMI rows	variables	$\sqrt{\mu}$	ξ_{min}	ϵ_{min}
4288	1921	37.5881	-0.4	0.1

To demonstrate the operation of the proposed controller, a simulation was carried out, considering a tracking task.

The first simulation considers pulse responses for the two angles, θ_A and θ_B, and the results are shown in Figure 29. Although somewhat oscillatory, the control effort did not affect the quality of the tracking of the controlled variables. The coupling effect is noted in the response of θ_B due to variations in θ_A.

Figure 30 shows the controller state variable x_c, which can be interpreted as an observation of the state vector that multiplies the matrix $A(\rho)$ of the LPV model $(x - x_{ref})$.

The second simulation considers a sinusoidal response, and it is presented in Figure 31. Once again the control effort presented an oscillatory behavior and the variation in θ_C is larger than the one observed in the previous simulation. However, the tracking performance was satisfactory. Furthermore, Figure 32 shows x_c compared to $(x - x_{\text{ref}})$.

With this simulation, we validate the proposed dynamic control technique. The technique showed great results, solving the tracking problem with a small error and considering only the feedback of the output.

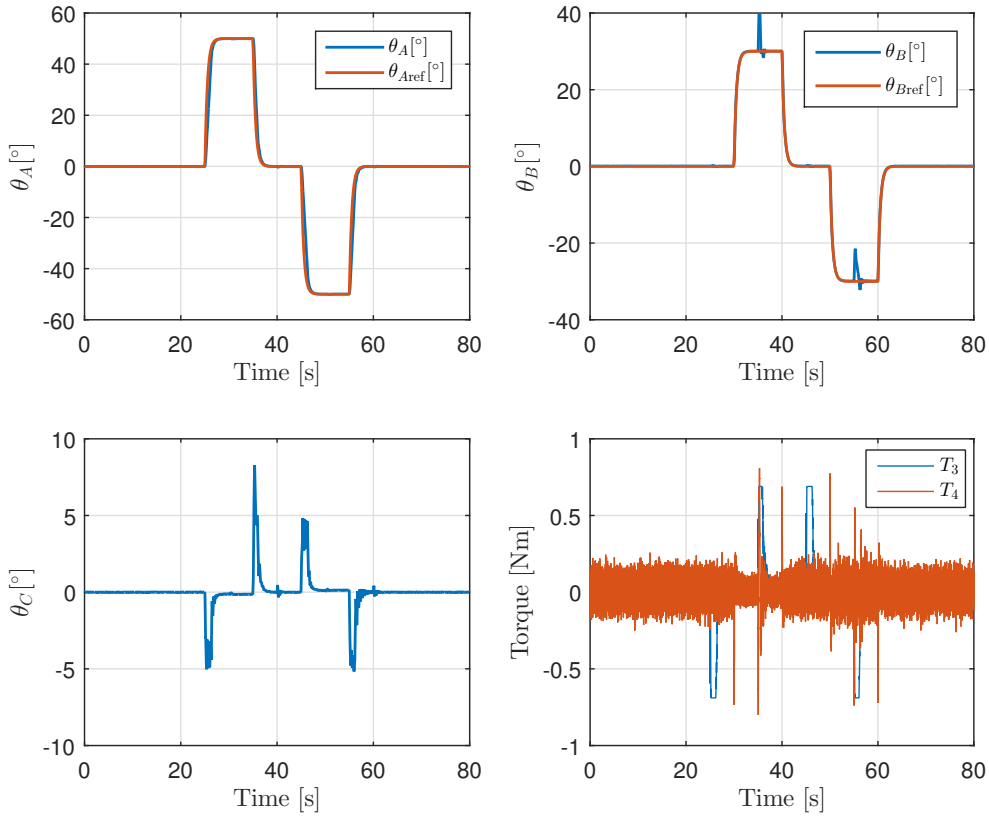

Figure 29: Simulation result of the $\mathcal{H}_2$ dynamic control applied to the CMG and considering a pulse as reference.

Differently from the static output-feedback case, which did not present feasible results in the examples presented in this work, the dynamic controller was successfully applied. However, the computational complexity is relatively higher when compared to static output-feedback and state-feedback. Moreover, as the design is performed in two stages, the design procedure can be considered more involved than in the case of state-feedback controllers.

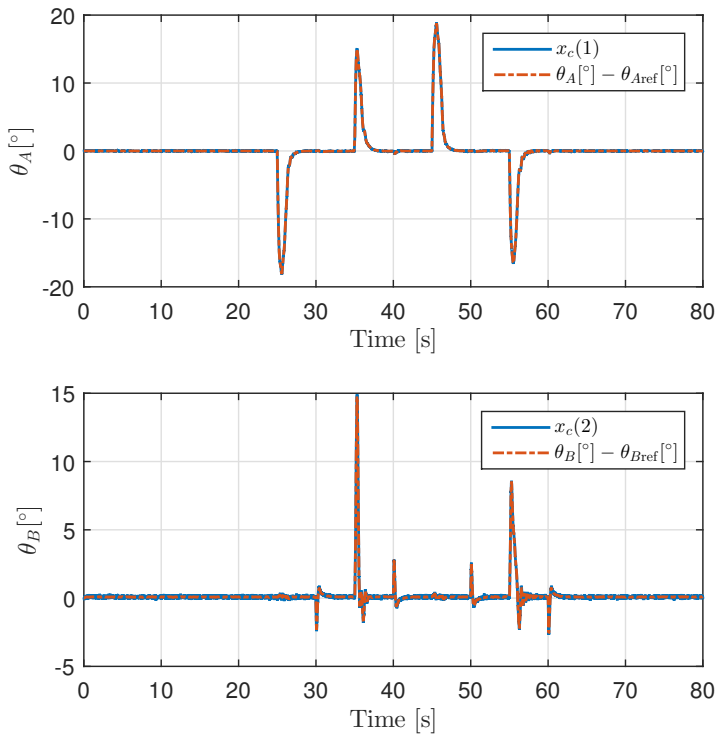

Figure 30: Controller state x_c result of the $\mathcal{H}_2$ dynamic control applied to the CMG and considering a pulse as reference.

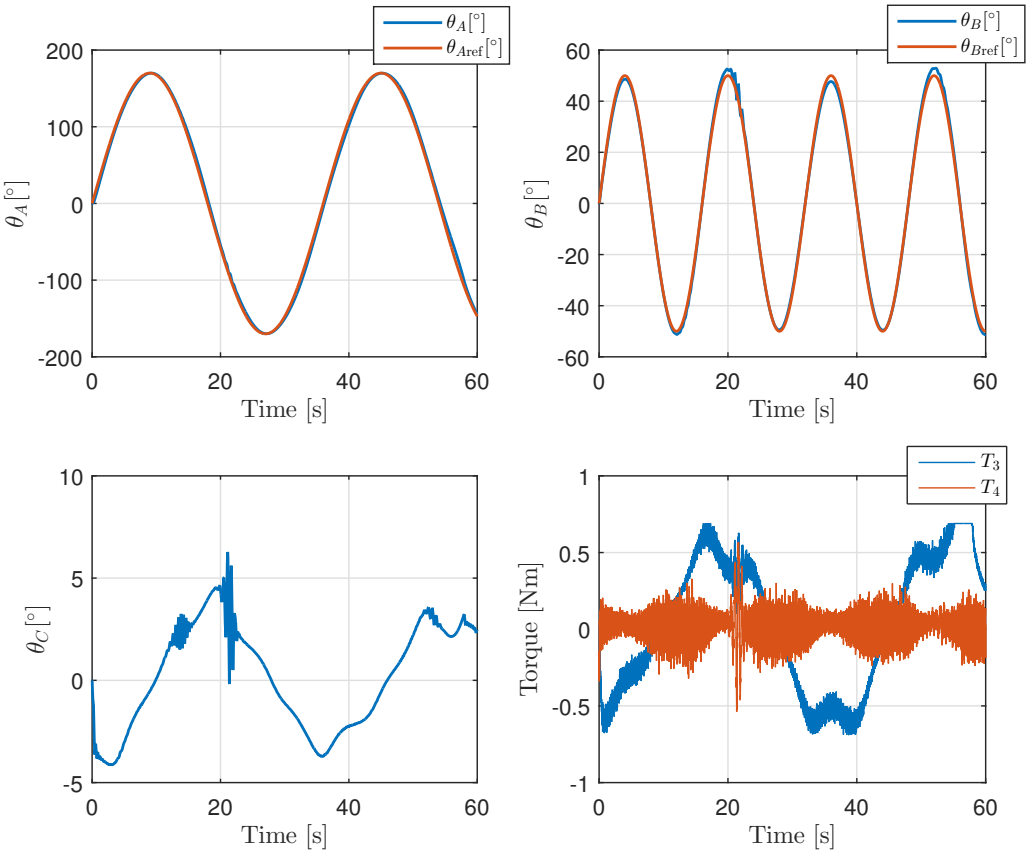

Figure 31: Simulation result of the $\mathcal{H}_2$ dynamic control applied to the CMG and considering a sinusoidal reference.

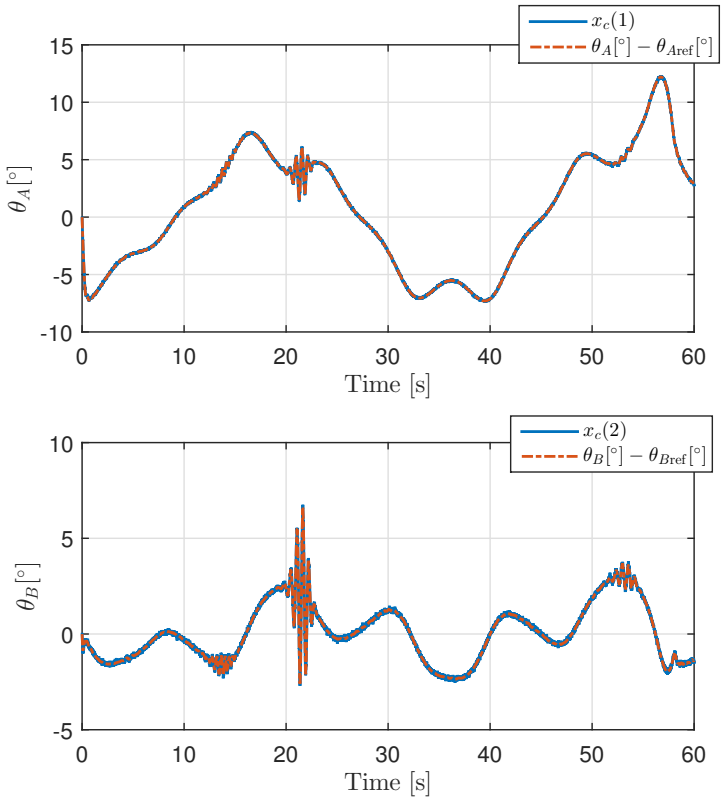

Figure 32: Controller state x_c result of the $\mathcal{H}_2$ dynamic control applied to the CMG and considering a sinusoidal reference.

5 CONCLUSION

This thesis presented *i)*- modeling techniques for a class of nonlinear systems in terms of LPV or quasi-LPV models; *ii)*- synthesis conditions based on convex optimization for gain-scheduled controllers with polynomial dependence on the scheduling variables, assuring stability and performance (in terms of the $\mathcal{H}_2$ and $\mathcal{H}_\infty$ norms) with less conservatism; *iii)*- simulations and experimental validations in practical systems of the proposed modeling and control methods.

5.1 Modeling

Regarding the modeling in terms of time-varying parameters, two approaches have been developed to obtain LPV and quasi-LPV models from a class of nonlinear systems. One focused on increase of region in which the model is capable to represent the dynamics of the plant with accuracy, and another focused on reference tracking problems.

In general, the high order Taylor expansion approach can generate models capable to represent with accuracy a larger region around a chosen operating point. As shown in the simulations, the models devised for the mechatronics systems investigated represented the associated nonlinear models quite well.

The second approach considered a polynomial regression to generate models with several operating points. The main strategy was to design an LPV (or quasi-LPV) model representing a family of linear models within the considered range of operation. To acomplish this task, an algorithm that generates generalized polynomial LPV (or quasi-LPV) models was proposed to cope with systems with a generic number of time-varying parameters and with arbitrary polynomial degrees. The algorithm presented good results when applied to the mechatronic plants under investigation, specially when dealing with the tracking problem. Generally, the price to be paid to obtain more accurate models is a progressive increase in the computational burden demanded to synthesize the polynomial models with larger degrees. At this point the designer must trade-off the accuracy of

the model and the computational complexity required to design the gain-scheduled controllers for the model. As a final conclusion about this topic, both the proposed modeling techniques are systematic and general methods to deal with a class of nonlinear systems, being an important first step for the challenging task of designing controllers for this class of systems.

5.2 Gain-scheduled Control

Concerning the problem of designing controllers, new LMI conditions for stabilization, $\mathcal{H}_2$ and $\mathcal{H}_\infty$ control were proposed for LPV (or quasi-LPV) systems with polynomial dependence on the time-varying parameters. The proposed synthesis conditions include a scalar parameter belonging to a bounded set, being an important extra degree of freedom to obtain controllers with improved performance.

Initially, the stabilization problem by means of gain-scheduled state-feedback controlllers was addressed. New synthesis conditions were provided with a scalar parameter limited to the range $(-1, 1)$, which facilitates the task of implementing a linear search. Exhaustive numerical simulations in the context of time-invariant systems were presented to evaluate the proposed technique, showing that the additional variables specially included to deal with the time-derivative of the Lyapunov matrix do not introduce conservativeness.

Next, extensions to cope with $\mathcal{H}_2$ and $\mathcal{H}_\infty$ gain-scheduled state-feedback control were proposed, both also considering the linear search presented in the stabilization condition. Finally, as a clear demonstration of the generality and utility of the proposed technique, extensions to deal with the more challeging problems of static and full-order dynamic output-feedback were also presented. The synthesis conditions are formulated in terms of a well established technique from the literature where the controllers are designed in two steps.

As all synthesis conditions from the literature based on LMI optimization, the proposed technique causes a rapidly increase in the computational burden necessary to design models and controllers as the degrees of the models and controllers grow, limiting the approach for systems with a small number of variables and parameters.

Although not presented, an extension to deal with the mixed $\mathcal{H}_2/\mathcal{H}_\infty$ gain-scheduled control design is possible. As all proposed conditions employ the slack variables to construct the gain, different Lyapunov matrices for both criteria can be used, potentially leading to less conservative results.

5.3 Simulations and Experimental Validations

Finally, simulation and practical results were presented, considering: State-feedback, static output-feedback and full-order dynamic output-feedback control. For the state-feedback case, the results were considered satisfactory, even though, for most cases, the Taylor-based modeling did not provide significant improvements (as previously mentioned). However, with the modeling scheme that interpolates linear models, the tracking problem was efficiently tackled without integrators or pre-filters.

Regarding the static output-feedback case, it was not possible to design a feasible controller for the real mechatronic plants investigated in this thesis. However, the proposed condition proved to be effective in a numerical example based on a randomly generated system.

The full-order dynamic output-feedback control presented good results in the simulation tests. However, in the case of CMG, there is a small oscillation in the control effort (worse in $\mathcal{H}_\infty$ case), which can harm the practical implementation of the controller. However, as the Furuta pendulum did not present this oscillation, other setups for the parameters involved in the design, as the values of ξ and ϵ and the polynomial degrees of the controller variables, can mitigate this undesired issue.

Another interesting point to mention about the dynamic controller is the fact that the dynamics $\dot{x}_c = A_c(\rho)x_c + B_c(\rho)y$ is working like as an observer to estimate $(x - x_{ref})$. This is due to the first stage of the synthesis condition, which considers $u = C_c(\rho)x_c$, where $C_c(\rho)$ is chosen as a stabilizing state-feedback controller. As a consequence, in order to maintain stability, x_c converges to $(x - x_{ref})$.

5.4 Future Works

As future works, the following extensions and tasks can be mentioned:

- We first intend to carry out a practical implementation of the dynamic controller;
- We intend to test the high-order Taylor series-based modeling technique on systems that are more sensitive to the LPV parameter;
- Another future direction of investigation could be the application of the polynomial interpolation method in discrete systems, as there is no restriction for that in the procedure;

- Finally, since the proposed time-varying control conditions are very model dependent (exact measurement of the LPV variable is required), the extension of the method to cope with modeling or measurement errors (LACERDA et al., 2016) would be an interesting direction as well.

5.5 Publication and submissions

Two conference papers were published from the results obtained in this thesis:

- G. P. Neves, F. Y. Toriumi, B. A. Angélico and R. C. L. F. Oliveira, "A new approach for quasi-LPV modeling and state-feedback control of nonlinear systems with application on a 5-DOF pendulum", Proceedings of the 2021 American Control Conference (ACC), 2021, pp. 4920-4925, doi: 10.23919/ACC50511.2021.9483001.

- G. P. Neves B. A. Angélico and R. C. L. F. Oliveira, "$\mathcal{H}_2$ gain-scheduled state-feedback synthesis conditions applied to a quadruple tank system", Anais do Congresso Brasileiro de Automática 2020, doi: 10.48011/asba.v2i1.1584.

Beside that, two journal papers were submitted:

- G. P. Neves B. A. Angélico and R. C. L. F. Oliveira, "$\mathcal{H}_2$ gain-scheduled state-feedback design with experimental validation in a control moment gyroscope represented as a polynomial LPV model", Mechatronics.

- G. P. Neves B. A. Angélico and R. C. L. F. Oliveira, "Quasi-LPV modeling and H_∞ gain-scheduled state-feedback control applied to a control moment gyroscope", International Journal of Control.

REFERENCES

ABBAS, H. S.; ALI, A.; HASHEMI, S. M.; WERNER, H. LPV state-feedback control of a control moment gyroscope. **Control Engineering Practice**, v. 24, p. 129 – 137, 2014.

AGULHARI, C. M.; FELIPE, A.; OLIVEIRA, R. C. L. F.; PERES, P. L. D. Algorithm 998: The Robust LMI Parser — A toolbox to construct LMI conditions for uncertain systems. **ACM Transactions on Mathematical Software**, v. 45, n. 3, p. 36:1–36:25, August 2019.

AGULHARI, C. M.; OLIVEIRA, R. C. L. F.; PERES, P. L. D. LMI relaxations for reduced-order robust $\mathcal{H}_\infty$ control of continuous-time uncertain linear systems. **IEEE Transactions on Automatic Control**, v. 57, n. 6, p. 1532–1537, jun. 2012.

ANDERSEN, E. D.; ANDERSEN, K. D. The MOSEK interior point optimizer for linear programming: An implementation of the homogeneous algorithm. In: FRENK, H.; ROOS, K.; TERLAKY, T.; ZHANG, S. (Ed.). **High Performance Optimization**. [S.l.]: Springer US, 2000, (Applied Optimization, v. 33). p. 197–232. ⟨http://www.mosek.com⟩.

APKARIAN, P.; ADAMS, R. J. Advanced gain-scheduling techniques for uncertain systems. **IEEE Transactions on Control Systems Technology**, v. 6, n. 1, p. 21–32, 1998.

APKARIAN, P.; GAHINET, P. A convex characterization of gain-scheduled $\mathcal{H}_\infty$ controllers. **IEEE Transactions on Automatic Control**, v. 40, n. 5, p. 853–864, maio 1995.

APKARIAN, P.; GAHINET, P.; BECKER, G. Self-scheduled $\mathcal{H}_\infty$ control of linear parameter-varying systems: A design example. **Automatica**, v. 31, n. 9, p. 1251–1261, 1995.

ARZELIER, D.; PEAUCELLE, D.; SALHI, S. Robust static output feedback stabilization for polytopic uncertain systems: Improving the guaranteed performance bound. In: **Proceedings of the 4th IFAC Symposium on Robust Control Design (ROCOND 2003)**. Milan, Italy: [s.n.], 2003. p. 425–430.

BIANCHI, F. D.; KUNUSCH, C.; OCAMPO-MARTINEZ, C.; SÀNCHEZ-PEÑA, R. S. A gain-scheduled LPV control for oxygen stoichiometry regulation in pem fuel cell systems. **IEEE Transactions on Control Systems Technology**, v. 22, n. 5, p. 1837–1844, Sep. 2014.

BIANCHI, F. D.; MANTZ, R. J.; CHRISTIANSEN, C. F. Gain scheduling control of variable-speed wind energy conversion systems using quasi-LPV models. **Control Engineering Practice**, v. 13, n. 2, p. 247–255, 2005.

BLIMAN, P.-A. An existence result for polynomial solutions of parameter-dependent LMIs. **Systems & Control Letters**, v. 51, n. 3-4, p. 165–169, mar. 2004.

BLIMAN, P.-A. Stabilization of LPV systems. In: HENRION, D.; GARULLI, A. (Ed.). **Positive Polynomials in Control**. Berlin: Springer-Verlag, 2005, (Lecture Notes in Control and Information Sciences, v. 312). p. 103–117.

BOYD, S.; GHAOUI, L. E.; FERON, E.; BALAKRISHNAN, V. **Linear Matrix Inequalities in System and Control Theory**. [S.l.]: Society for Industrial and Applied Mathematics, 1994.

BRIAT, C. **Linear Parameter-Varying and Time-Delay Systems — Analysis, Observation, Filtering and Control**. Berlin Heidelberg: Springer-Verlag, 2015. v. 3. 394 p. (Advances in Delays and Dynamics, v. 3).

CHESI, G.; GARULLI, A.; TESI, A.; VICINO, A. Robust stability of time-varying polytopic systems via parameter-dependent homogeneous Lyapunov functions. **Automatica**, v. 43, n. 2, p. 309–316, fev. 2007.

DAAFOUZ, J.; BERNUSSOU, J. Parameter dependent Lyapunov functions for discrete time systems with time varying parameter uncertainties. **Systems & Control Letters**, v. 43, n. 5, p. 355–359, ago. 2001.

DE CAIGNY, J.; CAMINO, J. F.; OLIVEIRA, R. C. L. F.; PERES, P. L. D.; SWEVERS, J. Gain-scheduled $\mathcal{H}_2$ and $\mathcal{H}_\infty$ control of discrete-time polytopic time-varying systems. **IET Control Theory & Applications**, v. 4, n. 3, p. 362–380, March 2010.

DE CAIGNY, J.; CAMINO, J. F.; SWEVERS, J. Interpolation-based modeling of MIMO LPV systems. **IEEE Transactions on Control Systems Technology**, v. 19, n. 1, p. 46–63, 2011.

DE OLIVEIRA, M. C.; BERNUSSOU, J.; GEROMEL, J. C. A new discrete-time robust stability condition. **Systems & Control Letters**, v. 37, n. 4, p. 261–265, jul. 1999.

DE OLIVEIRA, M. C.; GEROMEL, J. C.; BERNUSSOU, J. Design of dynamic output feedback decentralized controllers via a separation procedure. **International Journal of Control**, v. 73, n. 5, p. 371–381, mar. 2000.

DE SOUZA, C. E.; BARBOSA, K. A.; TROFINO, A. Robust $\mathcal{H}_\infty$ filtering for discrete-time linear systems with uncertain time-varying parameters. **IEEE Transactions on Signal Processing**, v. 54, n. 6, p. 2110–2118, jun. 2006.

DE SOUZA, C. E.; TROFINO, A. Gain-scheduled $\mathcal{H}_2$ controller synthesis for linear parameter varying systems via parameter-dependent Lyapunov functions. **International Journal of Robust and Nonlinear Control**, v. 16, n. 5, p. 243–257, mar. 2006.

DEAECTO, G. S.; GEROMEL, J. C.; GARCIA, F. S.; POMILIO, J. A. Switched affine systems control design with application to DC–DC converters. **IET Control Theory & Applications**, v. 4, n. 7, p. 1201–1210, 2010.

EBIHARA, Y.; HAGIWARA, T. New dilated LMI characterizations for continuous-time multiobjective controller synthesis. **Automatica**, v. 40, n. 11, p. 2003–2009, nov. 2004.

ECP. **Model 750: Control Moment Gyroscope**. 1990. Educational Control Products. 30 Jul. 2019 ¡http://www.ecpsystems.com/controls_ctrlgyro.htm¿.

ECP, T. P. **Manual for model 750 Control Moment Gyroscope**. [S.l.], 1999.

GAHINET, P.; APKARIAN, P.; CHILALI, M. Affine parameter-dependent Lyapunov functions and real parametric uncertainty. **IEEE Transactions on Automatic Control**, v. 41, n. 3, p. 436–442, mar. 1996.

GEROMEL, J. C.; COLANERI, P. Robust stability of time varying polytopic systems. **Systems & Control Letters**, v. 55, n. 1, p. 81 – 85, 2006.

GEROMEL, J. C.; COLANERI, P. Stability and stabilization of continuous-time switched systems. **SIAM Journal on Control and Optimization**, v. 45, n. 5, p. 1915–1930, 2006.

GEROMEL, J. C.; DE OLIVEIRA, M. C.; HSU, L. LMI characterization of structural and robust stability. **Linear Algebra and Its Applications**, v. 285, n. 1–3, p. 69–80, dez. 1998.

GEROMEL, J. C.; KOROGUI, R. H.; BERNUSSOU, J. $\mathcal{H}_2$ and $\mathcal{H}_\infty$ robust output feedback control for continuous time polytopic systems. **IEE Proceedings — Control Theory and Applications**, v. 1, n. 5, p. 1541–1549, set. 2007.

HANIFZADEGAN, M.; NAGAMUNE, R. Smooth switching LPV controller design for LPV systems. **Automatica**, v. 50, n. 5, p. 1481–1488, 2014.

HESPANHA, J. P. **Linear systems theory**. [S.l.]: Princeton university press, 2018.

HESPANHA, J. P.; NAGHSHTABRIZI, P.; XU, Y. A survey of recent results in networked control systems. **Proceedings of the IEEE**, v. 95, n. 1, p. 138–162, jan. 2007.

HOFFMANN, C.; WERNER, H. A survey of linear parameter-varying control applications validated by experiments or high-fidelity simulations. v. 23, n. 2, p. 416–433, mar. 2015.

HUANG, Y.; JADBABAIE, A. Nonlinear $\mathcal{H}_\infty$ control: An enhanced quasi-LPV approach. **IFAC Proceedings Volumes**, v. 32, n. 2, p. 2754–2759, 1999.

LACERDA, M. J.; TOGNETTI, E. S.; OLIVEIRA, R. C. L. F.; PERES, P. L. D. A new approach to handle additive and multiplicative uncertainties in the measurement for $\mathcal{H}_\infty$ LPV filtering. **International Journal of Systems Science**, v. 47, n. 5, p. 1042–1053, 2016.

LIBERZON, D. **Switching in Systems and Control**. Boston, MA: Birkhäuser, 2003. (Systems and Control: Foundations and Applications).

MOHAMMADPOUR, J.; SCHERER, C. W. (Ed.). **Control of Linear Parameter Varying Systems with Applications**. New York: Springer, 2012.

MONTAGNER, V. F.; OLIVEIRA, R. C. L. F.; PERES, P. L. D. Design of $\mathcal{H}_\infty$ gain-scheduled controllers for linear time-varying systems by means of polynomial Lyapunov functions. In: **Proceedings of the 45th IEEE Conference on Decision and Control**. San Diego, CA, USA: [s.n.], 2006. p. 5839–5844.

MONTAGNER, V. F.; OLIVEIRA, R. C. L. F.; PERES, P. L. D.; BLIMAN, P.-A. Stability analysis and gain-scheduled state feedback control for continuous-time systems with bounded parameter variations. **International Journal of Control**, v. 82, p. 1045–1059, June 2009.

MOREIRA, H. R.; OLIVEIRA, R. C. L. F.; PERES, P. L. D. Robust $\mathcal{H}_2$ static output feedback design starting from a parameter-dependent state feedback controller for time-invariant discrete-time polytopic systems. **Optimal Control Applications and Methods**, v. 32, n. 1, p. 1–13, January/February 2011.

MORI, S.; NISHIHARA, H.; FURUTA, K. Control of unstable mechanical system control of pendulum†. **International Journal of Control**, Taylor & Francis, v. 23, n. 5, p. 673–692, 1976.

NEVES, G. P.; ANGÉLICO, B. A.; AGULHARI, C. M. Robust $\mathcal{H}_2$ controller with parametric uncertainties applied to a reaction wheel unicycle. **International Journal of Control**, Taylor & Francis, v. 0, n. 0, p. 1–11, 2019.

Oliveira, R. C. L. F.; de Oliveira, M. C.; Peres, P. L. D. Robust state feedback lmi methods for continuous-time linear systems: Discussions, extensions and numerical comparisons. In: **Proceedings of the 2011 IEEE International Symposium on Computer-Aided Control System Design (CACSD)**. [S.l.: s.n.], 2011. p. 1038–1043.

OLIVEIRA, R. C. L. F.; PERES, P. L. D. Parameter-dependent LMIs in robust analysis: Characterization of homogeneous polynomially parameter-dependent solutions via LMI relaxations. **IEEE Transactions on Automatic Control**, v. 52, n. 7, p. 1334–1340, jul. 2007.

PEAUCELLE, D.; ARZELIER, D. An efficient numerical solution for $\mathcal{H}_2$ static output feedback synthesis. In: **Proceedings of the 2001 European Control Conference**. Porto, Portugal: [s.n.], 2001. p. 3800–3805.

RODRIGUES, L.; OLIVEIRA, R.; CAMINO, J. Parameterized LMIs for robust and state feedback control of continuous-time polytopic systems. **International Journal of Robust and Nonlinear Control**, v. 28, n. 3, p. 940–952, 2018.

RODRIGUES, L. A.; OLIVEIRA, R. C. L. F.; CAMINO, J. F. New extended LMI characterization for state feedback control of continuous-time uncertain linear systems. In: **Proceedings of the 2015 European Control Conference (ECC)**. [S.l.: s.n.], 2015. p. 1992–1997.

ROTONDO, D.; NEJJARI, F.; PUIG, V. Quasi-LPV modeling, identification and control of a twin rotor MIMO system. **Control Engineering Practice**, v. 21, n. 6, p. 829–846, 2013.

RUGH, W. J.; SHAMMA, J. S. Research on gain scheduling. **Automatica**, v. 36, n. 10, p. 1401 – 1425, 2000. ISSN 0005-1098.

SATO, M. Performance analysis of LPV systems using higher-order Lyapunov functions. In: **Proceedings of the 16th IFAC World Congress**. Prague, Czech Republic: [s.n.], 2005.

SATO, M.; PEAUCELLE, D. Gain-scheduled output-feedback controllers using inexact scheduling parameters for continuous-time LPV systems. **Automatica**, v. 49, n. 4, p. 1019–1025, abr. 2013.

SEBER, G.; WILD, C. **Nonlinear Regression**. [S.l.]: John Wiley & Sons, 1989. ISBN 9780471617600.

SHU-QING, L.; SHENG-XIU, Z. A modified LPV modeling technique for turbofan engine control system. In: **Proceedings of the 2010 International Conference on Computer Application and System Modeling (ICCASM 2010)**. [S.l.: s.n.], 2010. v. 5, p. 99–102.

STURM, J. F. Using SeDuMi 1.02, a MATLAB toolbox for optimization over symmetric cones. **Optimization Methods and Software**, v. 11, n. 1–4, p. 625–653, 1999. ⟨http://sedumi.ie.lehigh.edu/⟩.

SZNAIER, M. Receding horizon: an easy way to improve performance in LPV systems. In: **Proceedings of the 1999 American Control Conference**. Albuquerque, NM, USA: [s.n.], 1999. v. 4, p. 2257–2261.

TAN, W.; PACKARD, A.; BALAS, G. J. Quasi-LPV modeling and LPV control of a generic missile. In: **Proceedings of the 2000 American Control Conference**. Chicago, IL, USA: [s.n.], 2000. v. 5, p. 3692–3696.

TANAKA, K.; WANG, H. **Fuzzy Control Systems Design and Analysis: A Linear Matrix Inequality Approach**. New York, NY: John Wiley & Sons, 2001.

TARBOURIECH, S.; GARCIA, G.; GOMES DA SILVA JR., J. M.; QUEINNEC, I. **Stability and Stabilization of Linear Systems with Saturating Actuators**. London, UK: Springer, 2011.

TOH, K. C.; TODD, M. J.; TÜTÜNCÜ, R. SDPT3 — A Matlab software package for semidefinite programming, Version 1.3. **Optimization Methods and Software**, v. 11, n. 1, p. 545–581, 1999.

TORIUMI, F.; ANGELICO, B. Passivity-based nonlinear control approach for tracking task of an underactuated CMG. **IEEE/ASME Transactions on Mechatronics**, PP, p. 1–1, 11 2020.

TORIUMI, F. Y.; ANGéLICO, B. A. Nonlinear controller design for tracking task of a control moment gyroscope actuator. **IEEE/ASME Transactions on Mechatronics**, v. 25, n. 1, p. 438–448, Feb 2020.

TORIUMI, F. Y.; ANGéLICO, B. A.; TANNURI, E. A. Feedback linearization approach applied to a control moment gyroscope with SISO configuration. In: **Proceedings of the 2018 13th IEEE International Conference on Industry Applications (INDUSCON)**. [S.l.: s.n.], 2018. p. 174–179.

TÓTH, R. **Modeling and identification of linear parameter-varying systems**. Heidelberg, Germany: Springer-Verlag, 2010. v. 403. (Lecture Notes in Control and Information Sciences, v. 403).

TROFINO, A.; DE SOUZA, C. E. Biquadratic stability of uncertain linear systems. **IEEE Transactions on Automatic Control**, v. 46, n. 8, p. 1303–1307, ago. 2001.

WANG, F.; BALAKRISHNAN, V. Improved stability analysis and gain-scheduled controller synthesis for parameter-dependent systems. **IEEE Transactions on Automatic Control**, v. 47, n. 5, p. 720–734, maio 2002.

WU, F. A generalized LPV system analysis and control synthesis framework. **International Journal of Control**, v. 74, n. 7, p. 745–759, maio 2001.

WU, F.; YANG, H. X.; PACKARD, A.; BECKER, G. Induced L_2-norm control for LPV systems with bounded parameter variation rates. **International Journal of Robust and Nonlinear Control**, v. 6, n. 9-10, p. 983–998, 1996.

XIE, W. $\mathcal{H}_2$ gain scheduled state feedback for LPV system with new LMI formulation. **IEE Proceedings — Control Theory and Applications**, v. 152, n. 6, p. 693–697, nov. 2005.

APPENDIX A – REACTION WHEEL INVERTED PENDULUM

The reaction wheel pendulum consists of a wheel (called reaction wheel) positioned on top of a rod. Its operation consists of using the reaction of the torque applied to the wheel to act on the rod and, thus, balance the pendulum. Consider the schematic drawing with the coordinate systems fixed on each body shown in Figure 33.

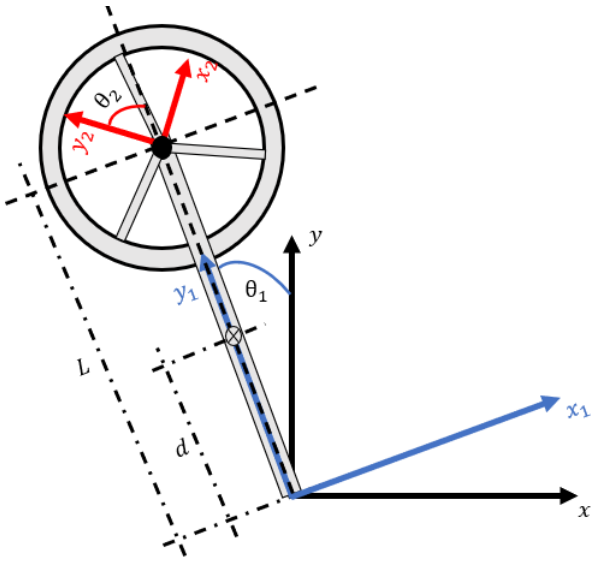

Figure 33: Reaction wheel pendulum schematic drawing.

The variables θ_1 and θ_2 are the angles of the wheel and the reaction wheel, respectively. Besides, the parameters of the built pendulum are informed in Table 24. The coordinate system (system $\{0\}$) depicted in black is fixed to the base, the blue one (system $\{1\}$) is fixed to the body, and the red one (system $\{2\}$) is fixed to the wheel.

Table 24: Reaction wheel pendulum parameters

	Parameter	Value
M_1	Body mass [kg]	0.117
M_2	Wheel mass [kg]	0.119
L	Body length [m]	0.14298
I_2	Wheel moment of inertia [kgm^2]	9.4559×10^{-4}
I_1	Body moment of inertia [kgm^2]	6.2533×10^{-4}
d	Distant between base and body center of mass [m]	0.0987
g	Gravity acceleration [m/s^2]	9.81
K_t	Torque constant motor	0.0601
K_e	Velocity constant motor [V/(rad/s)]	0.1836
R_m	Motor resistance [Ω]	2.44

The system rotation matrices are

$$
\begin{aligned}
{}^1_0R &= R_1 = \begin{bmatrix} \cos(\theta_1) & -\sin(\theta_1) & 0 \\ \sin(\theta_1) & \cos(\theta_1) & 0 \\ 0 & 0 & 1 \end{bmatrix}, \\
{}^2_1R &= R_2 = \begin{bmatrix} \cos(\theta_2) & -\sin(\theta_2) & 0 \\ \sin(\theta_2) & \cos(\theta_2) & 0 \\ 0 & 0 & 1 \end{bmatrix},
\end{aligned}
$$

and the velocities of each system is calculated by

$$
\begin{aligned}
\omega_1 &= R_1^\top \begin{bmatrix} 0 & 0 & 0 \end{bmatrix}^\top + \begin{bmatrix} 0 & 0 & \dot{\theta}_1 \end{bmatrix}^\top, \\
v_{1c} &= \omega_1 \times \begin{bmatrix} 0 & d & 0 \end{bmatrix}^\top, \\
\omega_2 &= R_2^\top \omega_1 + \begin{bmatrix} 0 & 0 & \dot{\theta}_2 \end{bmatrix}^\top, \\
v_2 &= v_{2c} = R_2 \left(\omega_2 \times \begin{bmatrix} 0 & L & 0 \end{bmatrix}^\top \right).
\end{aligned} \tag{A.1}
$$

To compute the dynamic model using the Lagrange equation it is necessary to determine the Lagrangian

$$
\mathcal{L} = \mathcal{K} - \mathcal{U},
$$

where $\mathcal{K}$ and $\mathcal{U}$ are the kinetic and potential energies, respectively, which are calculated as

$$
\begin{aligned}
\mathcal{K} &= \frac{1}{2} v_{1c}^\top M_1 v_{1c} + \frac{1}{2} v_{2c}^\top M_2 v_{2c} + \frac{1}{2} \omega_1^\top I_1 \omega_1 + \frac{1}{2} \omega_2^\top I_2 \omega_2, \\
\mathcal{U} &= M_1 d \cos(\theta_1) + M_2 L \cos(\theta_2).
\end{aligned}
$$

Defining $q = \begin{bmatrix}\theta_1 & \theta_2\end{bmatrix}^\top$, the Lagrange equation is

$$\frac{d}{dt}\frac{\partial \mathcal{L}}{\partial \dot{q}} - \frac{\partial \mathcal{L}}{\partial q} = \tau_{ext},$$

where

$$\tau_{ext} = \begin{bmatrix} 0 \\ \frac{K_t}{R_m}(12u - K_v\dot{\theta}_2) \end{bmatrix}.$$

Finally, the resulting nonlinear model is given by

$$M(q)\ddot{q} + V(q,\dot{q}) + G(q) = Pu,$$

where

$$\begin{aligned} M(q) &= \begin{bmatrix} 0.0051 & 0.0009 \\ 0.0009 & 0.0009 \end{bmatrix}, \\ V(q) &= \begin{bmatrix} 0 \\ 0.00452\dot{\theta}_2 \end{bmatrix}, \\ G(q) &= \begin{bmatrix} -0.28\sin(\theta_1) \\ 0 \end{bmatrix}, \\ P &= \begin{bmatrix} 0 \\ 0.2956 \end{bmatrix}. \end{aligned}$$

APPENDIX B – ROTATIONAL PENDULUM MODEL

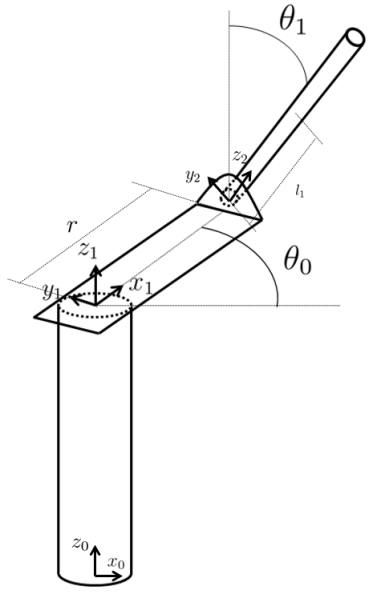

Figure 34: Rotational pendulum schematic drawing.

According to Figure 34, the rotation matrices can be written as

$$
\begin{aligned}
{}^{1}_{0}R &= R_0 = \begin{bmatrix} \cos(\theta_0) & -\sin(\theta_0) & 0 \\ \sin(\theta_0) & \cos(\theta_0) & 0 \\ 0 & 0 & 1 \end{bmatrix}, \\
{}^{2}_{1}R &= R_1 = \begin{bmatrix} 1 & 0 & 0 \\ 0 & \cos(\theta_1) & -\sin(\theta_1) \\ 0 & \sin(\theta_1) & \cos(\theta_1) \end{bmatrix},
\end{aligned}
$$

where θ_0 is the arm angle and θ_1 is the pendulum angle. Then, the velocities can be

calculated by

$$\begin{aligned}
\omega_0 &= R_0^\top \begin{bmatrix} 0 & 0 & 0 \end{bmatrix}^\top + \begin{bmatrix} 0 & 0 & \dot{\theta}_0 \end{bmatrix}^\top, \\
v_{0c} &= \omega_0 \times \begin{bmatrix} r/2 & 0 & 0 \end{bmatrix}^\top, \\
\omega_1 &= R_1^\top \omega_0 + \begin{bmatrix} \dot{\theta}_1 & 0 & 0 \end{bmatrix}^\top, \\
v_1 &= R_1 \left(\omega_0 \times \begin{bmatrix} r & 0 & 0 \end{bmatrix}^\top \right), \\
v_{1c} &= \omega_1 \times \begin{bmatrix} 0 & 0 & l_1 \end{bmatrix}^\top.
\end{aligned}$$

The potential (U) and kinetics (T) energies are

$$\begin{aligned}
T1 &= \frac{1}{2}\omega_0^\top I_b \omega_0 + \frac{1}{2} v_{0c}^\top M_b v_{0c}, \\
T2 &= \frac{1}{2}\omega_1^\top I_p \omega_1 + \frac{1}{2} v_{1c}^\top M_p v_{1c}, \\
T &= T1 + T2, \\
U &= M_p l_1 \cos(\theta_1).
\end{aligned}$$

Using the Lagrange equations, we has

$$\begin{aligned}
L &= T - U, \\
\frac{d}{dt}\frac{\partial L}{\partial \dot{q}} - \frac{\partial L}{\partial q} &= \tau_{ext},
\end{aligned}$$

where $q = \begin{bmatrix} \theta_0 & \theta_1 \end{bmatrix}^\top$ are the generalized variables. The generalized torque is $\tau_{ext} = \begin{bmatrix} \tau - B_0\dot{\theta}_0 & -B_1\dot{\theta}_1 \end{bmatrix}^\top$. The torque τ is applied by a DC motor, so, its dynamic is

$$\tau = \frac{K_t}{R}(12V - K_v\dot{\theta}_0),$$

where K_t is the torque constant, K_v is the speed constant, R the resistance and V is the percentage of input voltage ranging from -1 to 1. The values of the parameters of the built prototype are shown in Table 25.

Hence, the following nonlinear model is obtained:

$$M(q)\ddot{q} + V(q, \dot{q}) + G(q) = Pu,$$

Table 25: Rotational inverted pendulum parameters.

	Parameter	Value
M_0	Arm mass	$0.393Kg$
M_1	Pendulum mass	$0.068Kg$
r	Arm Length	$0.365m$
l_1	Distance of the center of mass	$0.1035m$
I_b	Arm inertia moment	$6.3725e-04Kgm^2$
I_p	Pendulum inertia moment	$3.9583e-04Kgm^2$
K_t	Torque constant	$0.02Nm/A$
K_v	Speed constant	$0.08V/(rad/s)$
R	Motor resistance	2.4Ω

where

$$
\begin{aligned}
M(q) &= \begin{bmatrix} 0.008603 - 0.001188\cos(\theta_1)^2 & -0.002375\cos(\theta_1) \\ -0.002375\cos(\theta_1) & 0.001583 \end{bmatrix}, \\
V(q,\dot{q}) &= \begin{bmatrix} 0.002375\sin(\theta_1)\dot{\theta}_1^2 + 0.001188\dot{\theta}_0\sin(2\theta_1)\dot{\theta}_1 + 0.004868\dot{\theta}_0 \\ -0.0005938\sin(2\theta_1)\dot{\theta}_0{}^2 + 0.0001\dot{\theta}_1 \end{bmatrix}, \\
G(q) &= \begin{bmatrix} 0 \\ -0.09319\sin(\theta_1) \end{bmatrix}, \\
P &= \begin{bmatrix} 0.3933 \\ 0 \end{bmatrix}.
\end{aligned}
$$

APPENDIX C – UNICYCLE

The unicycle has three parts with center of mass determined by $\overrightarrow{p_1}$, $\overrightarrow{p_2}$ and $\overrightarrow{p_3}$, respectively, for the position of the travel wheel, body and reaction wheel (NEVES; ANGÉLICO; AGULHARI, 2019). Furthermore, the unicycle is considered to be positioned on the $\overrightarrow{x}$ axis, as shown in Figure 35.

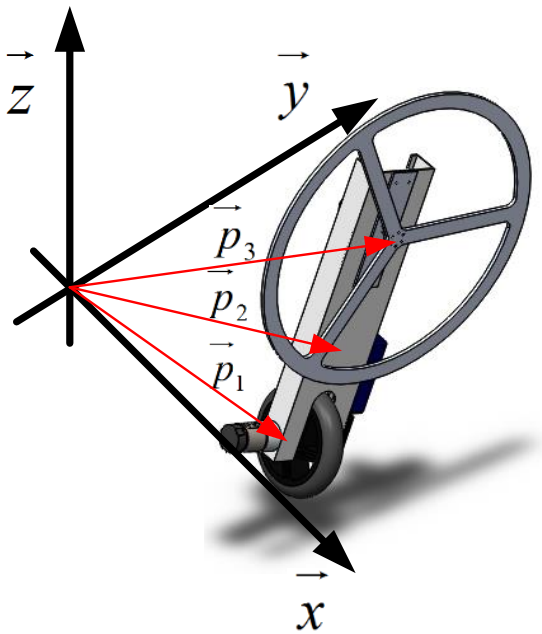

Figure 35: Positions of the bodies.

The position vectors are determined by

$$
\begin{aligned}
\overrightarrow{p_1} &= \begin{bmatrix} R_w\theta_w & R_w\sin(\varphi) & R_w\cos(\varphi) \end{bmatrix}, \\
\overrightarrow{p_2} &= \begin{bmatrix} R_w\theta_w + L\sin(\psi) & (R_w + L\cos(\psi))\sin(\varphi) & (R_w + L\cos(\psi))\cos(\varphi) \end{bmatrix}, \\
\overrightarrow{p_3} &= \begin{bmatrix} R_w\theta_w + (L+d)\sin(\psi) & (R_w + (L+d)\cos(\psi))\sin(\varphi) \\ & (R_w + (L+d)\cos(\psi))\cos(\varphi) \end{bmatrix}.
\end{aligned}
$$

The translational kinetic energy is calculated by

$$E_T = \frac{1}{2}\overrightarrow{v}^\top M \overrightarrow{v},$$

where M is the mass of the object and $\overrightarrow{v}$ is the velocity vector of the center of mass in relation to the inertial system. Thus, the translational kinetic energy of the unicycle is given by

$$E_T = \frac{1}{2}\overrightarrow{v_1}^\top M_w \overrightarrow{v_1} + \frac{1}{2}\overrightarrow{v_2}^\top M_b \overrightarrow{v_2} + \frac{1}{2}\overrightarrow{v_3}^\top M_r \overrightarrow{v_3},$$

where

$$\begin{aligned}\overrightarrow{v_1} &= \frac{d}{dt}\overrightarrow{p_1},\\ \overrightarrow{v_2} &= \frac{d}{dt}\overrightarrow{p_2},\\ \overrightarrow{v_3} &= \frac{d}{dt}\overrightarrow{p_3}.\end{aligned}$$

The rotational kinetic energy is calculated as

$$E_R = \underbrace{\frac{1}{2}J_w\dot{\theta}_w^2}_{1} + \underbrace{\frac{1}{2}J_{br}\dot{\psi}^2}_{2} + \underbrace{\frac{1}{2}J_r(\dot{\theta}_r + \dot{\varphi})^2}_{3} + \underbrace{\frac{1}{2}J_{bw}\dot{\varphi}^2}_{4},$$

where part 1 of the equation corresponds to the travel wheel rotation, part 2 is the rotation of the pitch angle, part 3 corresponds to the rotation of the reaction wheel and its center of mass and part 4 is the rotation of the roll angle.

The potential energy is

$$U = M_w g R_w \cos(\varphi) + M_b g((R_w + L\cos(\psi))\cos(\varphi)) + M_r g(R_w + (L+d)\cos(\psi))\cos(\varphi).$$

The Lagrange equation is used to determine the dynamic model of the system. The Lagrangian is defined as

$$L = E_T + E_R - U,$$

where E_T, E_w and U are the translational kinetic energy, rotational kinetic energy and the potential energy, respectively.

Given $q = \begin{bmatrix}\theta_r & \varphi & \theta_w & \psi\end{bmatrix}^\top$ (vector of the variables corresponding to the degrees of freedom), and τ the vector of external torques and force, the Lagrange equation is written as

$$\frac{d}{dt}\frac{\partial L}{\partial \dot{q}} - \frac{\partial L}{\partial q} = \tau - B_v,$$

where $B_v = \begin{bmatrix} B_{vr}\theta_r & -B_{vr}\theta_r & B_{vw}\theta_w & -B_{vw}\theta_w \end{bmatrix}^\top$ is the vector of the viscous friction.

In this case, the external torque is caused by the motors and their reactions, such that

$$\tau = \begin{bmatrix} \tau_r & -\tau_r & \tau_w & -\tau_w \end{bmatrix}^\top,$$

where τ_r is the torque caused by the motor connected to the reaction wheel, and τ_w the torque caused by the motor connected to the travel wheel. The equations of the DC motors are

$$\begin{aligned} \tau_r &= \frac{K_{tr}}{R_{er}}(12V_r - K_{er}\dot{\theta}_r), \\ \tau_w &= \frac{K_{tw}}{R_{ew}}(12V_w - K_{ew}(\dot{\theta}_w - \dot{\psi})), \end{aligned}$$

where V_r and V_w are inputs of the motor coupled with the reaction wheel and the travel wheel, respectively, with $-1 \leq V_r \leq 1$ and $-1 \leq V_w \leq 1$.

The practical unicycle can be seen in Figure 36 and the physical parameters in Table 26.

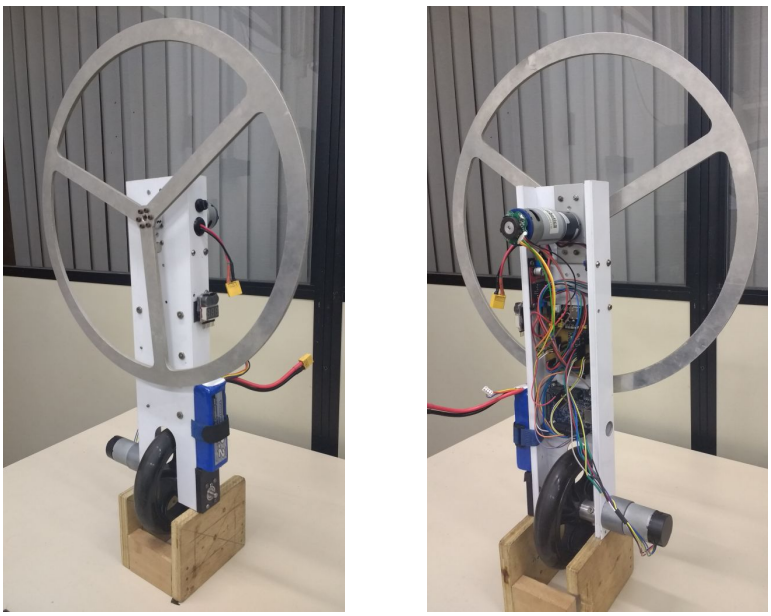

(a) View 1. (b) View 2.

Figure 36: Practical unicycle

Table 26: Unicycle physical parameters.

	Parameter	Value
R_r	Reaction wheel radius $[m]$	0.2
R_w	Wheel radius $[m]$	0.071
L	Distance of the center of mass (CM) of the body $[m]$	0.18632
d	Distance between the CM of the body and reaction wheel $[m]$	0.1503
M_r	Reaction wheel mass $[Kg]$	0.47568
M_b	Body mass $[Kg]$	1.23913
M_w	Wheel mass $[Kg]$	0.30220
g	Acceleration of gravity $[m/s^2]$	9.8
J_r	Reaction wheel moment of inertia $[Kgm^2]$	0.013472
J_w	Wheel moment of inertia $[Kgm^2]$	0.00077
J_{br}	Moment of inertia of the body plus reaction wheel $[Kgm^2]$	0.03937
J_{bw}	Moment of inertia of the body plus wheel $[Kgm^2]$	0.03458
n_r	Reduction of the reaction wheel motor	71
K_{tr}	Torque constant of the reaction wheel motor $[Nm/A]$	0.3383
K_{er}	Electrical constant of the reaction wheel motor $[Vs^2/rad]$	0.9454
R_{er}	Electrical resistance of the reaction wheel motor$[\Omega]$	0.6
n_w	Reduction of the wheel motor	131.25
K_{tw}	Torque constant of the wheel motor $[Nm/A]$	0.3531
K_{ew}	Electrical constant of the reaction wheel motor $[Vs^2/rad]$	1.3465
R_{ew}	Electrical resistance of the wheel motor$[\Omega]$	2.4
B_{vw}	Travel wheel viscous friction $[Ns^2/rad]$	0.1
B_{vr}	Reaction wheel viscous friction $[Ns^2/rad]$	0.1

From the Lagrange equation and the input vector $u = \begin{bmatrix} V_r & V_w \end{bmatrix}^\top$, the nonlinear model can be written as

$$M(q)\ddot{q} + V(q, \dot{q}) + G(q) = Pu,$$

where

$$
\begin{aligned}
M(q) &= \begin{bmatrix} 0.013 & 0.013 & 0 & 0 \\ 0.013 & 0.058\cos(\psi) + 0.1\cos(\psi)^2 + 0.1 & 0 & 0 \\ 0 & 0 & 0.011 & 0.029\cos(\psi) \\ 0 & 0 & 0.029\cos(\psi) & 0.14 \end{bmatrix}, \\
V(q,\dot{q}) &= \begin{bmatrix} 0.63\dot{\theta}_d \\ -0.63\dot{\theta}_d - 0.058\dot{\varphi}\dot{\psi}\sin(\psi) - 0.1\dot{\varphi}\dot{\psi}\sin(2\psi) \\ -0.029\sin(\psi)\dot{\psi}^2 - 0.2\dot{\psi} + 0.3\dot{\theta}_w \\ 0.3\dot{\psi} - 0.2\dot{\theta}_w + 0.029\dot{\varphi}^2\sin(\psi) + 0.051\dot{\varphi}^2\sin(2\psi) \end{bmatrix}^\top, \\
G(q) &= \begin{bmatrix} 0 \\ -9.8\sin(\varphi)(0.41\cos(\psi) + 0.15) \\ 0 \\ -4\cos(\varphi)\sin(\psi) \end{bmatrix}, \\
P &= \begin{bmatrix} 6.7664 & 0 \\ -6.7664 & 0 \\ 0 & 1.7654 \\ 0 & -1.7654 \end{bmatrix}.
\end{aligned}
$$

APPENDIX D – CONTROL MOMENT GYROSCOPE

For the Control Moment Gyroscope (CMG) (TORIUMI; ANGéLICO; TANNURI, 2018), consider the four coordinate systems illustrated in Figure 37. The coordinate systems are located at the center of mass, but for ease of viewing, they are set aside in the figure.

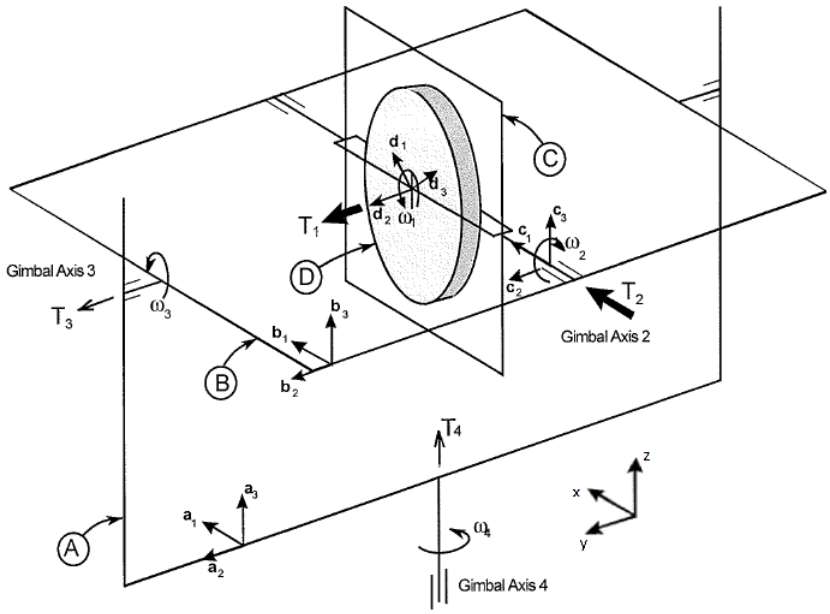

Figure 37: CMG schematic drawing.
Source: (ECP, 1999)

Thus, the rotational matrices are

$$
\begin{aligned}
{}^{A}_{N}R &= \begin{bmatrix} \cos(\theta_A) & -\sin(\theta_A) & 0 \\ \sin(\theta_A) & \cos(\theta_A) & 0 \\ 0 & 0 & 1 \end{bmatrix}, \\
{}^{B}_{A}R &= \begin{bmatrix} \cos(\theta_B) & 0 & \sin(\theta_B) \\ 0 & 1 & 0 \\ -\sin(\theta_B) & 0 & \cos(\theta_B) \end{bmatrix}, \\
{}^{C}_{B}R &= \begin{bmatrix} 1 & 0 & 0 \\ 0 & \cos(\theta_C) & -\sin(\theta_C) \\ 0 & \sin(\theta_C) & \cos(\theta_C) \end{bmatrix}, \\
{}^{D}_{C}R &= \begin{bmatrix} \cos(\theta_D) & 0 & \sin(\theta_D) \\ 0 & 1 & 0 \\ -\sin(\theta_D) & 0 & \cos(\theta_D) \end{bmatrix},
\end{aligned}
\tag{D.1}
$$

where θ_i is the angle of the gimbal i. Hence, the velocities are

$$
\begin{aligned}
\omega_N &= \begin{bmatrix} 0 & 0 & 0 \end{bmatrix}^\top, \\
\omega_A &= {}^{A}_{N}R^\top \omega_N + \begin{bmatrix} 0 & 0 & \dot{\theta}_A \end{bmatrix}^\top, \\
\omega_B &= {}^{B}_{A}R^\top \omega_A + \begin{bmatrix} 0 & \dot{\theta}_B & 0 \end{bmatrix}^\top, \\
\omega_C &= {}^{C}_{B}R^\top \omega_B + \begin{bmatrix} \dot{\theta}_C & 0 & 0 \end{bmatrix}^\top, \\
\omega_D &= {}^{D}_{C}R^\top \omega_C + \begin{bmatrix} 0 & 0 & \dot{\theta}_D \end{bmatrix}^\top,
\end{aligned}
$$

As the system only has rotational movement, there is no translational velocity. Then, the kinetics (T) energy is

$$
T = \frac{1}{2}\left(\omega_A^\top I_A \omega_A + \omega_B^\top I_B \omega_B + \omega_C^\top I_C \omega_C + \omega_D^\top I_D \omega_D\right),
$$

where the moment of inertia tensors are

$$
\begin{aligned}
I_A &= \mathrm{diag}(I_{Axx}, I_{Ayy}, I_{Azz}), \\
I_B &= \mathrm{diag}(I_{Bxx}, I_{Byy}, I_{Bzz}), \\
I_C &= \mathrm{diag}(I_{Cxx}, I_{Cyy}, I_{Czz}), \\
I_D &= \mathrm{diag}(I_{Dxx}, I_{Dyy}, I_{Dxx}).
\end{aligned}
$$

Using the Lagrange equation, one has

$$\frac{d}{dt}\frac{\partial T}{\partial \dot{q}} - \frac{\partial T}{\partial q} = \tau_{ext},$$

where $\tau_{ext} = \begin{bmatrix} -B_A\dot{\theta}_A & -B_B\dot{\theta}_B & T_3 - B_C\dot{\theta}_C & T_4 - B_D\dot{\theta}_D \end{bmatrix}^\top$, and T_3 and T_4 are the torques applied in the bodies 3 and 4, respectively.

The physical plant can be seen in the Figure 38, whereas Table 27 presents the prototype parameters.

Figure 38: Practical CMG.
Source: (ECP, 1990)

Finally, the nonlinear model is

$$M(q)\ddot{q} + V(q,\dot{q}) = Pu, \tag{D.2}$$

where[1]

$$M(q) = \begin{bmatrix} 0.021s\theta_C^2 - 0.024s\theta_B^2 - 0.021s\theta_B^2 s\theta_C^2 + 0.13 & 0.021c\theta_B c\theta_C s\theta_C & -0.027s\theta_B & 0.027c\theta_B s\theta_C \\ 0.021c\theta_B c\theta_C s\theta_C & 0.073 - 0.021s\theta_C^2 & 0 & 0.027c\theta_C \\ -0.027s\theta_B & 0 & 0.027 & 0 \\ 0.027c\theta_B s\theta_C & 0.027c\theta_C & 0 & 0.027 \end{bmatrix},$$

$$V(q,\dot{q}) = \begin{bmatrix} V_1 & V_2 & V_3 & V_4 \end{bmatrix}^\top,$$

$$P = \begin{bmatrix} 0 & 0 & 1 & 0 \\ 0 & 0 & 0 & 1 \end{bmatrix}^\top,$$

[1]To simplify the notation, $s\theta = \sin(\theta)$ and $c\theta = \cos(\theta)$.

Table 27: Gyroscope parameters.

	Parameter	Value
B_A	friction coefficient	$0.0027N/(rad/s)$
B_B	friction coefficient	$0.0027N/(rad/s)$
B_C	friction coefficient	$0.0118N/(rad/s)$
B_D	friction coefficient	$0.000187N/(rad/s)$
I_{Axx}	Inertia moment	$0Kgm^2$
I_{Ayy}	Inertia moment	$0Kgm^2$
I_{Azz}	Inertia moment	$0.0698Kgm^2$
I_{Bxx}	Inertia moment	$0.0119Kgm^2$
I_{Byy}	Inertia moment	$0.0178Kgm^2$
I_{Bzz}	Inertia moment	$0.0297Kgm^2$
I_{Cxx}	Inertia moment	$0.0124Kgm^2$
I_{Cyy}	Inertia moment	$0.0278Kgm^2$
I_{Czz}	Inertia moment	$0.0188Kgm^2$
I_{Dxx}	Inertia moment	$0.0148Kgm^2$
I_{Dyy}	Inertia moment	$0.0273Kgm^2$

Source: (ABBAS et al., 2014)

with

$$V_1 = 2.7e-3\dot{\theta}_A - 0.049\dot{\theta}_B\dot{\theta}_C c\theta_B - 0.046\dot{\theta}_A\dot{\theta}_B s2\theta_B - 0.027\dot{\theta}_B\dot{\theta}_D s\theta_B s\theta_C$$
$$+0.043\dot{\theta}_B\dot{\theta}_C c\theta_B c\theta_C^2 - 0.021\dot{\theta}_B^2 c\theta_C s\theta_B s\theta_C + 0.027\dot{\theta}_C\dot{\theta}_D c\theta_B c\theta_C$$
$$+0.043\dot{\theta}_A\dot{\theta}_B c\theta_B c\theta_C^2 s\theta_B + 0.043\dot{\theta}_A\dot{\theta}_C c\theta_B^2 c\theta_C s\theta_C,$$
$$V_2 = 2.7e-3\dot{\theta}_B + 5.7e-3\dot{\theta}_A\dot{\theta}_C c\theta_B - 0.027\dot{\theta}_C\dot{\theta}_D s\theta_C + 0.046\dot{\theta}_A^2 c\theta_B s\theta_B - 0.043\dot{\theta}_B\dot{\theta}_C c\theta_C s\theta_C$$
$$+0.027\dot{\theta}_A\dot{\theta}_D s\theta_B s\theta_C - 0.021\dot{\theta}_A^2 c\theta_B c\theta_C^2 s\theta_B + 0.043\dot{\theta}_A\dot{\theta}_C c\theta_B c\theta_C^2,$$
$$V_3 = 0.012\dot{\theta}_C - 5.7e-3\dot{\theta}_A\dot{\theta}_B c\theta_B + 0.027\dot{\theta}_B\dot{\theta}_D s\theta_C + 0.021\dot{\theta}_B^2 c\theta_C s\theta_C$$
$$-0.021\dot{\theta}_A^2 c\theta_B^2 c\theta_C s\theta_C - 0.043\dot{\theta}_A\dot{\theta}_B c\theta_B c\theta_C^2 - 0.027\dot{\theta}_A\dot{\theta}_D c\theta_B c\theta_C,$$
$$V_4 = 0.027\dot{\theta}_A\dot{\theta}_C c\theta_B c\theta_C - 0.027\dot{\theta}_A\dot{\theta}_B s\theta_B s\theta_C - 0.027\dot{\theta}_B\dot{\theta}_C s\theta_C + 1.9e-4\dot{\theta}_D.$$